UNIVERSITEIT VAN PRETORIA
UNIVERSITY OF PRETORIA
YUNIBESITHI YA PRETORIA

A THERMOGRAVIMETRIC STUDY OF THE REACTIONS OF MOLYBDENUM AND TUNGSTEN DISILICIDES WITH ANHYDROUS HYDROGEN FLUORIDE AND FLUORINE

Jabulani Selby Gama

Department of Chemical Engineering

University of Pretoria

A dissertation submitted in partial fulfilment of the requirements of the degree Master of Science in the Faculty of Engineering, Built Environment and Information Technology, University of Pretoria

Supervisor: Prof. P.L. Crouse

Co-supervisor: Dr J.B. Wagener

December 2011

Acknowledgements

I am deeply grateful to my supervisor, Prof. P.L. Crouse, Department of Chemical Engineering, University of Pretoria. His knowledge, persistence and logical thinking have been extremely helpful to me, as has his understanding, encouragement and guidance.

My warm thanks go to Dr J.B. Wagener, who gave me the opportunity to work with him and his associates in the Delta F group of the Department of Applied Chemistry at Necsa. His extensive discussions around my work and interesting explanations have been both enlightening and helpful.

I also wish to thank Dr H. Oosthuizen for her help, detailed review, constructive criticism and excellent advice during the preparation of this dissertation. I also wish to thank Mr B.M. Vilakazi for his instructions concerning the operation of the TGA instrument and the generation of thermogravimetric data.

During this work I have collaborated with many colleagues for whom I have great regard. I wish to extend my warmest thanks to all those who have contributed to this work, especially Dr E. Snyders, Mr D. Moolman and Mr O.S. Monnahela.

I would like to extend my recognition to the people and institutions that helped me with the analyses of the samples during the project: Pelindaba Analytical Laboratory (PAL) for the XRF results, SEM and XRD both from Necsa; and XRD from University of Pretoria.

I owe loving thanks to my family for unconditional support during the project.

The financial support of the National Research Foundation **(**NRF), Graduate in Training program (GiT) at Necsa, and the University of Pretoria is gratefully acknowledged.

Abstract

A study of the reactions between molybdenum and tungsten disilicide ($MoSi_2$ and WSi_2) with anhydrous hydrogen fluoride and fluorine was carried out to investigate the chemical behaviour of the materials. These two compounds were used as alternatives that resemble the chemical behaviour of uranium silicide (U_3Si_2). An extensive literature survey of U_3Si_2 processing techniques is included, which guided the process selection for this work.

The thermogravimetric results of a study into the dry fluorination of molybdenum and tungsten disicilides using both anhydrous hydrogen fluoride and dilute fluorine gas as fluorinating agents are reported. For both solids the observed reactions with fluorine follow the thermodynamically predicted routes, in which the formation of the volatile metal hexafluorides, along with gaseous silicon tetrafluoride was observed. The disilicides get fully converted at roughly 300 to 400 °C respectively.

The expected products for the reactions of both solids with hydrogen fluoride are solid tungsten metal, solid molybdenum metal, hydrogen gas, and gaseous silicon tetrafluoride. The metal fluorides (WF_4 and MoF_3) were not obtained because they form at low temperatures only. Therefore the metals of molybdenum and tungsten were obtained as final products respectively from both reactions; and were verified with the aid of XRF and XRD analyses.

Mass-transfer phenomena are shown to play a role in the reactions between hydrogen fluoride and both disilicides, preventing unrestrained complete fluorination of the two solids. Kinetic parameters are reported and the rate limiting mechanisms identified.

List of abbreviations and symbols

H^0	Enthalpy, standard
S^0	Entropy, standard
F_2	Fluorine gas
X_B	Fractional conversion
τ	Full time for complete conversion
G^0	Gibbs free energy, standard
Cp	Heat capacity
HEU	Highly enriched uranium
HF	Hydrogen fluoride gas
ICP-OES	Inductively coupled plasma optical emission spectroscopy
LEU	Low enriched uranium
LWR	Low water reactors
α	Mass fraction residue
$MoSi_2$	Molybdenum disilicide
PAL	Pelindaba Analytical Laboratory
PUREX	Plutonium - Uranium Extraction
RERTR	Reduced Enrichment for Research and Test Reactor
R&D	Research and Development
SCM	Shrinking core model
SPM	Shrinking particle model
SEM	Scanning electron microscopy
SNF	Spent nuclear fuel
TGA	Thermogravimetric analyser

WSi_2	Tungsten disilicide
XRD	X-Ray diffraction
XRF	X-Ray fluorescence

TABLE OF CONTENTS

List of figures

List of tables

UNIVERSITEIT VAN PRETORIA
UNIVERSITY OF PRETORIA
YUNIBESITHI YA PRETORIA

1. INTRODUCTION

1.1 Background

Historically, highly enriched uranium (HEU >20% ^{235}U enrichment) has been widely used in the manufacture of nuclear fuel for nuclear reactors. However, the international nuclear energy sector raised some concern about the use of HEU as nuclear fuel or targets in research and test reactors because HEU can also be used to manufacture atomic bombs. As a result, programmes have been put in place throughout the world to convert research and test reactors to low enrichment uranium (LEU <20% ^{235}U enrichment) fuel. An example is the Reduced Enrichment for Research and Test Reactors (RERTR) programme in the USA. It is expected that reducing the enrichment level of uranium in the nuclear fuel will not impair the performance of the reactor.

The reduction in the enrichment level of uranium has led to the development of new, high density, LEU silicide fuels, such as U_3Si_2 (U + 7.5 wt% Si), U_3Si (U + 4 wt% Si), and U_3SiAl (U + 3.5 wt% Si + 1.5 wt% Al) to replace HEU fuels such as UAl_2 and UO_x (Domagala et al., 1983). Uranium disilicide (U_3Si_2) is preferred because it is brittle and comminutes easily compared with other silicide compounds. It also has a high density compared with UAl_x and U_3O_8, and high uranium loadings. Thus increases the possibility of ^{99}Mo yields similar to HEU, for the isotope industry.

The manufacture of the silicide fuel from uranium silicide should ideally imply minimal changes in the engineering design and fabrication procedures currently used in the manufacture of UAl_x. Although replacing HEU with LEU in general is not unproblematic there are certain technical challenges. One problem is the need to develop a technique for recovering uranium from the used fuel and develop reprocessing techniques for obtaining the same amount of ^{99}Mo under the same irradiation conditions as HEU.

South Africa is one of the countries still in the process of converting from HEU to LEU. The South African Nuclear Energy Corporation (Necsa) is currently engaged in preparing and constructing a plant to manufacture LEU silicide (U_3Si_2) fuel, which will replace the HEU aluminide (UAl_2) fuel currently used in the SAFARI-1 research reactor. This is to comply with the decision taken by the South African government and international nuclear bodies to convert nuclear reactors from HEU to LEU. The replacement of UAl_2 with U_3Si_2 requires the development of a more efficient reprocessing method for the silicide fuel.

Recovery techniques of uranium from HEU are well known; they usually involve dissolving the fuel in acidic or basic solutions. However, the literature makes it clear that there are difficulties in processing LEU, especially U_3Si_2, using the techniques employed to treat HEU. Gates-Anderson et al. (2004) reported that the U_3Si_2 targets do not readily dissolve in bases, hence the need for a more aggressive reprocessing procedure.

1.2 Manufacturing process of uranium silicide fuel

The manufacturing process of LEU silicide fuel (U_3Si_2) has begun in a number of countries. For instance, France and the USA are already running some of their reactors with LEU silicide fuel. The foundation of the manufacturing procedure is to follow the engineering design applied in manufacturing HEU fuels such as UAl_x. This would be the most cost efficient.

The production process of LEU silicide fuel at Necsa consists of the following (main) steps:

- Preparation of the uranium before arc melting (e.g. cutting and cleaning).
- Arc melting of uranium (92.5 wt% U) and silicon metal (7.5 wt% Si) and subsequent crushing, milling and sieving of the ingot to produce a powder of U_3Si_2 alloy.
- Mixing and blending the powder with aluminium and subsequent pressing of the mixture to form an U_3Si_2-Al compact.
- Cladding of the silicide (U_3Si_2-Al) compact with Al-6061 alloy.

After the compacts are cladded, they are rolled to produce fuel plates of the required thickness. The fuel plates are attached to a fuel element, which is then ready for use in a nuclear reactor.

1.3 A research strategy for recovering uranium by dry fluorination

Necsa's objective is to develop a dry-processing method, where the scrap generated during the production process is treated with fluorine or hydrogen fluoride to produce a uranium fluoride compound. These compounds could be then further treated to extract uranium suitable to be re-used in the manufacture of new fuel elements.

Normally, the first step in reprocessing LEU silicide fuel is to remove the Al-6061 alloy cladding. Consequently, decladding techniques will need to be investigated.

After the decladding process, two methods will be investigated for treating the U_3Si_2-Al. The first method uses HF as a fluorinating agent, where $UF_4(s)$ and $SiF_4(g)$, $AlF_3(s)$ and $H_2(g)$ are expected as possible products. The possible reaction is as follows:

$$U_3Si_2\text{-}Al(s) + 23HF(g) \rightarrow 3UF_4(s) + 2SiF_4(g) + AlF_3(s) + 11.5H_2(g) \qquad (1.1)$$

The $SiF_4(g)$ and $H_2(g)$ gases are expected to be scrubbed before being vented to the atmosphere, leaving the $UF_4(s)$ and $AlF_3(s)$ solids behind. The challenge will be to separate the two solids. After separation, the $UF_4(s)$ will further be treated by a bomb-reduction method to obtain pure uranium metal.

The second method is to treat the U_3Si_2-Al with fluorine. In this case, complete volatilisation of the U_3Si_2 is anticipated, where $UF_6(g)$ and $SiF_4(g)$ are expected to be the gaseous products and $AlF_3(s)$ as the residual solid. The possible reaction is as follows:

$$U_3Si_2\text{-}Al(s) + 14.5F_2(g) \rightarrow 3UF_6(g) + 2SiF_4(g) + AlF_3(s) \quad (1.2)$$

A method of separating the two gaseous products (UF_6 and SiF_4) needs to be investigated. The separated $UF_6(g)$ will be then reduced to obtain $UF_4(s)$, which will be treated by the bomb-reduction method to yield uranium metal.

1.4 Objective of this study

Uranium is a highly toxic heavy metal as well as being radioactive. Its chemistry research can only be done under controlled conditions, licensed and monitored by the Nuclear Regulator. At the time of commencement of this study the Applied Chemistry laboratory at Necsa had not received its nuclear license and the research strategy outlined in section 1.3 above could not be implemented directly.

A decision was therefore made to study the behaviour of molybdenum and tungsten disilicides under anhydrous hydrogen fluoride and fluorine atmosphere. These alternative materials were chosen because the metals uranium, molybdenum, and tungsten have similar physical and chemical properties. For example: high melting points, the same crystal structure, and highest oxidation state of +6. They also display similar chemical behaviour under a fluorine atmosphere, forming hexafluorides when directly fluorinated with fluorine (Cotton & Wilkinson, 1962: 944-945). For this purpose, the molybdenum and tungsten disilicides ($MoSi_2$ and WSi_2) were elected.

Table 1.1 below, display some of the common properties between molybdenum, tungsten and uranium disilicide. All the materials have high melting points, and share the same kind of crystal structure.

Table 1.1: The properties of selected disilicide alloys (Yao et al., 1999)

Material	Melting point (°C)	Crystal structure	Density (g/cm^3)
$MoSi_2$	2030	Tetragonal	6.24
WSi_2	2160	Tetragonal	9.86
U_3Si_2	1660	Tetragonal	12.2

The alternative materials do not pose any hazards, and can therefore be handled without the need for major precautions, contrary to the hazardous (radioactivity) of U_3Si_2.

The objective of this study was thus to generate theoretical and practical understanding of the behaviour of $MoSi_2$ and WSi_2 and to provide a guideline in designing the experimental plan for U_3Si_2 research.

2. LITERATURE SURVEY

2.1 Introduction

The techniques for recovery of uranium from nuclear fuel can be divided into two categories: wet and dry methods. Wet processing methods involve the dissolution of the fuel in a solvent or solution followed by extraction, such as liquid-liquid extraction. Dry processing methods involve gases, where the fuel is exposed to a reactive gas such as chlorine or fluorine and solid and/or gaseous products are obtained. Where two or more gaseous products are obtained, a separation method would be applied to obtain the desired products.

Various wet and dry processing techniques for reprocessing LEU are reported. There are more wet methods reported (i.e. compared with dry methods), although these are not based on the use of hydrogen fluoride.

This literature study covers dry and wet processing techniques for LEU silicide fuel, as well as the chemical behaviour of the selected alternative materials under fluorine and anhydrous hydrogen fluoride atmospheres. This was done in order to compare the similarities in the silicide compounds. In the case of the dry processing methods, the focus was only placed on cases where F_2, HF, and other fluorine-containing gases are used, since the experimental work would only be carried out using HF and F_2.

2.2 Scope

Some of the literature in the survey was available in-house at Necsa, while the rest of the literature search was done electronically. Results were obtained from the following sources: Energy Citations database (ECD); European Patent Office; Science Direct; Scopus; Patentsonline.com; Sumobrain.com; Journalarchive.com; and Google-patents. The key words used for the electronic search (of the processing of HEU and LEU) were: “recovery of uranium”;

"recovery of uranium silicide fuel"; "reprocessing of LEU silicide fuel"; "fluoride volatility method for reprocessing uranium silicide fuel"; "dry processing routes for uranium silicide fuel"; "fluorination of uranium alloys"; "fluorination of uranium silicide fuels"; "wet processing routes for the recovery of uranium"; and "dissolution of uranium silicide". The key words used for searching the literature for alternative materials were: "fluorination of molybdenum silicide"; "fluorination of tungsten silicides"; "molybdenum fluorides"; "tungsten fluorides"; and "chemical behaviour of tungsten or molybdenum silicides".

2.3 Wet processing techniques

2.3.1 Aluminium cladding dissolution

Aluminium is used to clad both LEU and HEU nuclear fuels. The first step in processing LEU fuel is to remove this aluminium cladding. HEU fuels were usually cladded with the aluminium alloy Al-6061, which is also used to clad the new LEU silicide fuel. Other aluminium alloys used for fuel cladding are AG3NE, AG5NE, AlFeNi and A5.

The dissolution of these aluminium alloys is done in nitric acid (Juvenelle et al., 2003). The experiments with AG3N3 were done at temperatures ranging from 70 °C to the boiling point of the acid (~110 °C), with acid solutions ranging from 3 to 9 N. The dissolution kinetics of AG3NE was not affected by the concentration of the medium, but was affected by the temperature of the solution.

The other alloys were treated at the boiling temperature of the acid with an acid concentration of 9 N. All samples had a plate thickness ranging from 1 to 1.5 mm. Table 2.1 summarises the dissolution rates of the different aluminium alloys in nitric acid.

Table 2.1: The dissolution rates of different aluminium alloys

Material	Dissolution rate ($mg/cm^2/h$)	Main constituent elements (wt %)			
		Mg	Fe	Ni	Si
AG3NE	25 to 30	3.5 to 4.5	0.5	-	0.3
AG5NE	165	4.9 to 5.6	0.5	-	0.4
AlFeNi	20	0.8 to 1.2	0.8 to 1.2	0.8 to 1.2	-
Al-6061	25 to 30	0.8 to 1.2	0.7	-	0.4 to 0.8
A5	15	0.05	0.4	-	0.25

To simulate irradiated samples, plates were immersed in demineralised water for 200 h at 90 °C, after some time AlO(OH) appeared on the surface of the plates. The presence of AlO(OH) was confirmed by microscopic observation and X-ray diffraction analysis. AlO(OH) is normally observed on irradiated fuel plates. The demineralised samples initially had a high dissolution rate, which decreased to a value similar to that of the untreated samples. The initial dissolution rate of thicker samples was the same as those of thin samples, indicating that the initial increase in the rate is a surface phenomenon (Juvenelle et al., 2003).

2.3.2 Dissolution of U_3Si_2 in boiling 3 M HNO_3 – 0.002 M Hg^{2+}

The dissolution of non-irradiated and irradiated LEU silicide intermetallic compounds (U_3Si_2, U_3Si, and U_3SiAl) was carried out using mercury catalysed nitric acid in bench scale tests (Rodrigues & Gouge, 1983). The procedure consisted of the following steps: dissolution, clarification, and solvent extraction.

A boiling solution of 3 M HNO_3 - 0.002 M Hg^{2+} was used to completely dissolve both non-irradiated and irradiated fuel. The distributed silicide particles dissolved faster than the aluminium in the matrix and cladding.

The solution dissolved non-irradiated fuel faster than irradiated fuel. For example, the dissolution time for non-irradiated U_3Si was 5.9 h compared with 7.1 h for irradiated U_3Si.

Reducing the Hg^{2+} concentration from 0.002 to 0.0002 M increases the average dissolution time for the three non-irradiated fuels, but decreases the amount of mercury for waste storage. For example, the dissolution time for non-irradiated U_3Si_2 increases from 6.0 to 9.7 h. Increasing the nitric acid concentration to 8 M HNO_3 - 0.002 M Hg^{2+} did not significantly affect the overall dissolution time of the non-irradiated U_3SiAl fuel.

Analysis of the remaining solids by ICP-OES and neutron activation analysis revealed negligible amounts of uranium in the solids, but revealed a high level of silicon in the solid. The X-ray diffraction analysis showed no crystal structure. The remaining solid appears as fluffy, white amorphous silica.

More uranium was lost during dissolution of the non-irradiated fuel than for the irradiated fuel – 0.08 *versus* 0.01% respectively.

The clarification steps consisted of a reverse permanganate strike and a gelatine strike to reduce the levels of silicon so that the silicon does not interfere with the solvent extraction. Solvent extraction was successfully performed on both non-irradiated and irradiated fuel (Rodrigues & Gouge, 1983).

2.3.3 Dissolution of U_3Si_2 in hot nitric acid without a mercury catalyst

Touron and Cheroux (2001) studied the behaviour of silicon during the reprocessing of uranium silicide from fresh fuel using a nitric acid medium without a mercury catalyst, a technique that is compatible with the PUREX process. They found that uranium silicide powder, with or without

aluminium cladding, with a particle size of between 90 and 125 µm, was successfully dissolved at 100 °C in 3 to 6 N nitric acid.

In the process, two kinetic regimes were observed in samples containing an aluminium concentration of up to 1.3 M. The first corresponded to the initial attack on the edges of the fuel core and on the AG3NE cladding; the second, after elimination of the cladding, corresponded to the dissolution of the fuel. The cladding was totally eliminated after 3 h in nitric acid at 100 °C, and complete dissolution was obtained after 6 to 8 h at 100 ºC. The nitric acid consumption ranged from 3 to 4 moles per mole of dissolved aluminium. The U_3Si_2 powder without aluminium cladding was completely dissolved within one hour; it is assumed that this was due to the larger surface area of the powdered sample.

Using this method, silicon was found as hydrated silica at a concentration of 5 g/L. Uranium of less than 0.3% was found in the residues after separation, rinsing and drying. An X-ray diffraction spectrum revealed the appearance of the compound $U(Al, Si)_3$ and the formation of a silica gel layer. It is assumed that the appearance of this compound is due to the reaction of U_3Si_2 and the aluminium in the core, and that the appearance of the silica gel layer was due to oxidation and condensation of silicon at the interface of the U_3Si_2 particles and the solution. More than 97% of uranium was extracted during the first step.

2.3.4 Recovery of U_3Si_2 in an aqueous solution of NaOH-$NaNO_3$

A method for recovering non-irradiated LEU silicide fuel from scrap generated during the production process is reported in the literature. In it the claim is made that it is possible to lower the initial purchase of silicon by recovering an ingot of U_3Si_2 with small amounts of impurities (Gale et al., 2004).

In this case the fuel was made by arc melting uranium and silicon metals, crushing the silicide into powder, mixing with aluminium and then cladding with Al-6061. They dissolved the

aluminium in the cladding and matrix in an aqueous solution of NaOH and $NaNO_3$ at temperatures lower than 75 °C. To remove the impurities (Mg, Cu, and Fe), the remaining U_3Si_2 was repeatedly washed using proprietary techniques.

They claim that this technique is a straightforward process, both quick and cost-effective. Unfortunately, the article gives neither the details of the appropriate washing techniques required nor the concentration of solution required to achieve the targeted impurity levels.

Their analysis showed approximately 100% recovery of uranium and silicon, 91.56 wt% U and 7.64 wt% Si (recovered) versus 92.05 wt% U and 7.6 wt% Si (manufactured). The recovered fuel was mixed with new fuel in proportions of up to 50%.

One of the problems they encountered was an increased level of oxygen in the recovered fuel. They assumed that some of this oxygen was the result of oxidation during manufacturing and some is the result of the recovery process itself. They claimed that they managed to reduce the oxygen level, but did not describe the technique involved (Gale et al., 2004).

2.3.5 Dissolution of aluminium cladding and U_3Si_2 targets

The replacement of HEU with LEU requires the development of a more aggressive process to recover fission products such as ^{99}Mo under the same irradiation conditions. Historically, recovery of the fission products in HEU was done by dissolving the irradiated target in acidic or basic solutions, a process that is not possible with LEU. U_3Si_2 does not dissolve in basic and in acidic solutions; silica precipitates, and thus makes it difficult to recover ^{99}Mo.

Buchholz and Vandergrift (1995) developed a processing method based on work done previously by Vandergrift and his co-workers, where they dissolved 0.3 g of U_3Si_2 in 100 mL of liquid (3 M NaOH plus 30 wt% H_2O_2) at 70 °C after the cladding was removed in 3 M NaOH.

Buchholz and Vandergrift's procedure involved dissolving the non-irradiated silicide targets in two separate stages (because they were unable to dissolve the cladding and U_3Si_2 target in one step). Firstly, they dissolved the aluminium cladding and aluminium in the fuel matrix in a 3 M NaOH - 3 M $NaNO_3$ solution. The uranium silicide left after removing the solution containing the cladding was dissolved in a solution of 9.56 M H_2O_2 and 10 M NaOH at a temperature of 90 to 95 °C. The solution foamed vigorously, the foam then subsided and a dark red uranium solution was produced. The solution was removed and the undissolved U_3Si_2 was treated with a fresh solution of 30 wt% H_2O_2 (9.56 M) and 10 M NaOH. The process was repeated until all the uranium silicide had dissolved.

The procedure works extremely well for removing the aluminium cladding from non-irradiated, un-annealed, thermally annealed, and irradiated targets. The annealed samples took double the time of (cold) un-annealed samples to dissolve the aluminium matrix. The procedure is also very effective for dissolving non-irradiated U_3Si_2, although it failed to dissolve a nine year old irradiated LEU silicide target.

Buchholz and Vandergrift optimised the procedure given above to treat irradiated and thermally annealed samples. They treated samples thermally annealed at different times and temperatures. They dissolved the cladding using 20 ml of 3 M NaOH - 3 M $NaNO_3$ per gram of aluminium. The aluminium content was between 0.41 to 0.48 g and 10 mL of solution was used in each case. The mixture was continuously agitated at 88 °C and the cladding dissolved within 10 to 12 min, leaving the meat as a wafer containing U_3Si_2 particles and pure aluminium powder. The solution forms a hydroxide flocculent from the Al-6061 cladding, which catalyses the auto-destruction of H_2O_2.

The remaining aluminium powder in the matrix was dissolved by replacing the old solution with a fresh solution of the same volume (10 mL of 3 M NaOH - 3 M $NaNO_3$). The un-annealed samples dispersed into powder within 25 to 30 min, while the annealed samples required a displacement of the solution after 40 to 45 min and dispersed into particles after 60 to 70 min. Buchholz and Vandergrift claimed that the annealing did not influence the dissolution time, although the time needed to disperse the sample into powder differed significantly.

The problem encountered during the silicide dissolution was the auto-destruction of H_2O_2. The U_3Si_2 dissolution and H_2O_2 destruction was controlled by adjusting the base concentration. A high base concentration increases the U_3Si_2 dissolution and results in much greater H_2O_2 destruction.

Although they did not optimise conditions for irradiated silicide targets, Buchholz and Vandergrift's initial results showed that the ideal may be NaOH concentrations of 0.2 to 0.5 M and H_2O_2 concentrations of 5 M at temperatures between 80 and 90 °C.

2.3.6 Dissolution of LEU silicide targets with alkaline hydrogen peroxide

LEU metal and U_3Si_2 targets can also be dissolved using an alkaline peroxide solution for the recovery of the fission product ^{99}Mo (Chen et al., 1996). Comminuted and atomised particles with the same mass were treated. The comminuted particles dissolved faster, undoubtedly due to the larger surface area.

The U_3Si_2 target dissolves in two stages. Firstly, the aluminium cladding and matrix are easily dissolved with 3 M NaOH - 3 M $NaNO_3$ at 75 °C and the remaining fuel meat wafer is continuously treated with 3 M NaOH - 3 M $NaNO_3$ for 30 min until it breaks apart. The last stage involves dissolving the U_3Si_2 with 1.5 M NaOH - 5 M H_2O_2 solutions.

Analytical results using a high-purity germanium detector showed that approximately 26% ^{99}Mo was lost in the aluminium cladding dissolution, and approximately 9% of the ^{99}Mo was dissolved during the fuel treatment. The U_3Si_2 particles contained the balance (~65%) of ^{99}Mo.

Hutter et al. (1994) also developed a method for recovering ^{99}Mo from LEU silicide using an alkaline hydrogen peroxide solution. This method is similar to the one developed by both Chen

et al. (1996) and Buchholz and Vandergrift (1995). The solution of 3 M NaOH - 3 M $NaNO_3$ was used in all instances to dissolve the aluminium cladding and matrix at temperatures ranging from 70 to 90 °C.

Hutter et al. (1994) dissolved the aluminium cladding (Al-5052 and Al-6061) and U_3Si_2 in NaOH-$NaNO_3$ and hydrogen peroxide respectively. Typically, 3.77 g of Al-6061 was dissolved in 3 M NaOH - 3 M $NaNO_3$ (77.3 mL) at 70 °C and, within 5 min, with no un-dissolved cladding visible.

Silicide targets particles (3 g) were dissolved in a jacketed flask heated to 90 to 95 ºC with 5 mL of 30 wt% hydrogen peroxide (9.56 M) and 5 mL of 10 M NaOH. The solution was continuously renewed with 10 mL of 30 wt% H_2O_2 (9.56 M) and 10 mL of NaOH until the entire target was dissolved.

The researchers also studied the dissolution of irradiated U_3Si_2 targets in a hydrogen peroxide solution. The decladding procedure of 3 M NaOH - 3 M $NaNO_3$ worked successfully, but the silicide did not dissolve after 800 mL of 5 M NaOH - 5 M H_2O_2 had been used over a period of 10 h. It was assumed that the miniplate did not dissolve owing to the formation of a surface layer of $U(AlSi)_3$.

Eventually, they found the optimum conditions for dissolving non-irradiated U_3Si_2 to be 5 M NaOH - 5 M H_2O_2 at boiling temperature, but this procedure did not work for irradiated silicide targets.

2.4 Dry processing techniques

2.4.1 Fluoride volatility technique

Gabriac et al. (1995) claimed to have discovered a process for treating uranium alloys using dry gaseous fluorination. The process consists of three unit processes, specifically: the dry fluorination of the solid or finely divided alloy; distillation for the purification of the UF_6 product; and mixing the obtained UF_6 with depleted UF_6 to obtain the desired isotopic ratio.

For highly enriched material, the first unit process uses fluorine as treatment gas in a one-step process. Alternatively, a two-step method is followed, first using either hydrogen fluoride or UF_6 to obtain partial fluorination of the material, giving a lower oxidation-state solid compound (e.g. UF_4), followed by treatment with fluorine to obtain volatile metal fluorides.

For the two-step fluorination process a counter-current reaction is proposed, where the solid is fed into one end, the HF/UF_6 enters at an intermediate entry point, and the fluorine enters at the opposite end of the solid-feeding. This appears to be an elegant way of achieving a two-step fluorination technique in a single, continuous unit process.

They described three test cases. In the first case, a crushed U-Nb-Mo-Ti-Fe-Ni alloy was fluorinated in a Monel reactor using an F_2/N_2 mixture, the N_2 being used to control the temperature at $320 \pm 30\ ^{\circ}C$. The volatile fluorides, UF_6, MoF_6, NbF_5, and TiF_4, were collected and distilled. The final product is claimed to be pure UF_6, but the purity level was not quantified.

In the second test case, aluminium-encased U_3Si_2 (92 wt% U and 7.3 wt% Si) was treated. The aluminium cover was removed by a dissolution method. No details of this removal process were provided. The silicide was then crushed to a grain size less than 150 µm. The alloy particles were treated in a counter-current reactor, with depleted UF_6 used as the partially fluorinating gas. The UF_6 product was collected from the exit stream by condensation at -25 ºC. F_2 and SiF_4 do not

condense at this temperature and were successfully vented. The U_3Si_2 was not pre-irradiated and thus did not contain any fission products.

The third and final test case describes irradiated U_3Si_2 enriched with 20% ^{235}U, first treated with hydrogen fluoride and, finally, with fluorine. The U_3Si_2 contained 7% fission products, 10% aluminium, 3% silicon and 80% uranium. The cladding was evidently removed by alkaline dissolution. After hydrogen fluoride treatment, volatile fluorides (presumably SiF_4) were vented off, and the remaining solid fluorides (including UF_4) were then exposed to F_2 gas, again diluted with nitrogen. The volatiles thus obtained were passed through a metal-packed column and the UF_6 was separated from the product stream by distillation. This enriched UF_6 product was finally diluted with natural UF_6 to obtain an enrichment of 3.5%.

2.4.2 Fluoride volatility process using fractional distillation

Ippei and Koji (2008) described a similar fluorination process (i.e. as above) for treating spent oxide fuel containing UO_2 and PuO_2. The process consists of treating the oxide with HF as a partial fluorinating gas, treating the obtained products with fluorine to complete the fluorination, followed by distillation, a process that exploits the difference in volatility between uranium and plutonium hexafluoride.

The spent fuel oxide is first treated with HF to produce $UF_4(s)$ and $PuF_3(s)$. The HF contained 10 to 30 volume % of hydrogen in a fluidised bed furnace operated in a temperature range of 350 to 430 ºC.

Secondly, the obtained products (UF_4 and PuF_3) are treated with fluorine to produce UF_6 and PuF_6. The fluorine is diluted to 20 to 40 volume % with nitrogen and operated at a temperature of 500 to 750 °C.

The two-step fluorination process, starting with hydrogen fluoride, has the advantage of producing PuF_3 which is easily converted to PuF_6 (compared with PuF_4 produced in a single step using fluorine). The use of hydrogen fluoride reduces the amount of expensive fluorine gas used in a single step and avoids the formation of an intermediate PuF_4, which is difficult to convert to PuF_6.

Separation of UF_6 and PuF_6 is done by fractional distillation, recovering part of the UF_6 as a gas and volatilising the remaining UF_6 and PuF_6 at the same time. Distillation is done using cold traps and controlling the pressure so that UF_6 is in the gas phase and PuF_6 in the liquid phase, making it possible to separate the UF_6 and PuF_6.

One example was provided to confirm the partial fluorination which results in the formation of UF_4 and PuF_3: an oxide fuel made up of U, Pu, O, Zr, Nb, Mo, Tc, Ru, Sb, Te, Ce, Np, Am, and Cm. The oxide was treated with a mixture of HF/H_2 containing 70 volume % HF at an operating temperature of 400 ºC. Partially fluorinated UF_4 and PuF_3 were obtained with oxide, fluoride or oxy-fluoride impurities.

2.4.3 Fluorex processing technique

A technique known as the Fluorex process, which is similar to the one claimed by Ippei and Koji (2008) above, is described by Kani et al. (2009). The Fluorex process consists of several steps, including: fluorination of the spent fuel to remove most of the uranium as UF_6; purification of UF_6 from the fission product, plutonium and residual uranium; pyrohydrolysis of the fluorination residue to form oxides; and, finally, the dissolution of the unconverted residues.

The Fluorex method is considered suitable for spent nuclear fuel (SNF) from light water reactors (LWR). An SNF consisting of 93% U, 1% Pu and 6% fission products was treated. Firstly, the cladding was removed using a dry oxidation/reduction method. Then the SNF was treated with fluorine to obtain UF_6. Plutonium fluorides and volatile fission products were also found as

impurities in the gas stream. The UF_6 was purified by rectification and/or passing through adsorbents (e.g. NaF). The remaining residues, including non-volatile fluorides of plutonium, uranium, and fission products were converted to oxides by pyrohydrolysis, and then dissolved in nitric acid so that they could be treated by the PUREX method.

Kani et al. (2009) claim that 94 to 98% of the supplied uranium was volatilised as UF_6 and about 90% of the plutonium was volatilised to PuF_6. It was expected that the amount of uranium volatilised would depend on fluorine stoichiometry, fluorine concentration, feed rate and grain size. Decreasing the fluorine stoichiometric ratio decreases the amount of uranium volatilised, but decreasing the fluorine concentration has no significant changes on the amount of uranium volatilised.

2.4.4 Reprocessing methods using SF_6

A method for recovering uranium as UF_6 from irradiated uranium-containing nuclear fuels (e.g. UO_2, U_3O_8, and UC_2) was reported (Knacke et al. 1967). The irradiated fuel can be treated in a single step or two steps, depending on the desired purity of UF_6. A two-step process is used for obtaining high purity UF_6, whereby the fuel is first transformed into lower fluorides at 700 to 800 °C. Secondly, both the lower fluorides and the unconverted uranium is treated at high temperatures of 850 to 900 °C and converted to UF_6. During this two-step process, the fission products are driven off as fluorides.

A gaseous mixture of sulphur hexafluoride in the presence of an oxidizing medium (e.g. O_2, N_2, Ar, or air) is used. They found that the reaction is efficient at temperatures above 800 ºC, and that UF_6 can be produced in a single step. The single step is used when it is not important to obtain high purity UF_6. Fuel encapsulated in carbon or carbon-containing coatings is subjected to mechanical comminution and/or treatment at a temperature of 900 to 1100 ºC, with oxygen or argon containing gas alone or in admixture with SF_6. This reaction strips the carbonaceous compound encapsulating the fuel and carries it away as a gas.

Three test cases were described using this technique. In the first case, 10 g of U_3O_8 in a laminar-vortex furnace was treated with SF_6 and O_2 at 900 °C. The UF_6 was recovered by condensation at a temperature of -40 °C.

In the second case, 40 g of UO_2 was treated in a rotary-tube furnace with SF_6 and O_2 at 850 °C. Knacke et al. (1967) claim that after 40 minutes there was no UO_2 visible, only UF_6 and SO_2, which was in accordance with the anticipated reaction ($UO_2 + SF_6 \rightarrow UF_6 + SO_2$). The UF_6 was collected by condensation at a temperature of -30 °C.

In the last case, UC_2 fuel cladded with a pyrolytically precipitated carbon was pre-treated with pure O_2 at 900 °C for about 40 minutes. The products were then treated with SF_6 and O_2 to form UF_6, which could be recovered by condensation.

Using SF_6 has the following advantages: SF_6 is non-poisonous and non-corrosive at temperatures below about 500 ºC and the excess fluorine can be reconverted to SF_6 by reacting with sulphur. SF_6 was preferred, rather than HF and halogen fluorides, because HF and halogen fluorides are highly corrosive, while bromine fluorides and chlorine fluorides can form explosive mixtures in the presence of moisture.

Knacke et al. (1967) claim that this technique is suitable for coated fuel elements consisting of carbides, nitrides, and oxides of uranium covered in carbon, silicon carbides or other carbon-containing coatings.

2.5 Chemistry of uranium metal with HF and F_2

2.5.1 Properties of uranium metal

Uranium is a high density, hard, silver-white, radioactive metal. The metal is pyrophoric when finely divided and forms a protective oxide layer when exposed to air. The metal is very reactive,

is attacked by acids, but not by alkalis. Uranium is a very important metal in the nuclear industry since it is used as fission material.

The known metal fluorides of uranium are UF_3, UF_4, and UF_6, although UF_5, U_2F_9 and U_4F_{14} have been identified as intermediate fluorides (Cotton & Wilkinson, 1962).

2.5.2 Formation of uranium metal fluorides

Almost all the uranium metal fluorides can be synthesized by more than one method. In many cases, the low metal fluorides are produced by the reduction of the high oxidation state metal fluorides. Some methods of synthesizing the metal fluorides are given below, starting with the UF_3 to UF_6. The common method of synthesizing the trifluoride, UF_3, is by the reduction of UF_4 with aluminium as follows:

$$3UF_4 + Al \xrightarrow{900\,^{\circ}C} 3UF_3 + AlF_3 \qquad (2.1)$$

Another method is to react uranium tetrafluoride with uranium mononitride (UN) or uranium sesquinitride (U_2N_3) at temperatures between 900 and 950 °C. This reaction can be done in an inert atmosphere or in a vacuum. Both yield the same results.

The tetrafluoride UF_4 forms when UF_6 reacts with hydrogen gas in a vertical tube-type reactor. Alternatively, UF_4 can be prepared by reacting hydrogen fluoride (HF) with uranium dioxide (Cotton and Wilkinson, 1962: 944-962).

Uranium pentafluoride, UF_5, is prepared by the reduction of UF_6 with reducing agents such as HCl, SO_2 and CO in liquid HF (Adelhem et al., 1980). Another method is the reaction of UF_4 with fluorine at 240 °C or the reaction of UF_6 with hydrogen bromide (HBr) at about 65 °C (Tagawa and Japan, 1976).

The hexafluoride is obtained from the oxidation, or direct fluorination of the lower fluorides with fluorine at about 400 °C (Cotton & Wilkinson, 1962: 944 - 962).

2.5.3 Properties of uranium silicide (U_3Si_2)

The phase diagram (Fig. 2.1) shows the composition percentage of stable silicides. Five intermetallic compounds are found in the U-Si phase diagram, namely, USi, USi_2, USi_3, U_3Si_2 and U_3Si_5. Uranium disilicide is formed by arc melting uranium with 7.5 wt% Si (Okamoto, 1990).

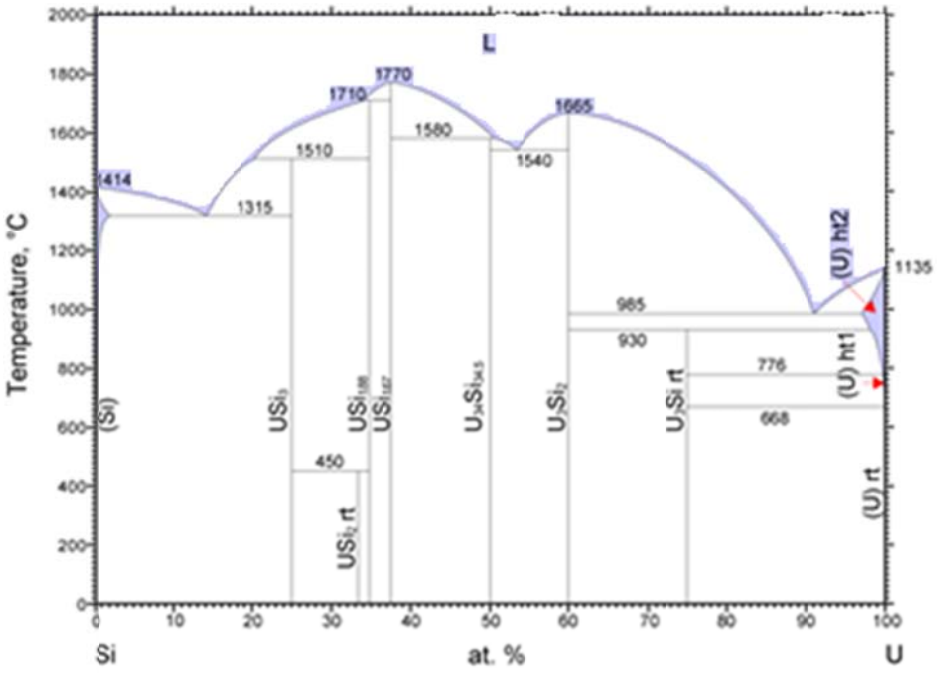

Figure 2.1: Phase diagram of the U-Si system (Okamoto, 1990)

Almost all the silicides have high melting points. The U_3Si_2 alloy is used in the nuclear industry as a replacement fuel for HEU fuel. As stated at the beginning of this document, this alloy was chosen because of its special properties: high uranium loading, high density, and brittleness. It also yields more or less the same amount of ^{99}Mo as obtained with HEU.

2.6 The relevant chemistry of molybdenum and tungsten disilicides

2.6.1 Properties of the pure metals (molybdenum and tungsten)

Molybdenum and tungsten are lustrous, silvery and fairly soft metals belonging to group six. Both metals have high melting points; 2620 °C for molybdenum and 3370 °C for tungsten. Tungsten has the highest melting point of all the non-alloyed metals and the second highest of all the elements after carbon (Greenwood & Earnshaw, 1984: 1167 – 1190).

Molybdenum has a d^5s^1 electron configuration, while tungsten has a d^4s^2 electron configuration. Despite the difference in their electron configurations, both metals have similar physical and chemical properties. For example, both react with halogens such as fluorine to form volatile hexafluorides, and both metals resist oxygen attack at ambient temperatures. However, molybdenum dissolves in hot concentrated sulphuric acid (H_2SO_4) and aqua regia, but not in hydrofluoric acid (HF) or alkali solutions, while tungsten resists attack by both acids and alkalis.

The oxidation state of the metals ranges from +1 to +6, with the highest oxidation states being formed using strong oxidizing agents. Compounds in the +6 state are stable against reduction.

The known metal fluorides for molybdenum are MoF_3, MoF_4, MoF_5 and MoF_6, and the metal fluorides for tungsten are WF_4, WF_5, WF_6, W_2F_{10}, W_3F_{15} and W_4F_{20} are known. The MoF_6 and WF_6 compounds are obtained by direct fluorination of the metals (Heslop & Robinson, 1967: 1167 - 1190). Gusarov et al., reported the presence of WF_5, W_2F_{10}, W_3F_{15} and W_4F_{20} through the reduction of WF_6 on a tungsten wire in vacuo at about 600 °C, and the compounds where detected by mass spectroscopy.

2.6.2 Properties and formation of the fluorides

2.6.2.1 The hexafluorides (MoF_6 and WF_6)

The hexafluorides, WF_6 and MoF_6, are volatile, corrosive and colourless compounds. They are formed using strong fluorinating agents such as F_2, BrF_3, and SF_6. Only molybdenum hexafluoride is hygroscopic. Tungsten hexafluoride is known as the densest gas at room temperature and a pressure of 1 atm, and has the same octahedral structure as MoF_6. Tungsten hexafluoride gas is mainly used in the production of semiconductor circuits and circuit boards (Glemser, 1986).

The direct exothermic fluorination of the metals with fluorine is the predominant method for synthesizing the hexafluorides. Jourdan and Morel (2001) and Settle et al. (1961) reported the formation of $WF_6(g)$ and $MoF_6(g)$ by the following reactions:

$$W + 3F_2 \rightarrow WF_6 \qquad \Delta H = -1721 \text{ kJ/mol at } 298 \text{ K} \tag{2.2}$$

$$Mo + 3F_2 \rightarrow MoF_6 \qquad \Delta H = -1559 \text{ kJ/mol at } 298 \text{ K} \tag{2.3}$$

According to the thermodynamic calculations, the reactions of the pure metals (tungsten and molybdenum) with fluorine in a ratio of 1:3 should form the hexafluorides at temperatures ranging from 25 to 1000 °C (Figs. 2.2 and 2.3). The calculations were done at standard atmospheric pressure (HSC software 6.1 package).

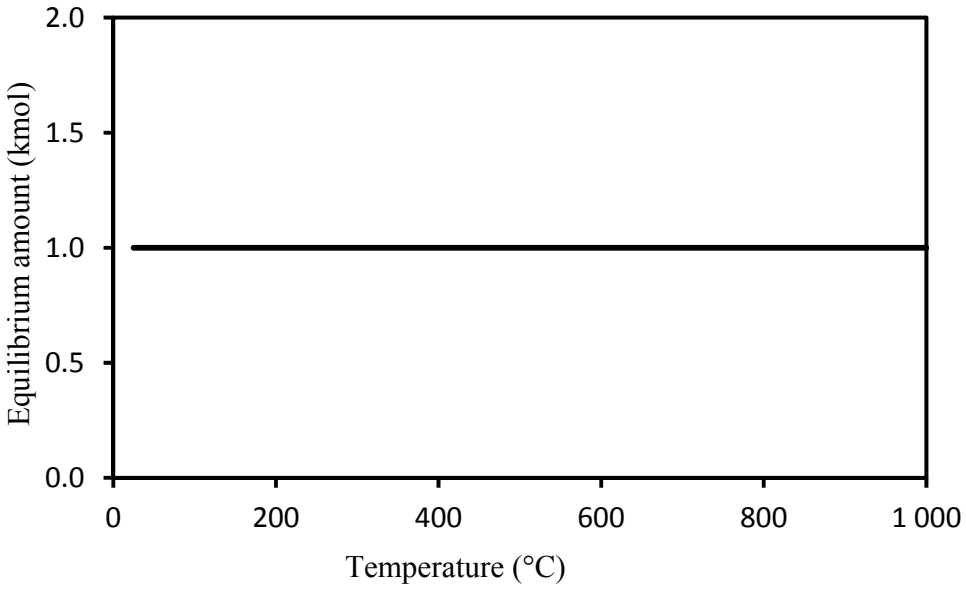

Figure 2.2: Equilibrium composition of the reaction between 1 kmol W and 3 kmol F_2

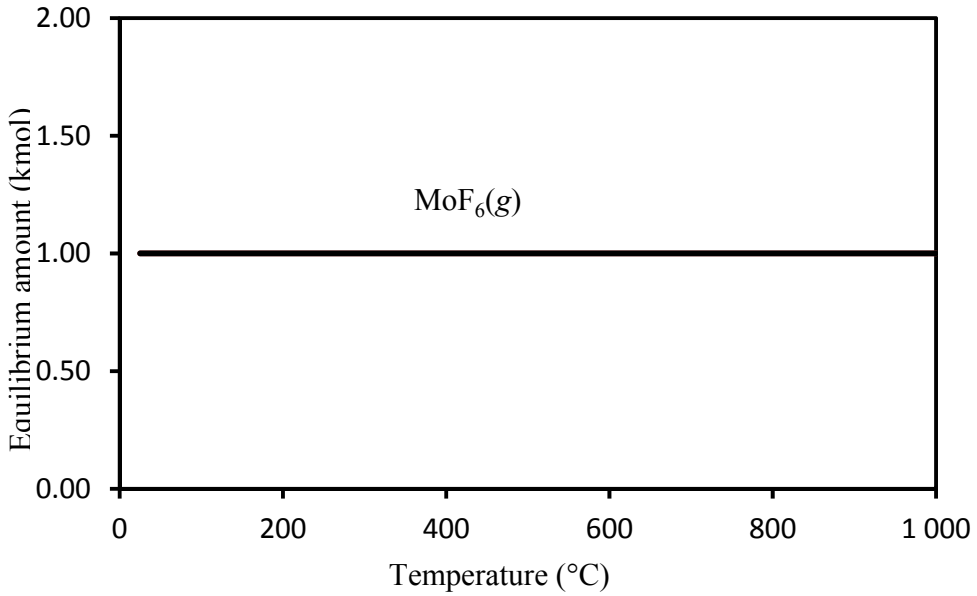

Figure 2.3: Equilibrium composition of the reaction between 1 kmol Mo and 3 kmol F_2

Johnson and Siegel (1996) used CF_4 and SF_6 as fluorine containing agents to produce the hexafluorides, WF_6 and MoF_6. The reaction between tungsten and SF_6 gave a yield of 80 to 90% WF_6 with either SF_4 or S(*s*) forming, depending on the molar ratio of SF_6/W.

$$W + 3SF_6(g) \rightarrow WF_6(g) + 3SF_4(g) \quad (2.4)$$

$$W + SF_6(g) \rightarrow WF_6(g) + S(s) \quad (2.5)$$

Molar ratios of SF_6/W exceeding three favoured the formation of SF_4, while a ratio less than two favoured the formation of S(*s*), but this does not affect the yield of WF_6.

In the case of molybdenum, varying the molar ratio also changes the product stoichiometry, but does not affect the yield percentage of MoF_6 (which is similar to the tungsten reaction).

$$Mo + 3SF_6(g) \rightarrow MoF_6(g) + 3SF_4(g) \quad (2.6)$$

$$Mo + SF_6(g) \rightarrow MoF_6(g) + S(s) \quad (2.7)$$

For example, a ratio of 4:1 of SF_6:Mo yielded 79 to 84% of MoF_6 and formed $SF_4(g)$. A ratio of less than 4 gave roughly the same yield, but formed solid sulphur.

In all the reactions of molybdenum with SF_6, a minor, thin, coloured film was observed, which was suspected to be a lower non-volatile molybdenum fluoride product, possibly MoF_5.

Overall, good yields of the hexafluoride were achieved for both tungsten (80 - 90%) and molybdenum (79 - 84%).

Only tungsten was treated with CF_4. Nothing was reported for molybdenum metal (presumably because of the low yield). The yield of WF_6 and the end stoichiometric product depends on the input energy and initial pressure of the fluorinating gas.

$$W + 1.5CF_4(g) \rightarrow WF_6(g) + 1.5C(s) \quad (2.8)$$

$$W + 3CF_4(g) \rightarrow WF_6(g) + 1.5C_2F_4(g) \quad (2.9)$$

The CF_4 produced a lower yield of WF_6 compared with SF_6. The highest yield obtained was 31%. Figure 2.4 shows the thermodynamically predicted products for the reaction of W (1 kmol) with CF_4 (1.5 kmol). Though the calculation was done at different conditions, such as the pressure, similar results were predicted, where both products would form at any temperature from 0 to 1000 °C.

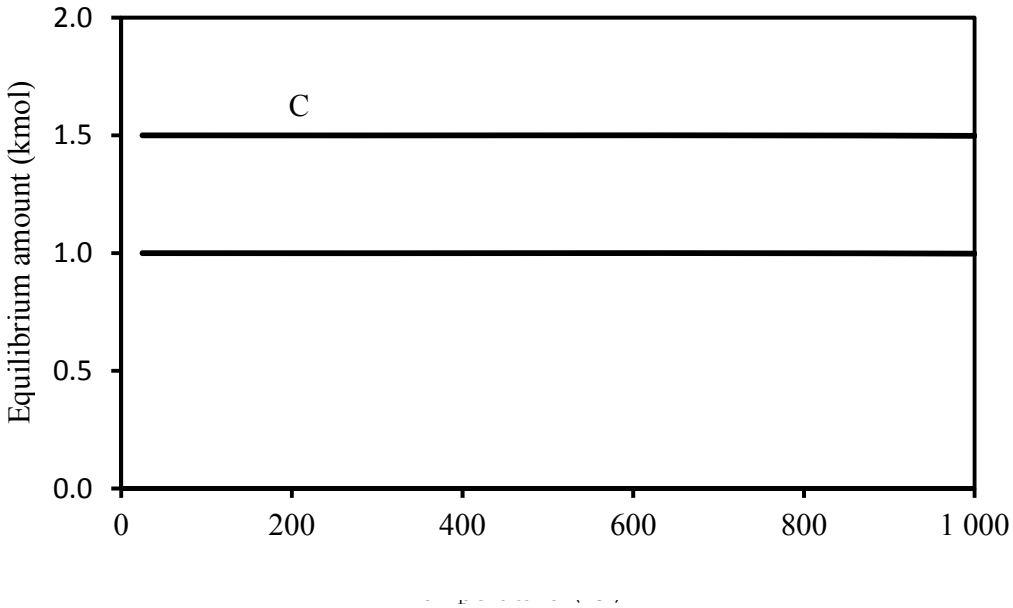

Figure 2.4: Equilibrium composition of the reaction between 1 kmol W and 1.5 kmol CF_4

Figure 2.5 shows the predicted products of the reaction between W and CF_4 at a higher molar ratio (1:3). In this case similar products forms at all temperature from 0 to 1000 °C with an excess amount of $CF_4(g)$. This simulation result does not correspond to the results of Johnson and Siegel. Since in their case they obtained WF_6 and $C_2F_4(g)$.

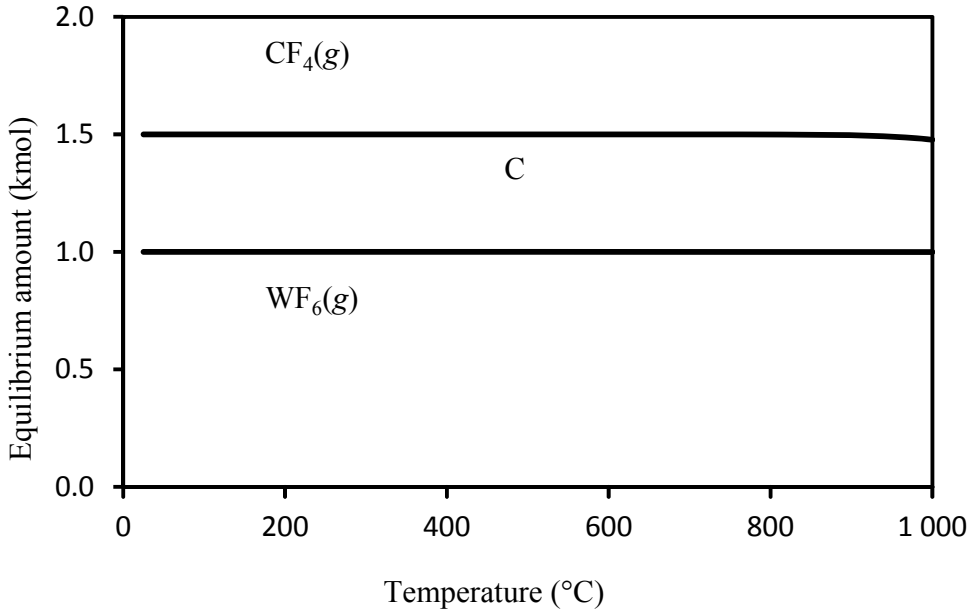

Figure 2.5: Equilibrium composition of the reaction between 1 kmol W and 3 kmol CF_4

Sulphur hexafluoride has a number of advantages as a reagent over carbon tetrafluoride and fluorine gas, since it has ideal handling properties, it is an inert fluorinating agent, and it gives a high yield of metal hexafluorides.

2.6.2.2 Molybdenum pentafluoride

Yellow, volatile, solid, molybdenum pentafluoride (MoF_5), is obtained by reducing the hexafluoride with the metal. Falconer et al. (1973) used a hot filament reduction cell and hot tungsten wire or molybdenum wire to obtain molybdenum pentafluoride. The hot filament reduction cell was immersed in a coolant bath for the duration of the reaction. The yield depended on the temperature of the coolant bath using either of the wires. A good yield was obtained with both wires at -40 to -50 °C after four hours, compared with a poor yield at -60 °C after seven hours.

Larson (1970) used phosphorus trifluoride, PF_3, $Mo(CO)_6$, or molybdenum powder to reduce MoF_6 to MoF_5. The phosphorus trifluoride has the advantage that the volatile by-products and excess PF_3 can easily be removed.

In their research, Cotton and Wilkinson (1962) referred to the formation of molybdenum pentafluoride by the direct fluorination of the metal with diluted fluorine at 400 °C. Unfortunately, no further experimental detail was given.

2.6.2.3 The tetrafluorides (MoF_4 and WF_4)

Tungsten tetrafluoride is only prepared by reducing the high oxidation state metal fluorides, while molybdenum tetrafluoride is prepared by reduction and disproportionation methods.

Priest and Schumb (1948) prepared tungsten tetrafluoride by reducing WF_6 with benzene in a nickel reactor at 110 °C. The reaction was very slow, since they obtained the products over a period of three to nine days.

Just over twenty years later, Larson (1970) formed the non-volatile pale green solid molybdenum tetrafluoride, MoF_4, by reacting $Mo(CO)_6$ with fluorine gas. Molybdenum pentafluoride was a byproduct, which was vacuum-distilled to leave solid molybdenum tetrafluoride. Molybdenum tetrafluoride was also prepared by the disproportionation of MoF_5 above 150 °C to MoF_4 and MoF_6.

2.6.2.4 Molybdenum trifluoride

Molybdenum trifluoride, MoF_3, is described as a brown solid with a rhombohedral crystal structure. It forms through the reduction of a higher oxidation state halide with the metal. LaValle et al. (1960) reduced molybdenum pentafluoride with molybdenum metal to obtain

molybdenum trifluoride. The reaction was carried out in an inert atmosphere to avoid the formation of molybdenum oxy-fluorides. Molybdenum trifluoride is stable up to 500 °C, but it disproportionates at 600 °C into molybdenum metal and higher oxidation state volatile fluorides.

2.6.3 Properties and reactions of molybdenum and tungsten disilicides

2.6.3.1 Properties of molybdenum and tungsten disilicide

Three known molybdenum silicide compounds can be identified from the molybdenum-silicon phase diagram (Fig. 2.6), namely, $MoSi_2$, Mo_3Si, and Mo_5Si_3 (Gokhale, 1990).

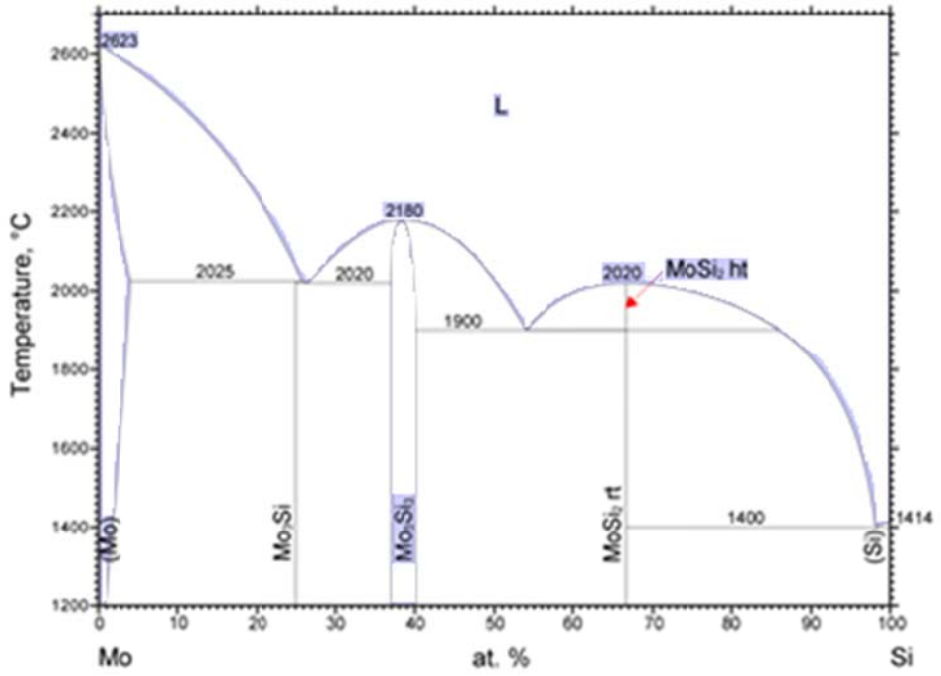

Figure 2.6: Mo-Si phase diagram

The molybdenum disilicide alloy is mainly used in high temperature applications because of its special physical properties, namely, a high melting point of 2030 °C, super high oxidation resistance, formation of a thin protective silica layer of SiO_2, and a high creep rate (Yao et al.

1999; Natesan and Deeve, 2000). The disadvantages of using this alloy at low temperatures include low fracture toughness, and pest oxidation in a temperature range of 400 to 600 °C through the formation of MoO_3 (Biamino et al., 2008).

Molybdenum silicide is not soluble in most inorganic acids including aqua regia, but is soluble in hydrofluoric and nitric acids.

There are two known tungsten silicide compounds as shown in the tungsten-silicon phase diagram (Fig. 2.7): namely, WSi_2 and W_5Si_3 (Nagender et al., 1990).

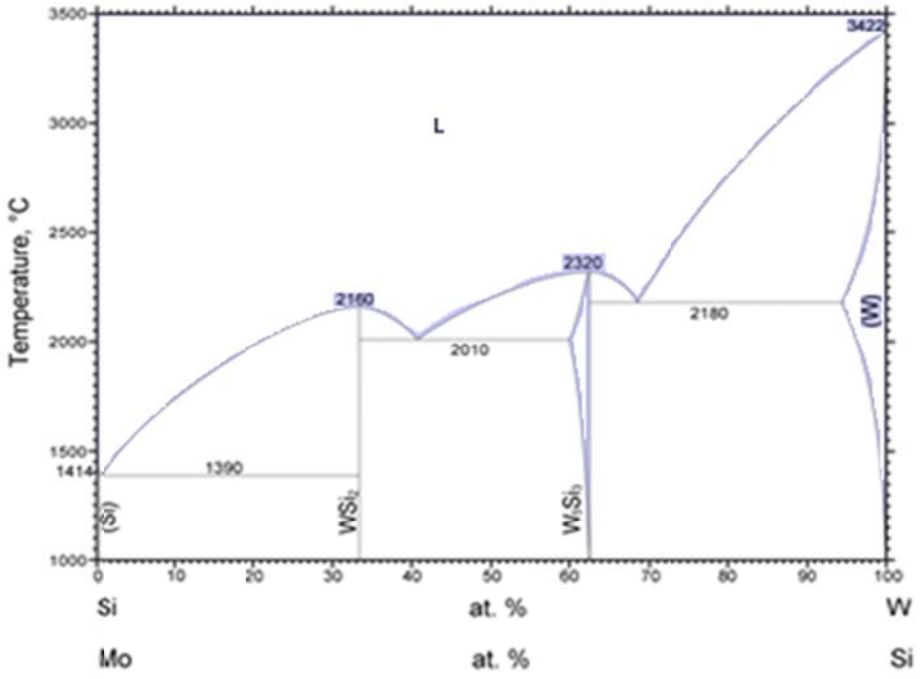

Figure 2.7: W-Si phase diagram

Tungsten disilicide is an electrically conductive ceramic material. It can react violently with substances such as strong acids, fluorine, oxidizers, and inter-halogens. It is used in microelectronics as a contact material, and is often used as a shunt over polysilicon lines to

increase their conductivity and increase signal speed. Tungsten disilicide is also used in micro electromechanical systems and as an oxidation-resistant coating.

2.6.3.2 Fluorination reactions of WSi_2 and $MoSi_2$ with F_2

Only two articles (O'Hare, 1992 and 1993) were found that discussed the fluorination of molybdenum or tungsten disilicide with fluorine. The purpose of O'Hare's study was to determine the standard molar enthalpy of formation using a fluorine combustion method. O'Hare treated WSi_2 with fluorine in the presence of tungsten (as an auxiliary substance) and sulphur (as a fuse) to achieve complete conversion. The reaction equation is as follows:

$$WSi_2 + 7F_2(g) \rightarrow WF_6(g) + 2SiF_4(g) \qquad (2.10)$$

Initial experiments without tungsten wire did not give complete conversion of the tungsten disilicide. In his later experiment, O'Hare (1993) used the same technique to fluorinate $MoSi_2$ to determine the standard molar enthalpy of WSi_2 formation. The fluorination was done in the presence of tungsten-metal foil as an auxiliary substance to achieve complete conversion of $MoSi_2$ to $MoF_6(g)$ and $SiF_4(g)$; again, sulphur was used as a fuse. The products were confirmed by FTIR spectroscopy.

$$MoSi_2 + 7F_2(g) \rightarrow MoF_6(g) + 2SiF_4(g) \qquad (2.11)$$

Thermodynamic calculations were performed to simulate the work done by O'Hare (O'Hare, 1992 and 1993), and a good correspondence was achieved (Figs 2.8 and 2.9). Both disilicides are predicted to be completely volatilised when exposed to fluorine. The volatile fluorides could form at any temperature form 0 to 1000 °C, according to the results in Figures 2.8 and 2.9 for the reaction between MSi_2 (1 kmol) and F_2 (7 kmol), where M = W or Mo.

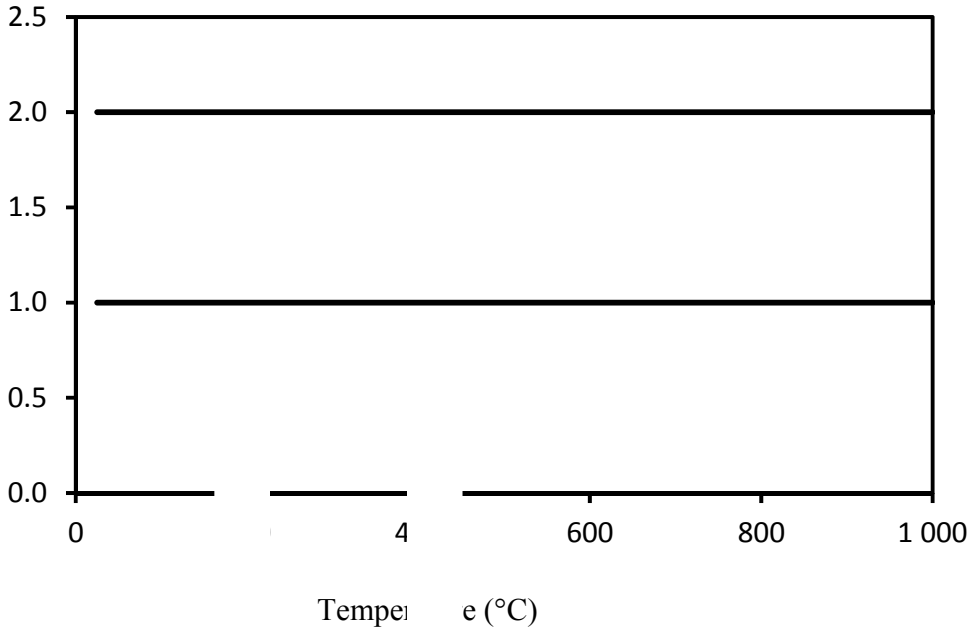

Figure 2.8: Equilibrium composition of the reaction between 1 kmol $MoSi_2$ and 7 kmol F_2

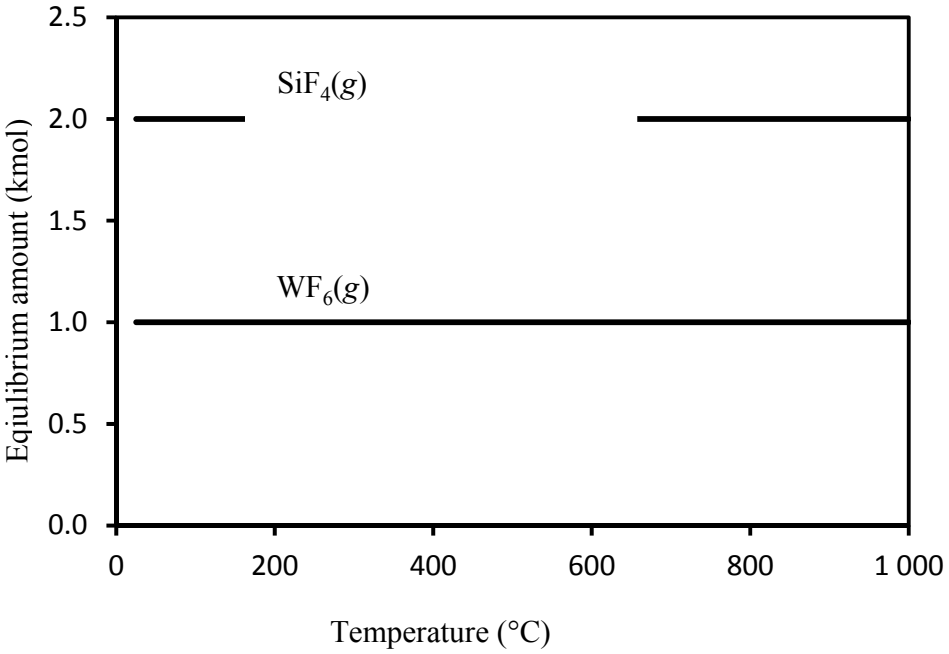

Figure 2.9: Equilibrium composition of the reaction between 1 kmol WSi_2 and 7 kmol F_2

2.7 Conclusion

In most of the wet processing methods, uranium silicide (U_3Si_2) fuel is dissolved in nitric acid with various concentrations at various temperatures. The cladding and U_3Si_2 matrix is dissolved simultaneously or in separate steps. The dissolution in nitric acid is successful in the case of both irradiated and non-irradiated silicide fuel.

The dry fluoride processing methods are successfully employed on UO_2 fuels to recover and separate uranium and plutonium. The method was applied successfully to U_3Si_2 fuel, in most instances without the aluminium cladding. The fluorination was carried out using fluorine only, or SF_6 only, or HF and UF_6, followed by fluorine treatment. The reprocessing technology based on the fluoride volatility method usually consists of (1) the removal of the cladding material, (2) the transformation of the fuel into powder, (3) fluorination of the powder fuel, and (4) purification of the products obtained.

Dry reprocessing methods seem very attractive at this stage and preferable to aqueous methods because it avoids the generation of high levels of liquid waste streams. In the case of irradiated fuel, it provides an easy way to recycle the fertile ^{235}U and unburned fissile transuranics.

In the literature very few reports of fluorination reactions of the tungsten and molybdenum disilicides were traced (O'Hare 1992 and 1993). Complete conversion of both disilicides was clearly obtained. Lower metal fluorides of both disilicides are not reported to be obtained through reaction with either HF or fluorine, but the lower fluorides of both the disilicides are reported to be achieved through the reduction of higher oxidation state fluorides.

3. THERMODYNAMIC EQUILIBRIUM CALCULATIONS

3.1 Introduction

This chapter discusses the thermodynamic equilibrium calculations of the reactions of WSi_2 and $MoSi_2$ with anhydrous hydrogen fluoride and fluorine. Anhydrous hydrogen fluoride was also used, in order to investigate the possibility of forming lower metal fluorides through the fluorination of the pure metals (tungsten and molybdenum) and to predicting the theoretical equilibrium composition for the reactions. Using these calculations, it is possible to predict the products formed for the reactions and provide guidelines for future experiments.

The calculations were done with the aid of two thermodynamic programs, namely, HSC Chemistry, version 6.1 (Outotec, 2007) and TERRA (Trusov, 2000). These programs calculate equilibrium compositions as a function of temperature, pressure and elemental composition. In this study the main calculation tool was the equilibrium module of the HSC Chemistry program. Since TERRA gave the same results, therefore is not reported. The results were cross-checked, and in general the two programmes predicted similar results.

The program, HSC Chemistry, has fourteen calculation options that utilize the same extensive thermo-chemical database, which contains enthalpy (*H*), entropy (*S*) and heat capacity (*Cp*) data for more than 20 000 chemical compounds. In the program HSC, the equilibrium composition is calculated based on the Gibbs free energy minimization method (Roine, 2006). By contrast the TERRA equilibrium composition calculations also are based on the principle of maximum entropy for isolated thermodynamic system (Mukashev et al., 2002) while it contains a data base similar to HSC Chemistry program.

3.2 Equilibrium composition calculations

The equilibrium composition calculations are based on the Gibbs free energy minimization method. The principle of minimum Gibbs free energy is essentially a restatement of the second law of thermodynamics. This law states that, for a closed system, with constant external parameters, the internal energy will decrease and approach a minimum value at equilibrium (Perry and Green, 1997; 4-5).

The Gibbs free energy is the maximum amount of non-expansion work that can be obtained in a closed system at constant temperature and pressure. When a system changes from a well-defined initial state to a well-defined final state, the change in Gibbs free energy (ΔG) equals the work done by the system on the surroundings, minus the work of the pressure forces during a reversible transformation of the system from the same initial state to the same final state.

The Gibbs free energy of a multi-component chemical system is equal to the sum of the Gibbs free energies of the individual components. To determine the equilibrium composition, it is therefore necessary to calculate the Gibbs free energies of all the components for all possible combinations of chemical elements in the system, and to minimise the total Gibbs free energy. The result will only be valid for a closed system (Lwin, 2000).

The equilibrium compositions calculations for all the reactions were done at standard atmospheric pressure and temperatures ranging from 0 to 1000 °C.

3.3 The reaction of WSi_2 and $MoSi_2$ with F_2

3.3.1 The WSi_2–F system

Fluorine is the strongest oxidizing agent of the elements of the periodic table; therefore no lower metal fluorides are expected to form. This was confirmed by the calculation which predicts the formation of the volatile fluorides WF_6 and SiF_4 between zero and 1000 °C (Fig. 3.1) when WSi_2 reacted with F_2 as shown in Equation 3.1:

$$WSi_2 + 7F_2(g) \rightarrow WF_6(g) + 2SiF_4(g) \quad (3.1)$$

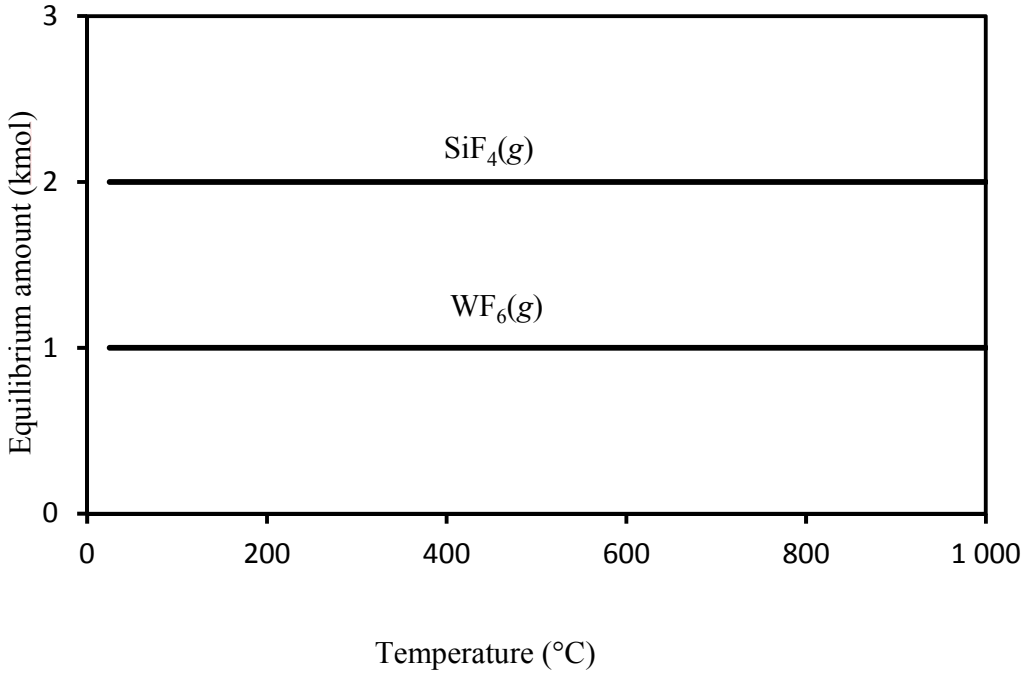

Figure 3.1: Equilibrium composition of the reaction between1 kmol WSi_2 and 7 kmol F_2

3.3.2 The Mo_2Si–F system

A similar calculation was done for the reaction between $MoSi_2$ (1 kmol) and F_2 (7 kmol) (Fig. 3.2). The disilicide of molybdenum behave similar to that of tungsten under a fluorine atmosphere. The volatile fluorides $MoF_6(g)$ and $SiF_4(g)$ are predicted to form at all temperatures from 0 to 1000 °C according to Equation 3.2.

$$MoSi_2 + 7F_2(g) \rightarrow MoF_6(g) + 2SiF_4(g) \quad (3.2)$$

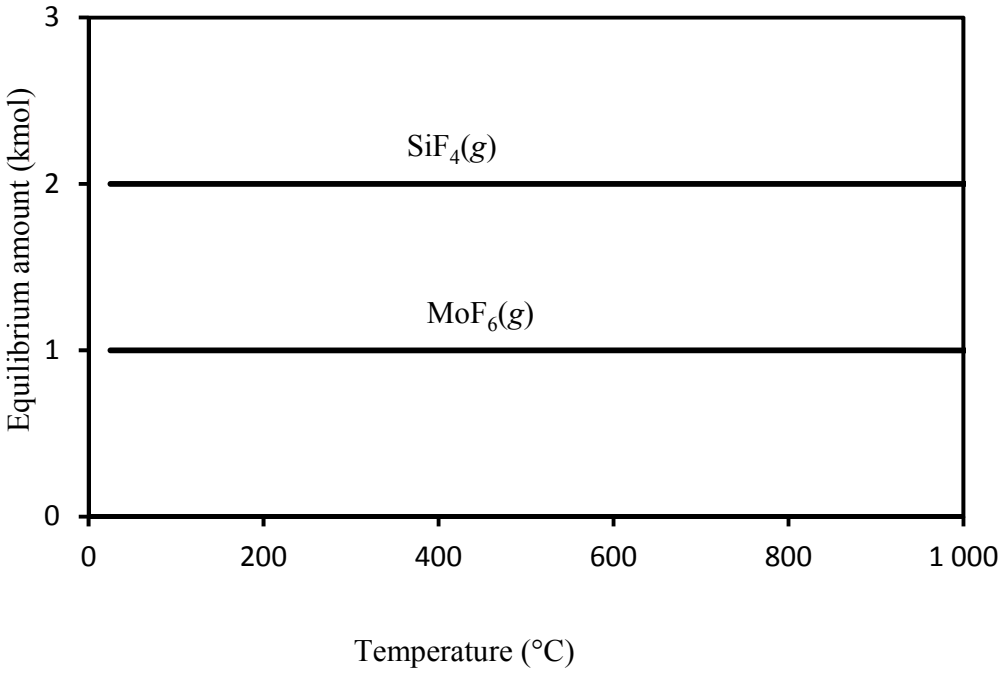

Figure 3.2: Equilibrium composition of the reaction between 1 kmol $MoSi_2$ and 7 kmol F_2

3.4 The reaction of WSi_2 and $MoSi_2$ with HF

3.4.1 The WSi_2–HF system

The calculation of WSi_2 with HF was done to investigate the possibility of forming lower metal fluorides. The predicted results of the reactions between WSi_2 (1 kmol) and HF (8 and 12 kmol, respectively) are shown in Figure 3.3 and 3.4.

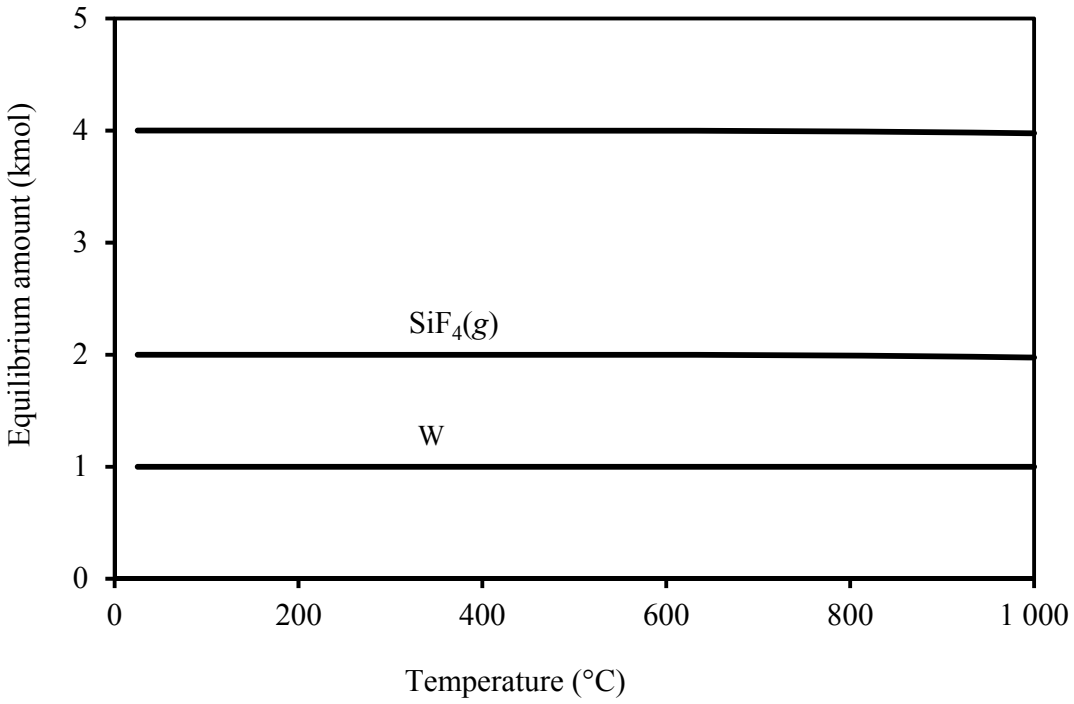

Figure 3.3: Equilibrium composition of the reaction between 1 koml WSi_2 and 8 kmol HF

For a WSi_2/HF ratio of 1:8, the products W, $SiF_4(g)$ and $H_2(g)$ should form at all temperatures from zero to 1000 °C (Fig 3.3), according to Equation 3.3.

$$WSi_2 + 8HF(g) \rightarrow W + 2SiF_4(g) + 4H_2(g) \quad (3.3)$$

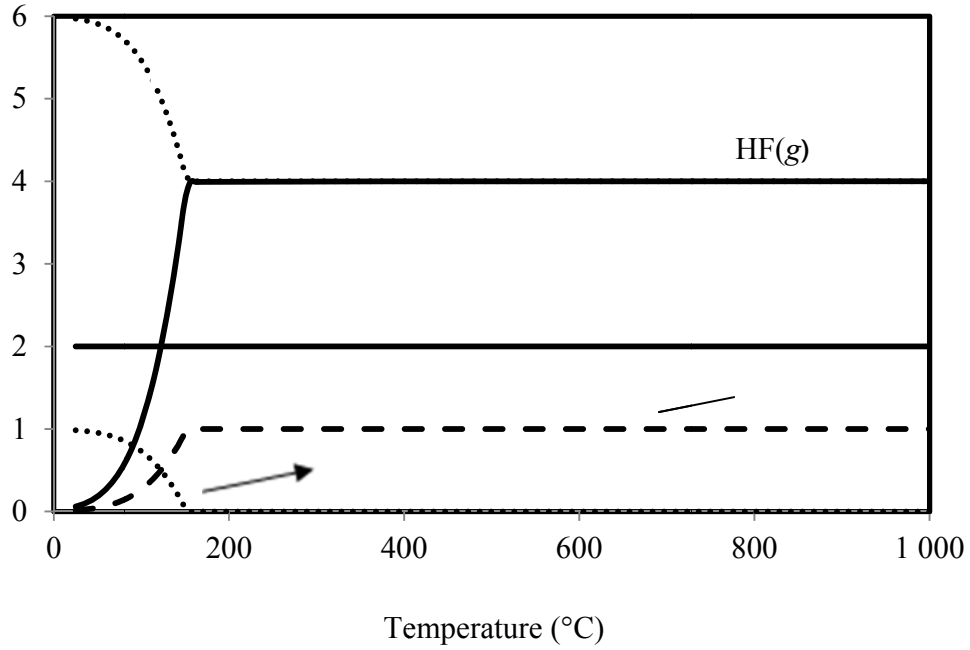

Figure 3.4: Equilibrium composition of the reaction between WSi_2 and HF (12 kmol)

With an excess amount of HF (12 kmol) WF_4 should form at low temperatures (ca. < 80 °C) according to Equation 3.4, but above about 150 °C only tungsten metal formed according to equation 3.3.

$$WSi_2 + 12HF(g) \rightarrow WF_4(s) + 2SiF_4(g) + 6H_2(g) \quad (3.4)$$

3.4.2 The $MoSi_2$-HF reaction

The predicted products of the reaction between $MoSi_2$ (1 kmol) and HF (8 kmol) are shown in Figure 3.5. The products Mo, $SiF_4(g)$ and $H_2(g)$ are predicted to form in the temperature range of 0 to 1000 °C. Similar to tungsten, no lower molybdenum fluoride compounds are predicted to form.

$$MoSi_2 + 8HF(g) \rightarrow Mo + 2SiF_4(g) + 4H_2(g) \quad (3.5)$$

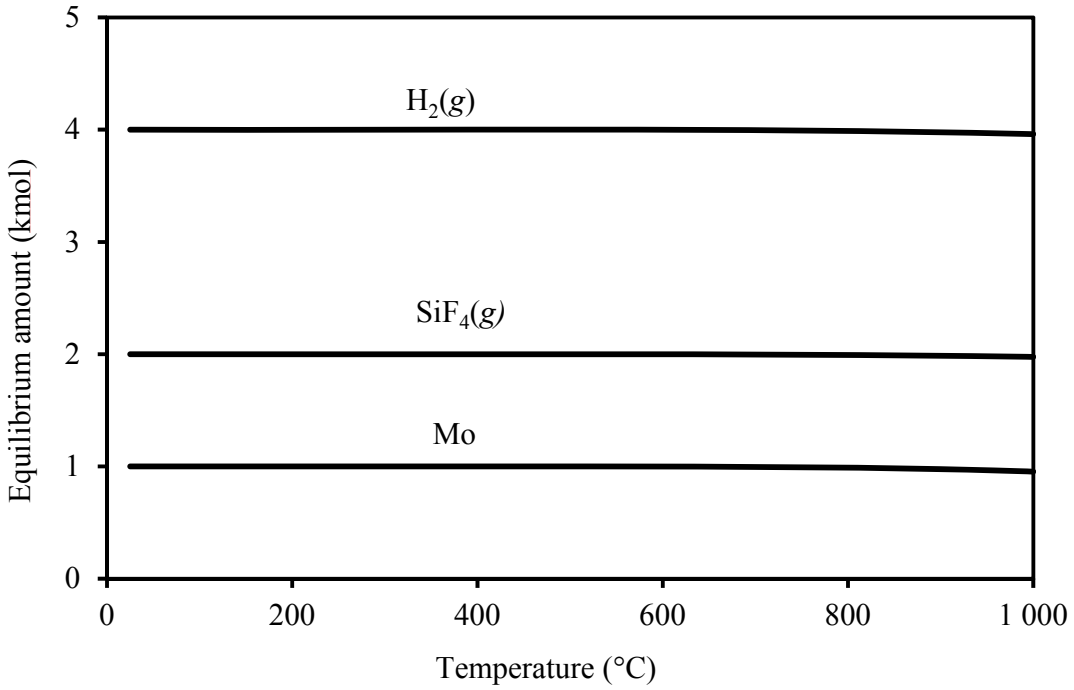

Figure: 3.5 Equilibrium composition of the reaction between $MoSi_2$ and HF (8 kmol)

With excess HF, the calculation predicts the formation of MoF_3 at low temperatures (< 80 °C) (Fig. 3.6), according to Equation 3.6, with only the competing reaction (equation 3.5) occurring above 80 °C.

$$MoSi_2 + 11HF(g) \rightarrow MoF_3(g) + 2SiF_4(g) + 5.5H_2(g) \quad (3.6)$$

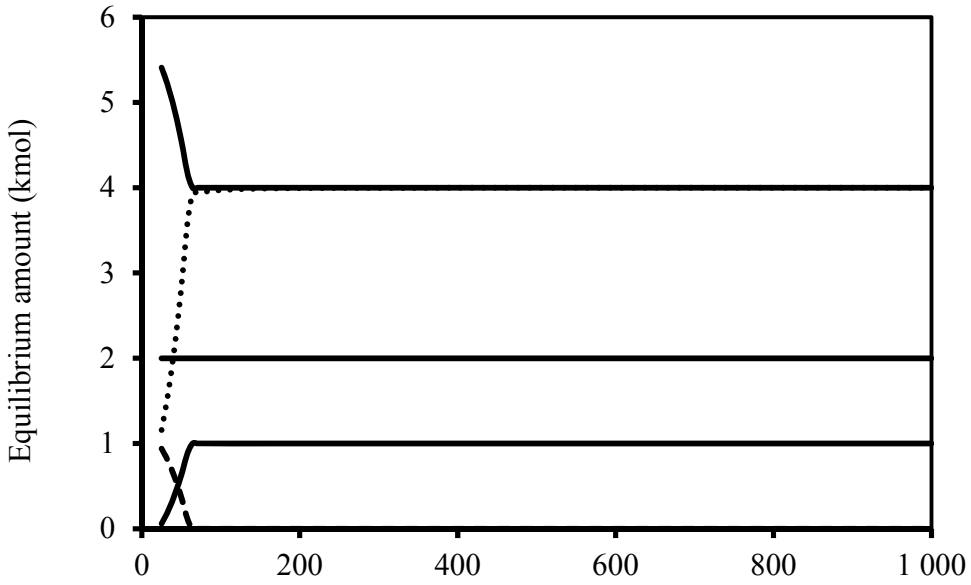

Figure 3.6: Equilibrium composition of the reaction between $MoSi_2$ and HF (12 kmol)

3.5 The reaction of molybdenum and tungsten metals with HF

3.5.1 The W-HF reaction

The behaviour of the pure metals (tungsten and molybdenum) under an HF atmosphere was investigated. Figure 3.7 shows the calculation results between the reaction of W (1 kmol) and HF (4 kmol).

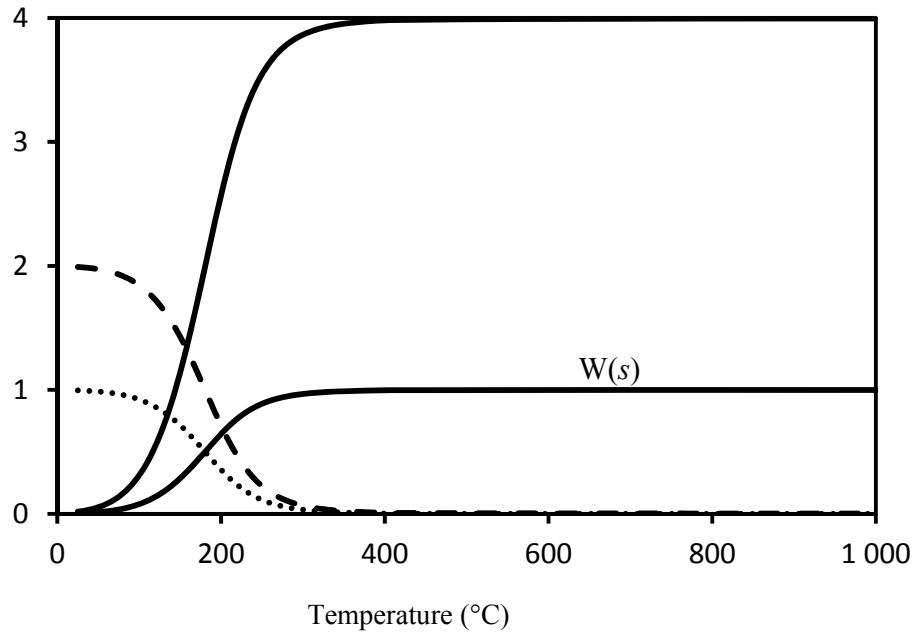

Figure 3.7: Equilibrium composition of the reaction between 1 kmol W and 4 kmol HF

At roughly 20 °C the reaction is predicted to occur as follows:

$$W + 4HF(g) \rightarrow WF_4 + 2H_2(g) \quad (3.7)$$

The amount of WF_4 decreases with temperature till no reactior ; above 200 °C.

3.5.2 The Mo-HF reaction

Similar results for the reaction between Mo (1 kmol) and HF (3 kmol) are predicted (Fig.3.8 and equation 3.10). The reaction is predicted to take place at low temperatures, and with no reaction above 200 °C.

$$Mo + 3HF(g) \rightarrow MoF_3 + 1.5H_2(g) \quad (3.8)$$

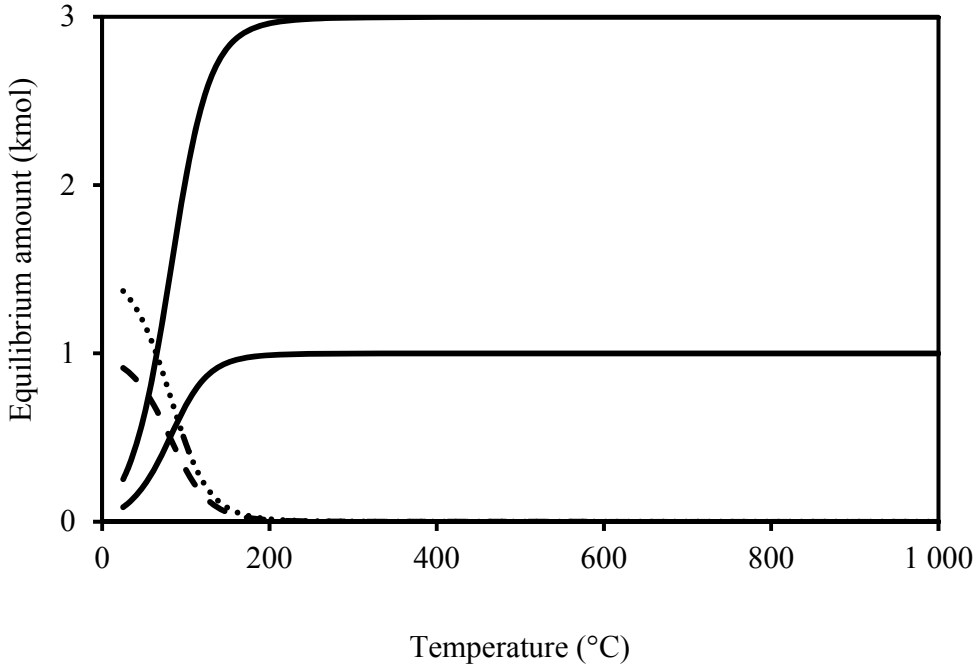

Figure 3.8: Equilibrium composition of the reaction between Mo and HF (3 kmol)

3.6 Theoretical mass change calculations

In order to interpret gravimetric results and identify the reactions taking place, the theoretical mass changes accompanying the possible reactions are calculated (Equation 3.9) for comparison with the experimental results.

$$\Delta m_{Theoretical} = \left(\frac{m_f - m_i}{m_i} \right) \times 100 \qquad (3.9)$$

Here m_f is the final mass of the products after the reaction and m_i is the mass of the starting material.

For example, the theoretical mass change for the formation of tungsten tetrafluoride from the reaction between WSi_2 and HF(*g*) could be given as follows:

$$WSi_2 + 12HF(g) \rightarrow WF_4(s) + 2SiF_4(g) + 6H_2(g) \quad (3.10)$$

$$\Delta m_{Theoretical} = \left(\frac{260 - 240}{240}\right) \times 100 = 8.3\%$$

A positive number indicates that a mass gain occurred during the reaction, while a negative number indicates a mass loss during the reaction. The gaseous products were not included in the calculations because the experiments were done in an open system, where the gaseous products were allowed to leave through the gas outlet. The reactions of both disilicides with HF and fluorine would form the products shown in Table 3.1.

Table 3.1: Summary of theoretical mass changes

Reactions	Solid predicted products	Theoretical mass change (%)	Remarks
$MoSi_2 + F_2(g)$	None	100	Formation of volatile products
$WSi_2 + F_2(g)$	None	100	Formation of volatile products
$MoSi_2 + HF(g)$	Mo	37.1	Mo metal forms by the reduction of MoF_3 at about 80 °C
$WSi_2 + HF(g)$	W	23.4	W metal forms by the reduction of WF_4 at about 150 °C

3.7 Conclusion

Both metals (tungsten and molybdenum) are predicted to behave the same under a hydrogen fluoride atmosphere.

The equilibrium composition calculations show similar chemical behaviour for both disilicides in a fluorine atmosphere, where a complete conversion of WSi_2 and $MoSi_2$ to the volatile fluorides SiF_4, and WF_6 and MoF_6 respectively could be expected.

In the case of anhydrous hydrogen fluoride, the lower metal fluorides, WF_4 and MoF_3, appear at low temperatures, but are not present at higher temperatures, where only the metals molybdenum and tungsten are expected.

The chemical behaviour for both disilicides is predicted to be different to uranium silicide. The overall reactions thus yield solid metal residues. The thermodynamic calculation of U_3Si_2 with HF(g) yield UF_4(s) at all temperatures from zero to about 1100 °C, after which sublimation starts.

4. EXPERIMENTAL

4.1 Thermal analysis

Measuring the physical and chemical properties of materials as a function of temperature or time is usually carried out with the aid of thermal analytical (TA) instruments. There are several TA techniques used for measuring specific properties, such as differential thermal analysis (DTA) and the differential scanning calorimeter (DSC), both for measuring calorimetric effects. A thermogravimetric analyser (TGA) is used to measure weight changes as a function of time or temperature (Brown, 1989).

In this study all the experiments were carried out using a modified TGA instrument, equipped to handle the corrosive gases, HF and fluorine. The instrument is built into a glove box in order to control the atmosphere. The technique of the TGA is to monitor the mass change of a substance as a function of time or temperature. Figure 4.1 gives an illustration of the instrument; the nickel sample pan is hanging inside a furnace and the reactive gas is introduced from the bottom. Gaseous products leaves through the gas outlet, via a special design scrubber before can be vented.

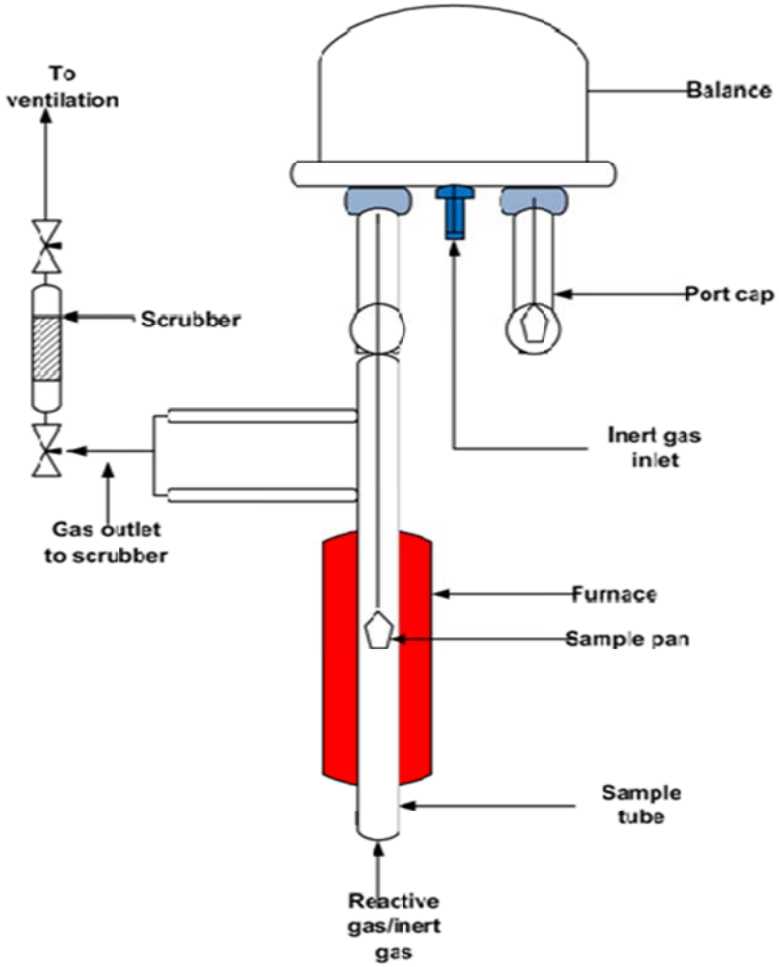

Figure 4.1: A schematic of a modified TGA instrument

A detailed description of a modified TGA instrument (TGA) is given by Rampersad (2005).

Two methods were used: In isothermal experiments the sample is first heated to a predetermined temperature and then maintained at a constant temperature to equilibrate before introducing the reactive gas. In non-isothermal experiments the reactive gas is introduced at the beginning of the experiment.

4.2 Materials

The tungsten disilicide powder (-325 mesh) and molybdenum disilicide powder (>99%) were purchased from Sigma-Aldrich. The samples were used without any pre-treatment, but were kept in a glove box to avoid oxidation. The reactive gases, anhydrous hydrogen fluoride (>99.99%) and fluorine (>99.4%), were both obtained from Pelchem, the chemical manufacturing division of Necsa.

4.3 Isothermal experimental procedure

A sample of $MoSi_2$ or WSi_2 of a weight between 20 and 60 mg was placed in a nickel TG pan. The pan has an inside diameter of 5.63 and a height of 1.64 mm. The sample was heated at a rate of 10 °C/min to the desired temperature. A mixture of 10% HF or F_2 diluted in N_2 was introduced at a flow rate of 60 mL/min to react with the samples, and pure nitrogen was used as purge gas with a flow rate of 54.2 mL/min. The mass change was recorded as a function of time and temperature. At the end a thermogravimetric curve was obtained. The isothermal experiments were done at temperatures in the range 200 to 700 °C.

The procedure of the mixtures of 10% HF or F_2 diluted in N_2 was developed at Necsa. For example, the fluorine mixture is made up to the desired volume% concentration. At first an empty cylinder is passivated with fluorine, then evacuated and cycle purge with nitrogen to remove the fluorine and impurities. It is again evacuated and cycle purge with fluorine to remove any residual nitrogen. The cylinder is then filled with pure fluorine followed by pure nitrogen to the desired pressures. It is left for at least for overnight for the gases to properly mix before use.

4.4 Non-isothermal experimental procedure

The non-isothermal experiments were conducted in a similar way, except that the sample was first heated to a predetermined temperature at a heating rate of 10 °C/min, and then maintained at a constant temperature to equilibrate. The reactive gas was introduced when the temperature has stabilised, which normally took 30 to 40 min. The isothermal experiments were carried out with HF on both disilicides at temperatures in the range 200 to 700 °C.

4.5 Analytical techniques

Several analytical techniques were used to assist in interpreting the results, including XRD for phase identification of a product, SEM for the morphology and topography of the samples, the SEM analysis were done at University of Pretoria and Necsa, while XRD was carried out at Necsa. XRF and ICP-OES were used for elemental analysis and chemical analysis respectively, and done by Pelindaba Analytical Laboratory (PAL).

5. RELEVANT KINETIC THEORY

5.1 Introduction

During a chemical reaction between a solid material and a gaseous reactant, the reaction rate is commonly determined by the available surface area. The mechanism is then typically described by shrinking core models (SCMs) or shrinking particle models (SPMs). In SCMs the rate limiting step can be gas film diffusion, product-layer diffusion or chemical reaction control. In SPMs the rate limiting step can be either the chemical reaction, or diffusion through the gas film surrounding the particle (Levenspiel, 1999; 566). In this chapter the various equations applicable to dry fluorination of solid material are described.

5.2 Fick's law and diffusion equation solutions

Steady state diffusion is expressed mathematically as Fick's first law, which relates the diffusive flux to the concentration field. Diffusive flux measures the amount of a chemical which passes through unit area per unit time. The general empirical equation is given as follows:

$$\text{Rate of transport process} = \frac{\text{driving force}}{\text{resistance}} \tag{5.1}$$

This equation generally states that a driving force is needed to overcome a resistance in order to transport a property. For diffusion the driving force is the concentration gradient of the species. Mathematically Fick's first law in one dimension is written as follows:

$$J_x = -D\frac{\partial c}{\partial x} \tag{5.2}$$

where J_x is the diffusive flux of a substance in mol.m^{-2}.s^{-1}, D is the diffusivity in m^2.s^{-1}, c is the concentration of the diffusing substance in mol.m^{-3}, and x is direction of the flux in m (Geankoplis, 1972).

Fick's second law describes how diffusion causes the concentration field to change with time. It is derived by assuming the change of concentration to be equal to the difference in the flux in and out of a control volume. It is expressed as:

$$\frac{\partial c}{\partial t} = D\frac{\partial^2 c}{\partial x^2} \tag{5.3}$$

Here, t is time (s). In three dimensions, it is expressed as follows:

$$\frac{\partial c}{\partial t} = D\nabla^2 C \tag{5.4}$$

with

$$\nabla^2 = \frac{\partial^2}{\partial x^2} + \frac{\partial^2}{\partial y^2} + \frac{\partial^2}{\partial z^2} \tag{5.5}$$

Two important quantities derived from Equation 5.4 and used for estimation purposes, are the diffusion length (L) and diffusion time (τ) related by,

$$L = 2\sqrt{D\tau} \tag{5.6}$$

Thus if either L or τ is known, the other can be estimated (Balluffi, 1924).

5.3 Shrinking core models (SCMs)

5.3.1 Introduction

A heterogeneous reaction where a gas contacts a solid and then transforms it into products can be expressed by the following Equation:

$$A(g) + bB(s) \rightarrow \text{products} \tag{5.7}$$

Here, A, represents the reactive gas (which is diluted HF(g) or F_2 in our case), b is the stoichiometric coefficient and B is the solid reactant (WSi_2 or $MoSi_2$).

The SCMs predict that the reaction always starts at the outer surface of the particle, proceeds to the core and results in completely converted material and inert solids. Five possible steps are visualized to occur in this model (Levenspiel, 2006; 570 - 571), namely,

(1) Diffusion of A through the gas film surrounding the solid to the surface of the solid,

(2) Diffusion of A through the ash (product) layer to the surface of the un-reacted core,

(3) Reaction of the gas with the solid,

(4) Diffusion of the gaseous products back to the exterior surface of the solid and, finally,

(5) Diffusion of gaseous products through the gas film back into the bulk.

In this chapter only the first three steps of the SCM are investigated, since in some cases the last two steps does not exist, especial if there are no gaseous products forming. The step with the highest resistance is considered to be rate controlling.

5.3.2 Gas film diffusion control

If diffusion through the surrounding stagnant gas film is the rate controlling step, the concentration gradient of the reactive gas is constant at all times during the reaction of the particle. A partially reacted particle is considered with an initial radius R, area of $4\pi r^2$, and an exterior surface S_{ex}, where S_{ex} does not change during the reaction. The partially reacted particle has an un-reacted core surrounded by an ash (product) layer and a stagnant gas film covering the surface. The disappearance of the original material as a function of time is given by Equation 5.8.

$$-\frac{1}{S_{ex}}\frac{dN_B}{dt} = -\frac{1}{4\pi R^2}\frac{dN_B}{dt} = -\frac{b}{4\pi R^2}\frac{dN_A}{dt} = b\,k_g\,C_{Ag} \tag{5.8}$$

where k_g is the mass transfer coefficient between gas and particle and C_{Ag} is the concentration of the reactive gas. After separation of variables, integration and appropriate substitution, an expression for the fractional conversion of the particle, X_B, is obtained.

$$\frac{t}{\tau} = 1 - \left(\frac{r_c}{R}\right)^3 = X_B \tag{5.9}$$

Where r_c is the radius of the reacted core and τ is the time for full conversion of the particle and k_g the mass transfer coefficient for diffusion through the stagnant gas film surrounding the particle. Where $r_c = 0$, then,

$$\tau = \frac{\rho_B R}{3b\,k_g\,C_{Ag}} \tag{5.10}$$

Using the residual mass fraction α defined as,

$$\alpha = 1 - X_B = \frac{M}{M_0} \tag{5.11}$$

Equation 5.9 becomes

$$\frac{t}{\tau} = 1 - \alpha \tag{5.12}$$

These expressions strictly apply to spherical particles.

5.3.3 Ash (product) layer diffusion control

If ash layer diffusion is the rate controlling step, the reactant A and the boundary of the un-reacted core move inward towards the centre of the particle. The rate of reaction of A at any instant is given by its rate of diffusion to the reaction surface. Expressed in terms of the applicable fluxes, the rate becomes (Levenspiel, 2006; 573):

$$-\frac{dN_A}{dt} = 4\pi r^2 Q_A = 4\pi R^2 Q_{AS} = 4\pi r_c^2 Q_{AC} \tag{5.13}$$

where Q_{As} is the flux of A through the exterior surface of the particle, Q_A the flux of A through the surface of any radius, and Q_{Ac} is the flux of A to the reaction surface. The fluxes provide measurements of the amount of a chemical that passes through the particle per unit area per unit time.

After appropriate integration and algebraic manipulation, the expression for the fractional conversion becomes

$$\frac{t}{\tau} = 1 - 3(1 - X_B)^{2/3} + 2(1 - X_B) \tag{5.14}$$

where the time for full conversion (τ) is given by Equation 5.15

$$\tau = \frac{\rho_B R^2}{6b D_e C_{Ag}} \tag{5.15}$$

D_e is the effective diffusion coefficient of the gaseous reactant. By using the residual mass fraction, Equation 5.14 becomes

$$\frac{t}{\tau} = 1 - 3\alpha^{2/3} + 2\alpha \tag{5.16}$$

5.3.4 Chemical reaction control

For chemical reaction control, a partially reacted particle is considered, and the rate of reaction is given as follows:

$$-\frac{1}{4\pi r_c^2}\frac{dN_B}{dt} = -\frac{b}{4\pi r_c^2}\frac{dN_A}{dt} = b k'' C_{ag} \tag{5.17}$$

After separation of the variables, integration and substitution, the fractional conversion expression becomes

$$\frac{t}{\tau} = 1 - \frac{r_c}{R} = 1 - (1 - X_B)^{1/3} \tag{5.18}$$

The time for full conversion is given as follows:

$$\tau = \frac{\rho_B R}{bk''C_{Ag}} \tag{5.19}$$

where *k"* is the first-order rate constant for the surface reaction. Using the residual mass fraction Equation 5.18 becomes

$$\frac{t}{\tau} = 1 - \alpha^{1/3} \tag{5.20}$$

5.4 Shrinking particle models (SPMs)

5.4.1 Introduction

In the shrinking particle model (SPM) the products are gaseous and no ash layer forms. Here three possible steps are visualized to occur in succession during the reaction (Levenspiel, 2006; 568):

(1) Diffusion of reactant A from the main body of a gas through the stagnant gas film to the surface of the solid

(2) Reaction on the surface between reactant A and solid, and finally

(3) The diffusion of reaction products from the surface of the solid through the stagnant gas film back into the main body of gas

As before, the chemical reaction is written as

$$A(g) + bB(s) \rightarrow \text{products} \tag{5.21}$$

A represents the reactive gas (HF or F_2 in this study) and B the solid (WSi_2 or $MoSi_2$).

5.4.2 Chemical reaction control

For chemical reaction control the conversion rate of solid B is proportional to the particle surface area, thus

$$-\frac{1}{S_{ex}}\frac{d\,N_B}{dt} = k'[n] = k \tag{5.22}$$

After integration and appropriate substitution, the expression for the time for full conversion is obtained as

$$\frac{t}{\tau} = 1 - \frac{r}{R} = 1 - \alpha^{1/3} \tag{5.23}$$

with

$$\tau = \frac{\rho_B R}{k} \tag{5.24}$$

5.4.3 Gas film diffusion

For small particles, in the Stokes law regime, the following two equations apply:

$$\frac{t}{\tau} = 1 - \left(\frac{r_c}{R}\right)^2 = 1 - \alpha^{2/3} \tag{5.25}$$

with

$$\tau = \frac{\rho_B R^2}{2bC_{Ag}D} \tag{5.26}$$

and D is the gas phase diffusion coefficient.

6. THE REACTIONS OF THE METAL DISILICIDES WITH HYDROGEN FLUORIDE

6.1 The reaction of anhydrous hydrogen fluoride with WSi_2

6.1.1 Introduction

Gaseous hydrogen fluoride (AHF) is not a good as fluorinating agent as fluorine and is frequently used to obtain lower metal fluorides (Muetterties and Castle, 1961). However, the lower fluorides of molybdenum and tungsten (MoF_3, MoF_4, and WF_4) are not obtained through the reaction of the pure metals or molybdenum and tungsten disilicide with HF. Priest and Schumb (1948) and Larson (1970) have shown that these are only obtained through the reduction of the high oxidation state metal fluorides.

The experimental work in this section was carried out to study the chemical behaviour of WSi_2 and $MoSi_2$ under an HF atmosphere to investigate the possibility of forming the lower metal fluorides. The experimental work was carried out using a modified TGA instrument according to the procedures described in Chapter 4.

The thermodynamic predictions (Chapter 3) were used as guidelines in designing the experiments. The thermodynamic calculations strictly apply to closed systems, while our experiments were carried out under open conditions, where the gaseous products were allowed to leave through the gas stream. Therefore derivation from the thermodynamic predictions might be expected.

The reaction between WSi_2 with HF is predicted to form the lower metal fluoride (WF_4) at temperatures less than 100 °C, at high temperature tungsten metal was the predicted final product.

6.1.2 Non-isothermal TG results of the reaction between WSi_2 and HF

Although the thermodynamic calculations predicted the formation of WF_4 at low temperatures less than 150 °C, no reaction occurred up to 200 °C in the non-isothermal reaction (Fig. 6.1).

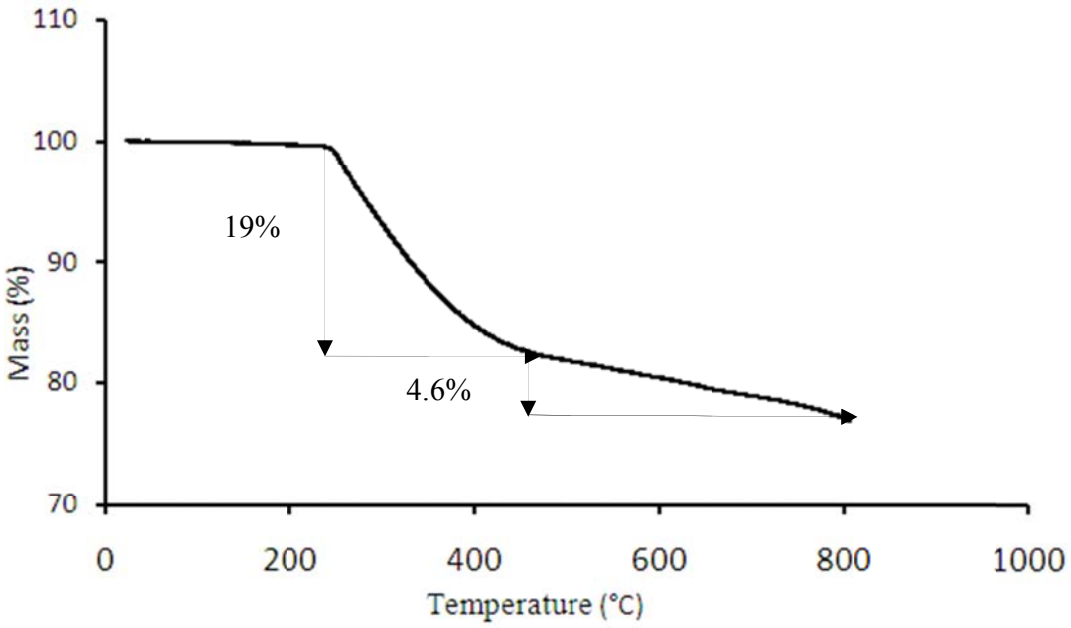

Figure 6.1: Thermogravimetric curve of the reaction between WSi_2 and HF

The mass loss process occurred in two steps, starting just above 200 °C. The total observed mass loss (23.6%) is taken to be equal to the expected mass loss of 23.4%, (considering the instrumental error of 1%). The first mass loss process indicates a fast reaction, while the second-step mass loss process starting at roughly 400 °C was slow or indicating the presence of a limiting mechanism. In the second step, the reaction proceeded slowly, but eventually reached the expected theoretical mass loss (23.4%).

Unexpectedly, the TG curve (Fig. 6.1) did not level off. However, the XRD analysis of the solid product corresponded to the expected product by showing tungsten metal as the major phase,

even though small amounts of silicon were still present (this was possibly due to the incomplete fluorination of the sample).

6.1.3 Isothermal results between the reaction of WSi_2 and HF

The isothermal experiments were carried out using the same TG instrument, but according to the procedure given in Section 4.3. The isothermal reactions were performed at temperatures in the range of 200 to 700 °C. These conditions had the potential to by-pass the intermediate product (WF_4), since it was predicted to form at low temperatures (less than 150 °C). The reactive gas (HF) was introduced after about 50 min, when the sample had become stable at that particular temperature. These isothermal reactions (Fig. 6.2) provided the data required to produce the chemical kinetics.

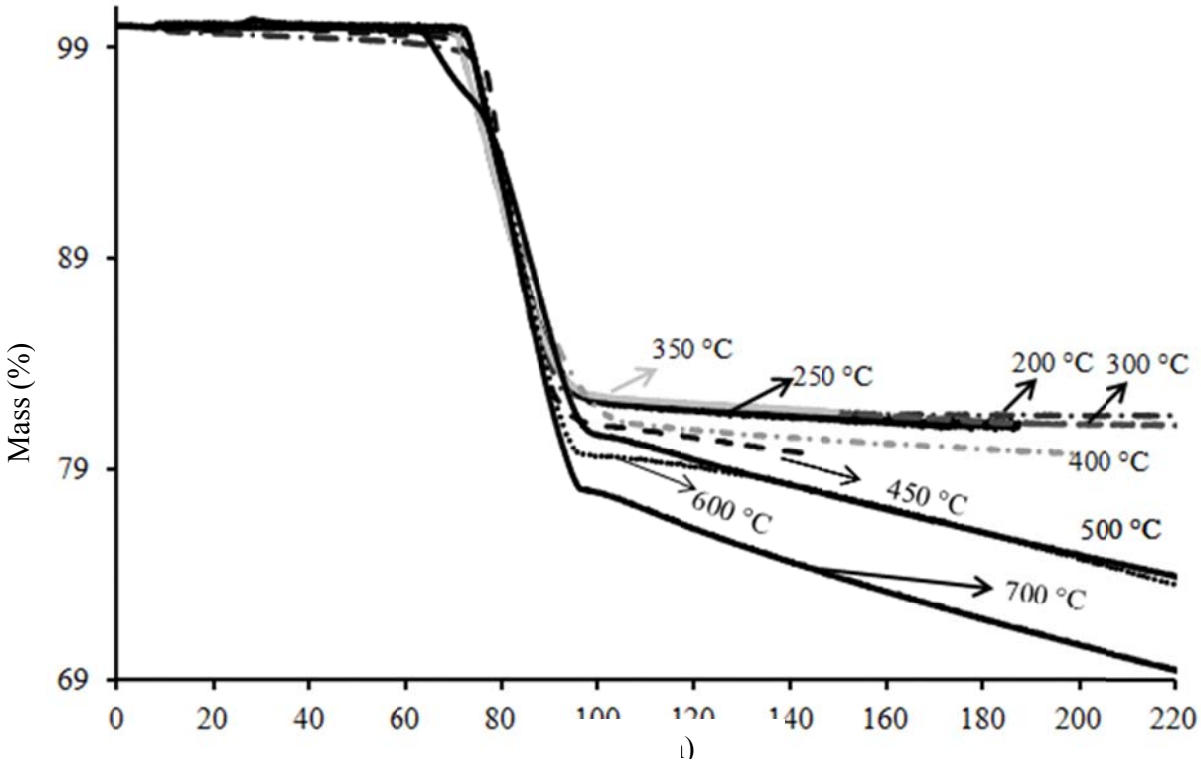

Figure 6.2: Thermogravimetric curves of the isothermal reactions between WSi_2 and HF

All the reactions finished with different mass percentages, the reactions done at 200 to 400 °C reached stable mass losses of 17.5, 18.5 19.0, and 19.5%, respectively. The reactions from 450 to 700 °C had a continuous mass loss up to 5 h; these reactions displayed the same slope as those from 200 to 400 °C, even though resulted in mass losses well above the expected (23.4%).

At high temperatures (i.e. 450 to 700 °C) further volatilisation of the samples appears to take place. It could be the formation of WF_6, where the produced tungsten metal reacted with hydrogen fluoride gas and formed volatile WF_6. Due to the limitations in the experimental set up volatile products could not be collected and analysed. A summary of the isothermal results is given in Table 6.1.

Table 6.1: Summary of the isothermal results of the reaction between WSi_2 and HF(*g*)

Isothermal temperature (°C)	Observed mass loss (%)	Remarks
200	17.5	For the reactions done at 200 to 400 °C the mass loss was approaching the expected mass loss of forming tungsten metal as the temperature increases
250	18.5	
300	19.0	
350	19.5	
400	20.3	
450	The mass loss from 450 to 700 °C was continuously, exceeding 27% after about 3 hours	The reactions done from 450 to 700 °C showed further volatilisation of the samples
500		
600		
700		

None of the experiments between WSi_2 and HF(*g*) showed a mass gain as an indication of the formation of WF_4.

6.1.4 SEM analysis of the reaction products of WSi_2 and HF

SEM analyses of untreated and treated WSi_2 samples are shown in Figures 6.3, 6.4, and 6.5. Figure 6.3 shows the untreated sample, while figures 6.4 and 6.5 show the products at 300 and 600 °C, respectively.

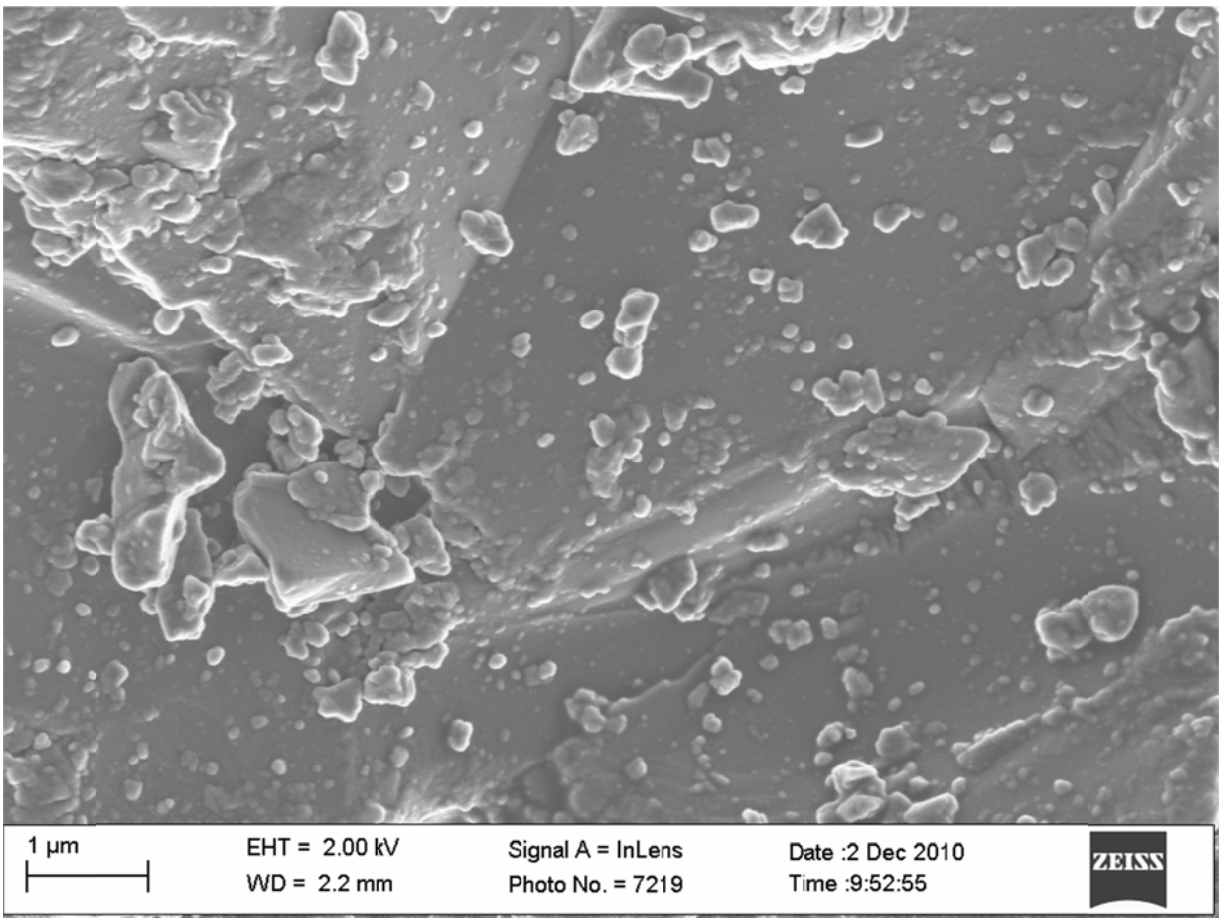

Figure 6.3: SEM analysis of untreated WSi_2

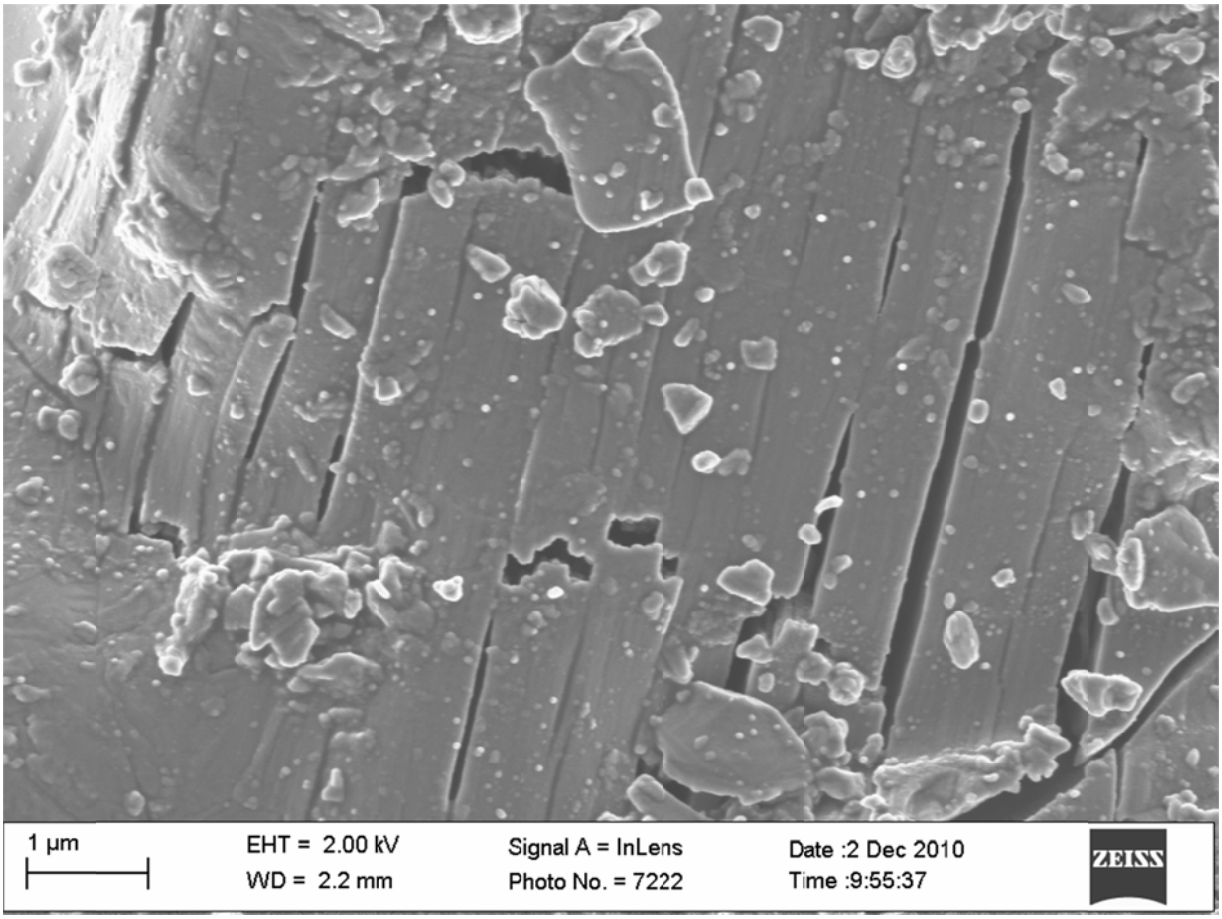

Figure 6.4: SEM analysis of WSi_2 treated with HF(*g*) at 300 °C

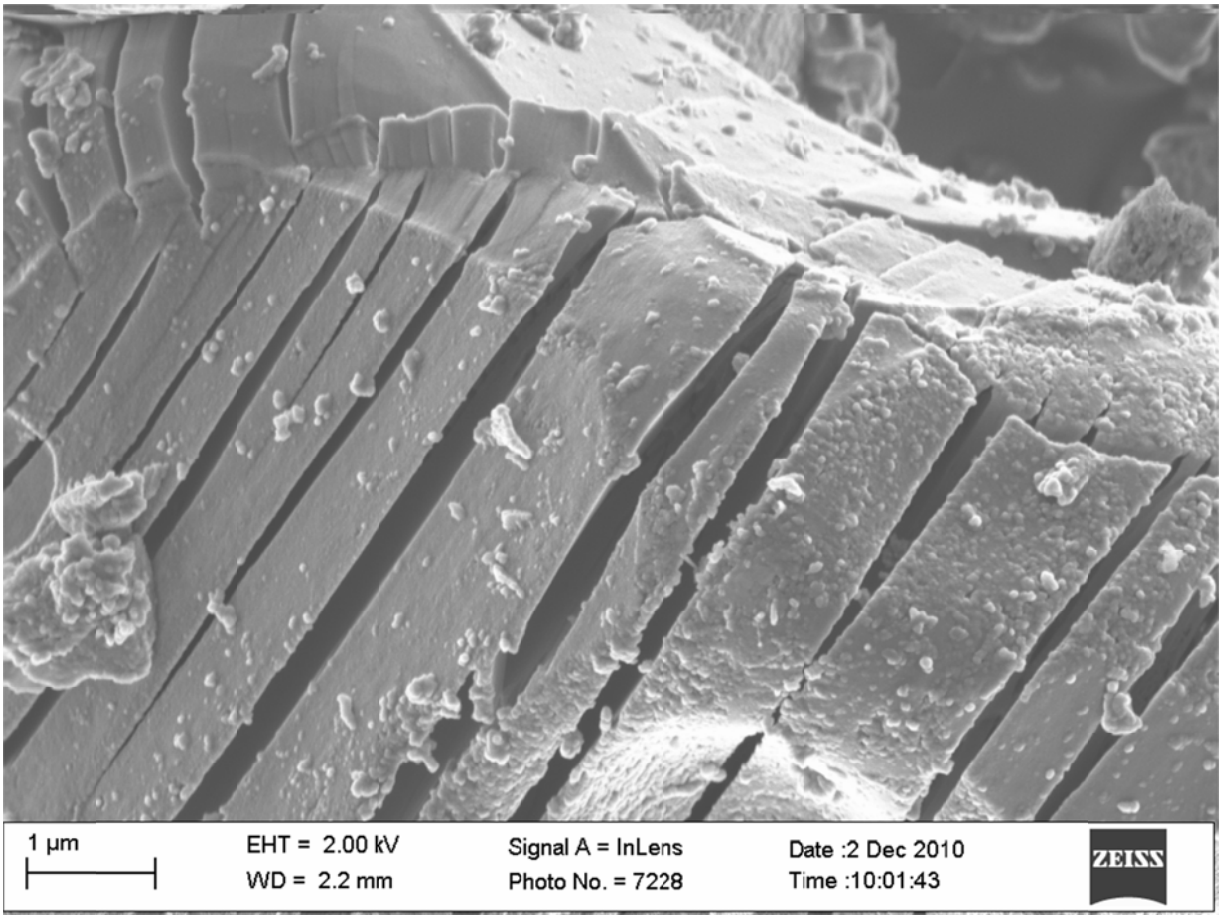

Figure 6.5: SEM analysis of WSi_2 treated with HF(*g*) at 600 °C

The particles of WSi_2 have the same size (about 10 µm) before and after treatment with HF at different temperatures. The treated samples from 300 to 700 °C showed cracks on the surface of the particles. This fracture of the particles was possibly caused by the removal of silicon, which would cause the structure to collapse or lose shape. Some of the particles remain unchanged at the reaction done at 200, 250 and 300 °C, probably due to the incomplete fluorination of the sample. Furthermore no shrinkage was observed, indicating that the volatile products had diffused out of a porous structure.

6.1.5 XRD analysis of the reaction products between WSi_2 and HF

The XRD patterns for the products of the reactions between WSi_2 and HF are presented in Fig 6.6 and 6.7. The reactions done at intermediate temperatures, like 250, 350 and 450 °C were not included. Figure 6.6 shows the patterns of the all the reactions *versus* a pattern of tungsten metal, where all the reactions match the reference pattern of tungsten metal, except at 200 and 300 °C. The product at 200 and 300 °C matched a pattern of WSi_2 with a tetragonal structure (Figure 6.6), due to the incomplete fluorination of the sample. The patterns of the products at 500 and 700 °C also give extra clear reflection between 20-30 2theta, which matched a pattern of WSi_2 with a hexagonal structure.

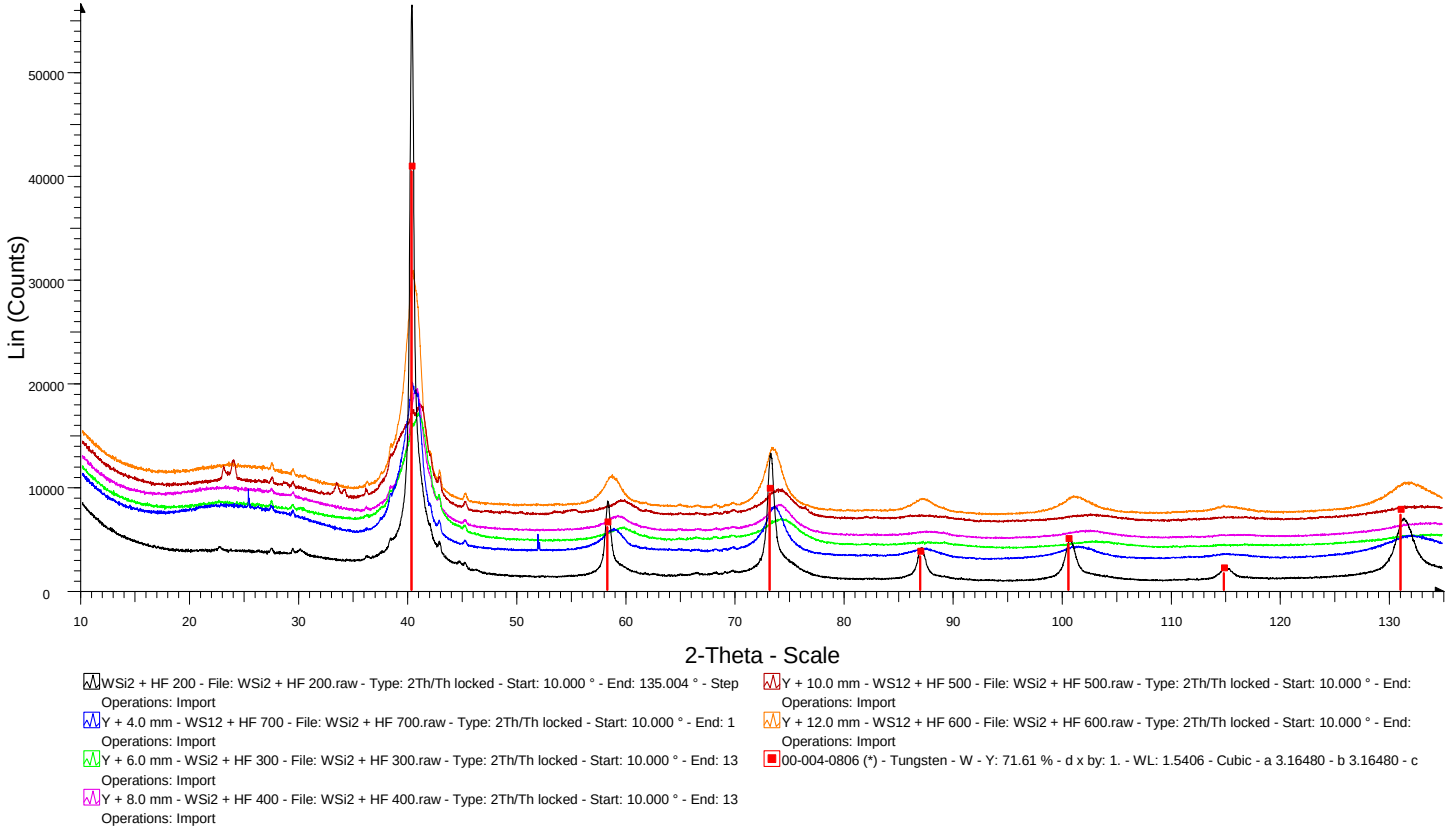

Figure 6.7 show that the treatment of WSi_2 with HF results in a micro structure change. The reaction at 200 °C did not match every peak of the WSi_2 reference pattern, especial above 60-130 2thatha. The two reference patterns of WSi_2 tetragonal and hexagonal were not matched in full, in all cases there were few peaks overlapping.

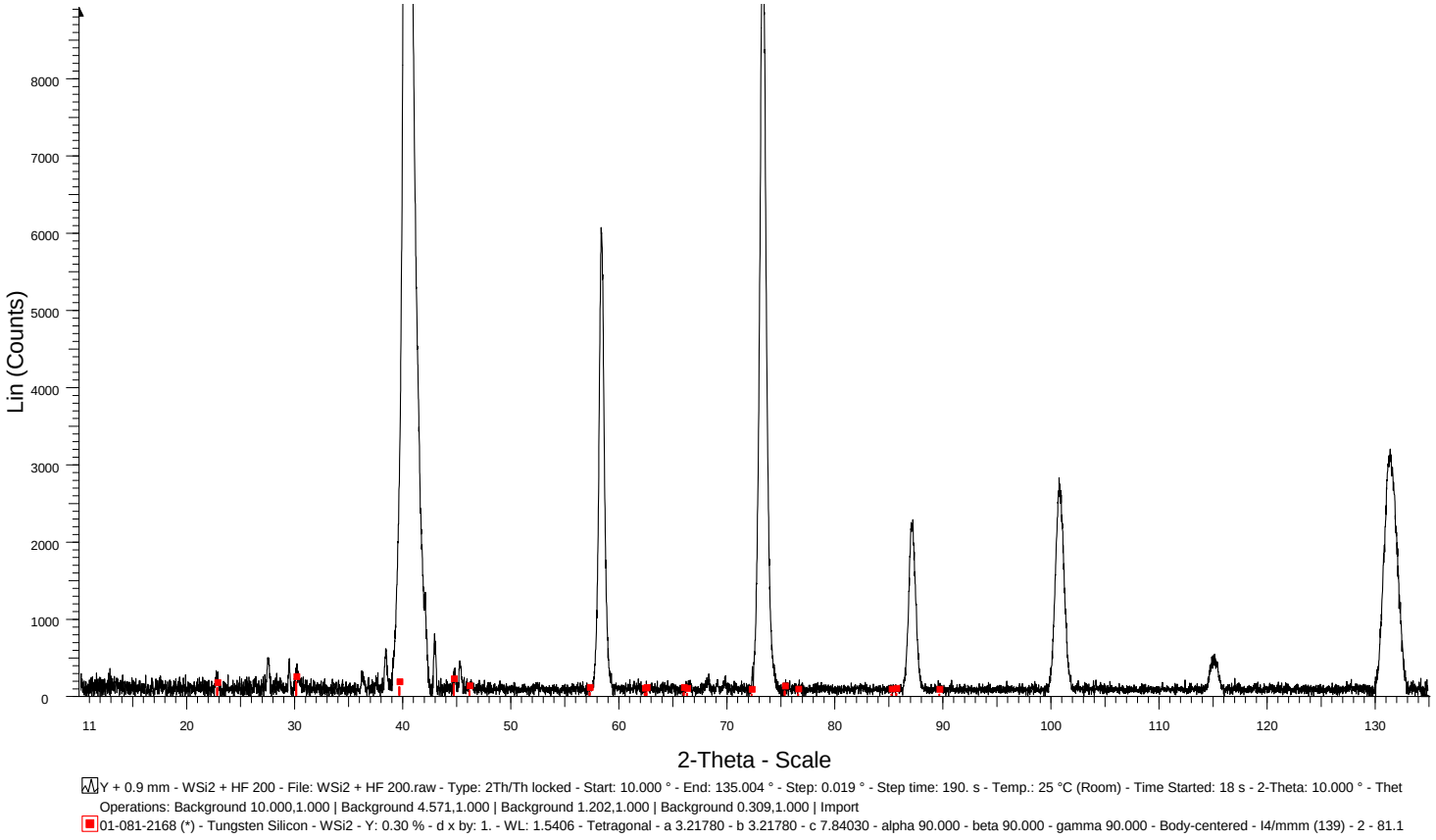

Figure 6.7: Background subtracted powder diffraction pattern of WSi_2 at 200 °C overlaid with stick patterns of the proposed WSi_2

6.2 Non-isothermal results of the reaction between $MoSi_2$ with HF

6.2.1 Introduction

According to the literature, the lower metal fluorides of molybdenum are not obtained through the reaction with HF, but can only be prepared through the reduction of high oxidation state fluorides (Falconer et al., 1973 and Larson, 1970). The chemical behaviour of $MoSi_2$ in an HF atmosphere was studied to determine whether the lower molybdenum fluoride forms under these conditions.

As discussed in Chapter 3, the thermodynamic calculations predicted the formation of MoF_3 at temperatures less than 80 °C (Equation 6.3). Above 80 °C molybdenum should form.

$$MoSi_2 + 8HF(g) \rightarrow Mo(s) + 2SiF_4(g) + 4H_2(g) \quad (6.3)$$

6.2.2 Non-isothermal TG results between $MoSi_2$ with HF

According to the TG results (Fig. 6.8) no reaction occurred below 200 °C, except the very small mass loss of about 2%, which is possibly due to the removal of the silicon oxide layer (SiO_2), which forms when $MoSi_2$ is exposed to air. Although the sample was kept in a glove box, oxidation may have occurred during the preparation stage.

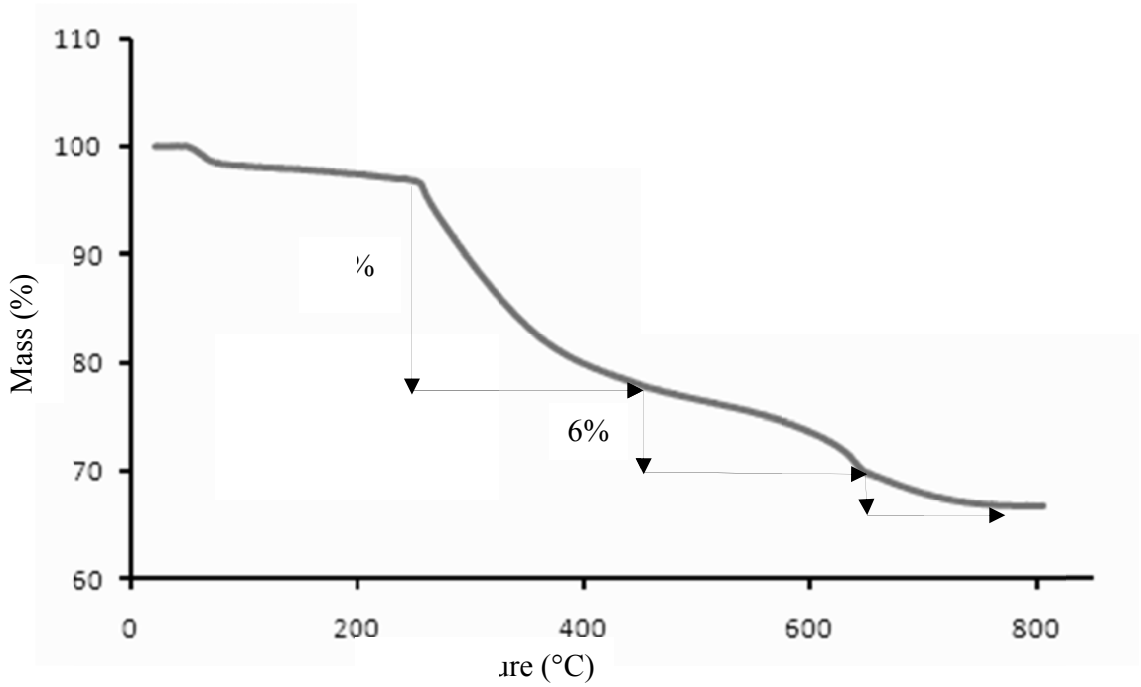

Figure 6.8: Thermogravimetric curve of the reaction between $MoSi_2$ and HF up to 800 °C

In this reaction a number of mass loss processes were observed that resulted in a total loss of 33.3%. The first mass loss is the 2% step, and then followed by the second mass loss process of about 22% which is most probably caused by the start of the formation of the products and a release of the gaseous products. The last two steps are probably the continuation of the formation of the products, but with some restrictions since are not as fast as the second mass loss process.

The final product from this reaction correspond to the predicted results showing molybdenum metal as the major phase, (XRD analysis), although a small amount of silicon was also present

(<1%). The small amount of silicon indicates the incomplete fluorination of the sample, which is caused by the limiting mechanism.

6.2.3 Isothermal results of the reaction between $MoSi_2$ and HF

The isothermal results of the reaction between $MoSi_2$ with HF performed at temperatures in the range of 200 to 700 °C are shown in Figure 6.9.

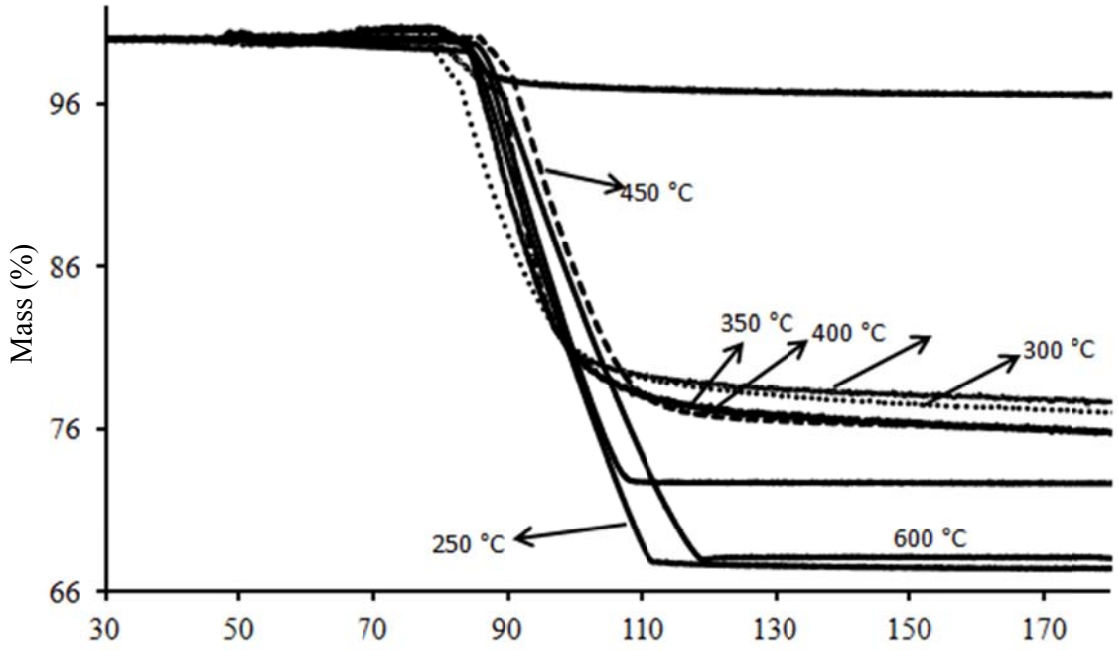

Figure 6.9: Thermogravimetric curve of the isothermal reaction between $MoSi_2$ and HF

Here all the nine reactions end up with different mass percentages, but show a common mass loss process. The reaction at 200 °C shows a very small mass loss of 3.7%. This possible indicates the removal of a silicon oxide layer, as explained above. The mass loss of these isothermal reactions increases as the temperature was increased. The common mass loss process

has the same slope, and is undoubtedly due to the formation of the volatile $SiF_4(g)$. A summary of the isothermal results is given in Table 6.2.

Table 6.2: Summary of the isothermal results between $MoSi_2$ and $HF(g)$

Isothermal temperature (°C)	Observed mass loss (%)	Remarks
200	3.7	The small mass loss at 200 °C was possibly due to the removal of the silicon oxide layer (SiO_2), which forms when $MoSi_2$ is exposed to air.
250	23.2	From 250 to 700 °C, increasing the temperature increases the mass loss. The mass losses get closer to the theoretical for forming Mo metal. Even the reaction at 700 °C did not yield the expected mass loss of 37 *versus* 32.7%.
300	23.8	
350	24.1	
400	24.5	
450	26.5	
500	27.4	
600	32.6	
700	32.7	

6.2.4 XRD analysis of the reaction products of $MoSi_2$ and HF

In the case of the molybdenum disilicide reactions, almost all the products form 200 to 600 °C matchde the pattern of $MoSi_2$ with a tetragonal structure (Fig 6.10 and 6.11). The pattern at 200 °C display additional narrow peaks throughout the scale from 20 to 130 2theta, however those extra peaks did not give any match to either $MoSi_2$ or Mo metal. The pattern at 700 °C gave was total different form the rest, giving a good match to a pattern of Mo metal.

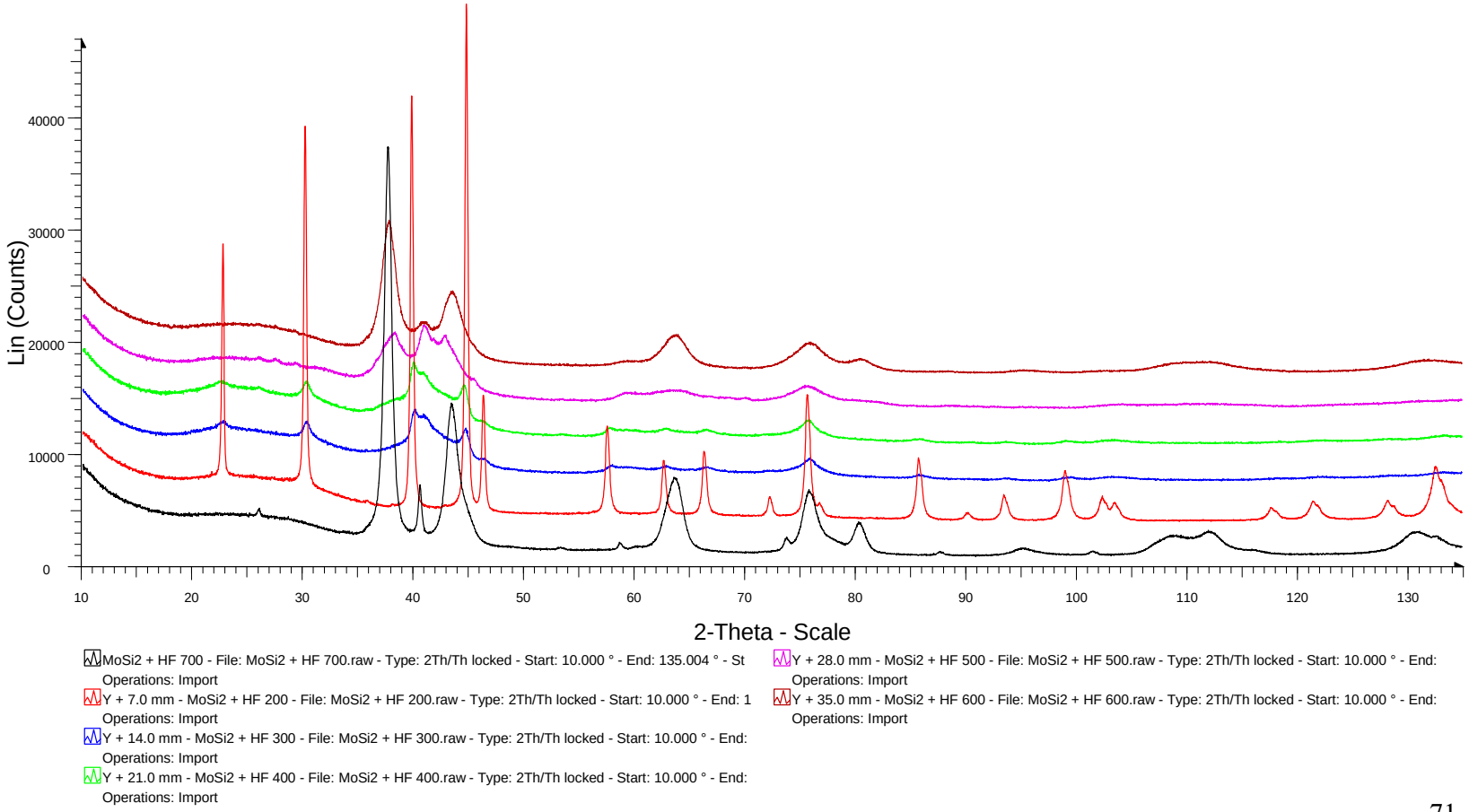

Only the reaction at 700 °C gives a good match to the reference pattern of Mo. This is possible, because the mass loss observed at this temperature was very close to the expected mass loss. The other reactions gave a good match to $MoSi_2$, (Fig. 6.10).

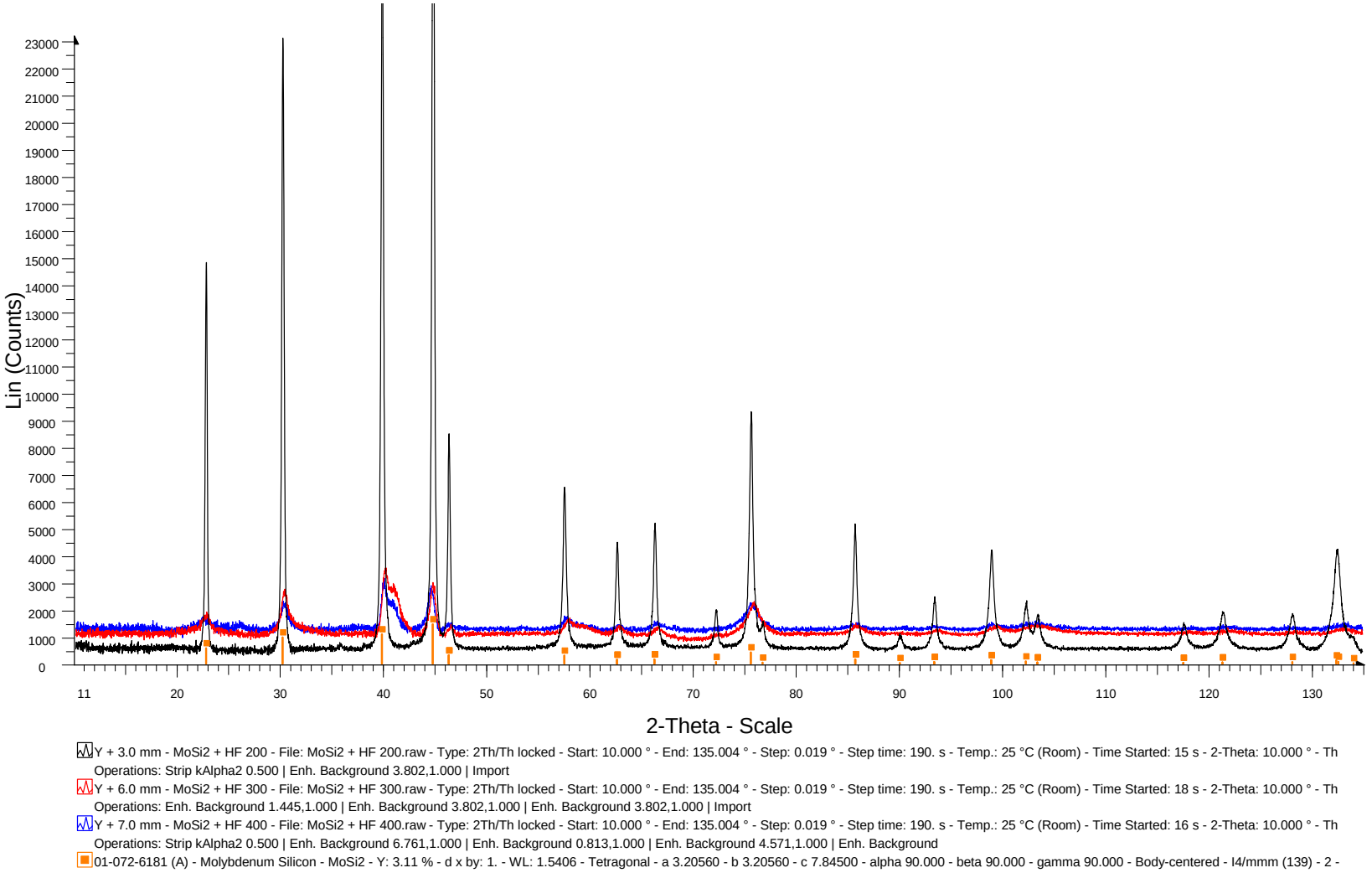

6.2.5 SEM analysis of the reaction products of $MoSi_2$ and HF

Figures 6.12, 6.13 and 6.14 give the SEM micrographs of the untreated and treated samples of $MoSi_2$.

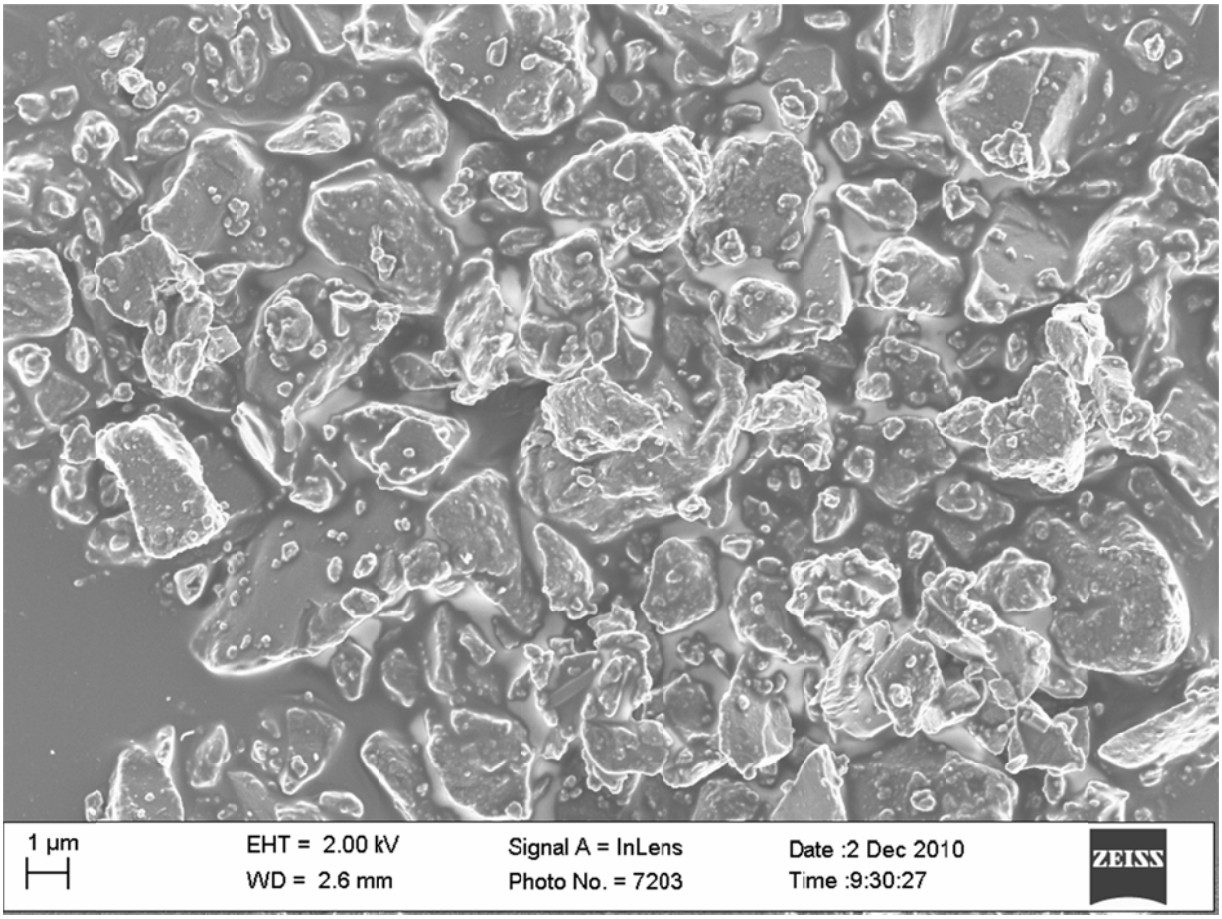

Figure 6.12: SEM analysis of untreated $MoSi_2$

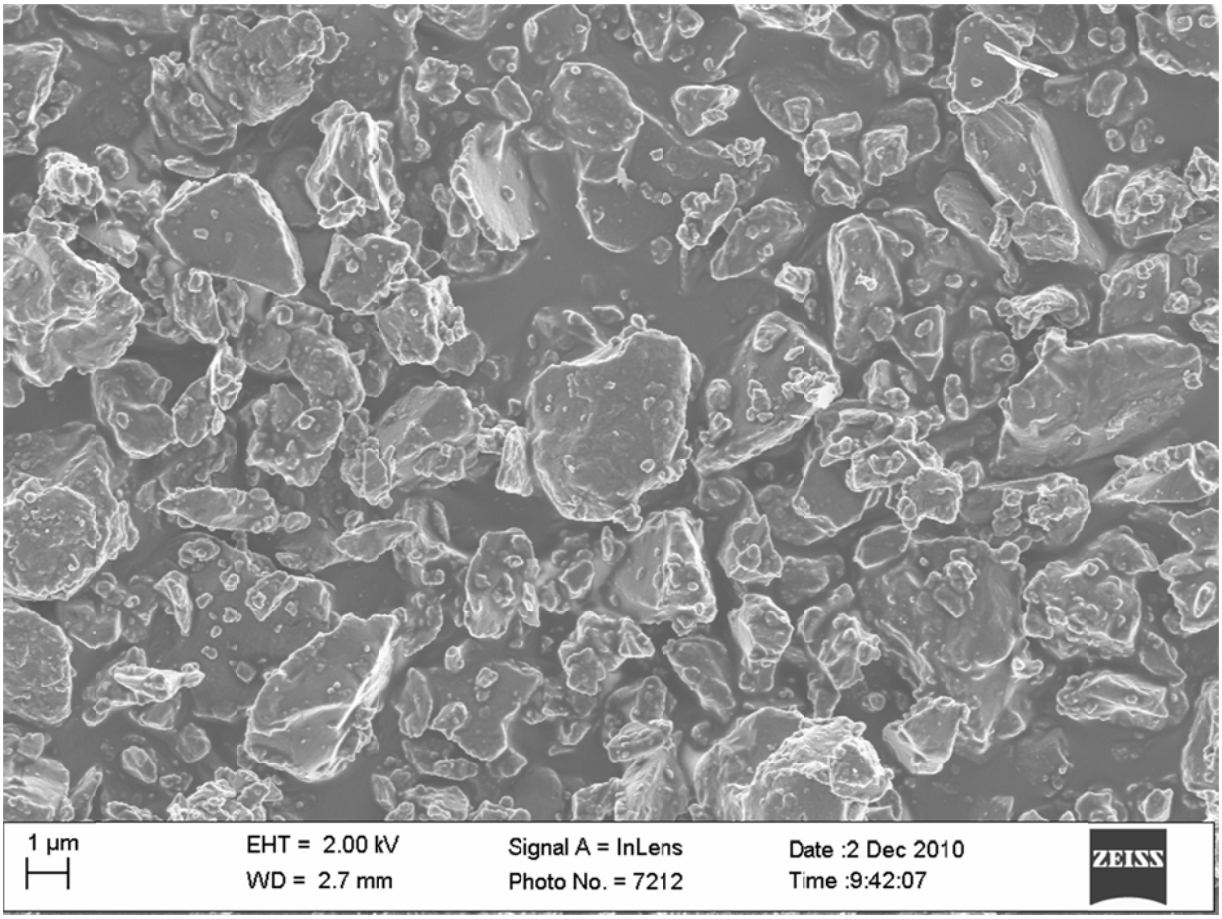

Figure 6.13: SEM analysis of $MoSi_2$ treated with HF at 600 °C

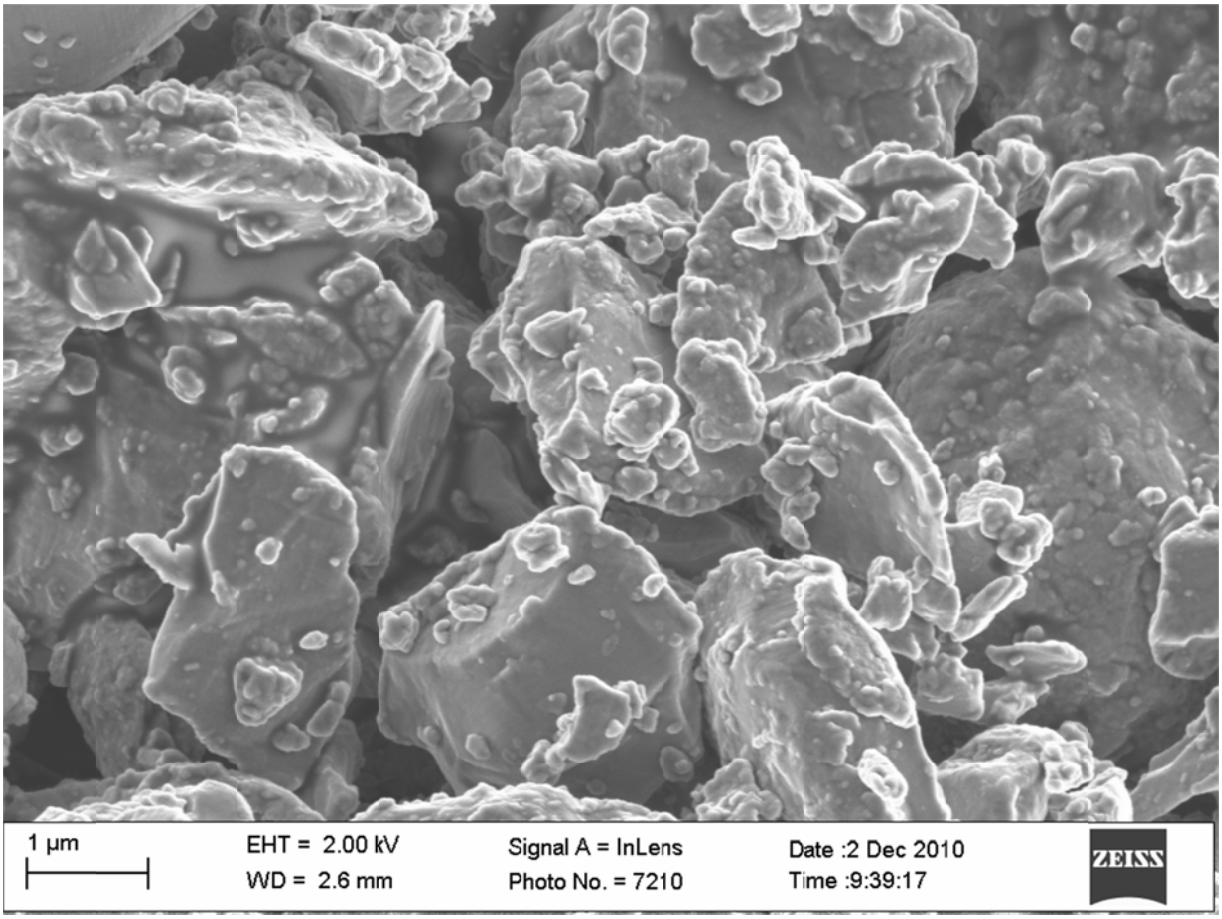

Figure 6.14: SEM analysis of $MoSi_2$ treated with HF at 300 °C

The structure of $MoSi_2$ did not change or collapse due to the treatment with HF(*g*). No surface cracks were observed on the surface, as for WSi_2.

6.3 Reaction kinetics

6.3.1 Introduction

This section deals with the chemical kinetics, reaction rates, and development of a mathematical description of the reactions conducted. Since in all the cases where WSi_2 and $MoSi_2$ react with HF, solid products form, only SCMs apply, not SPMs. Only three models need therefore to be considered. Their algebraic expressions equations 5.12, 5.23 and 5.25, as discussed in Chapter 5, are given as follows:

$$1-\alpha=\frac{t}{\tau} \qquad \text{(Diffusion through gas film control)}$$

$$1-\alpha^{1/3}=\frac{t}{\tau} \qquad \text{(Chemical reaction control)}$$

$$1-3\alpha^{2/3}+2\alpha=\frac{t}{\tau} \qquad \text{(Diffusion through ash layer control)}$$

Plots of the left-hand side of the three expressions against time should yield straight lines for a model to be valid, each with a slope $\left(\frac{1}{\tau}\right)$. The slopes are used to calculate the three constants, *viz*. k_g, D_e, and k'', using the equations of time for complete conversion (τ) of a single particle for each model, as given below:

$$\tau=\frac{\rho_B R}{3b k_g C_{Ag}} \qquad \text{(Diffusion through gas film control)}$$

$$\tau=\frac{\rho_B R^2}{6b D_e C_{Ag}} \qquad \text{(Diffusion through ash layer control)}$$

$$\tau=\frac{\rho_B R}{6b k'' C_{Ag}} \qquad \text{(Chemical reaction control)}$$

Here, ρ_B is the molar density of the solid, b is the stiochiometric coefficient of the reacting solid, C_{Ag} the concentration of the reactive gas, k_g the mass transfer coefficient for diffusion through the stagnant gas film surrounding the particle, D_e the effective diffusion coefficient through the product layer, and k'' is the first order rate constant.

For model fitting purposes, the fractional residue, α, was referenced to the amount of silicon present. That is, m_0, the initial sample mass was taken as the mass of silicon present in the silicide, and the time-dependent mass was taken as the sample mass minus the mass of metal in present. The span of α is thus 1 to 0 in each case.

Since the LHSs of the model equations tend to zero at $t = \tau$, the linear data plots were done for a zero y-intercept in each case.

The experimental TGA data are displayed in figures 6.15 to 6.23 below, for all temperatures, along with the three models fitted for evaluation.

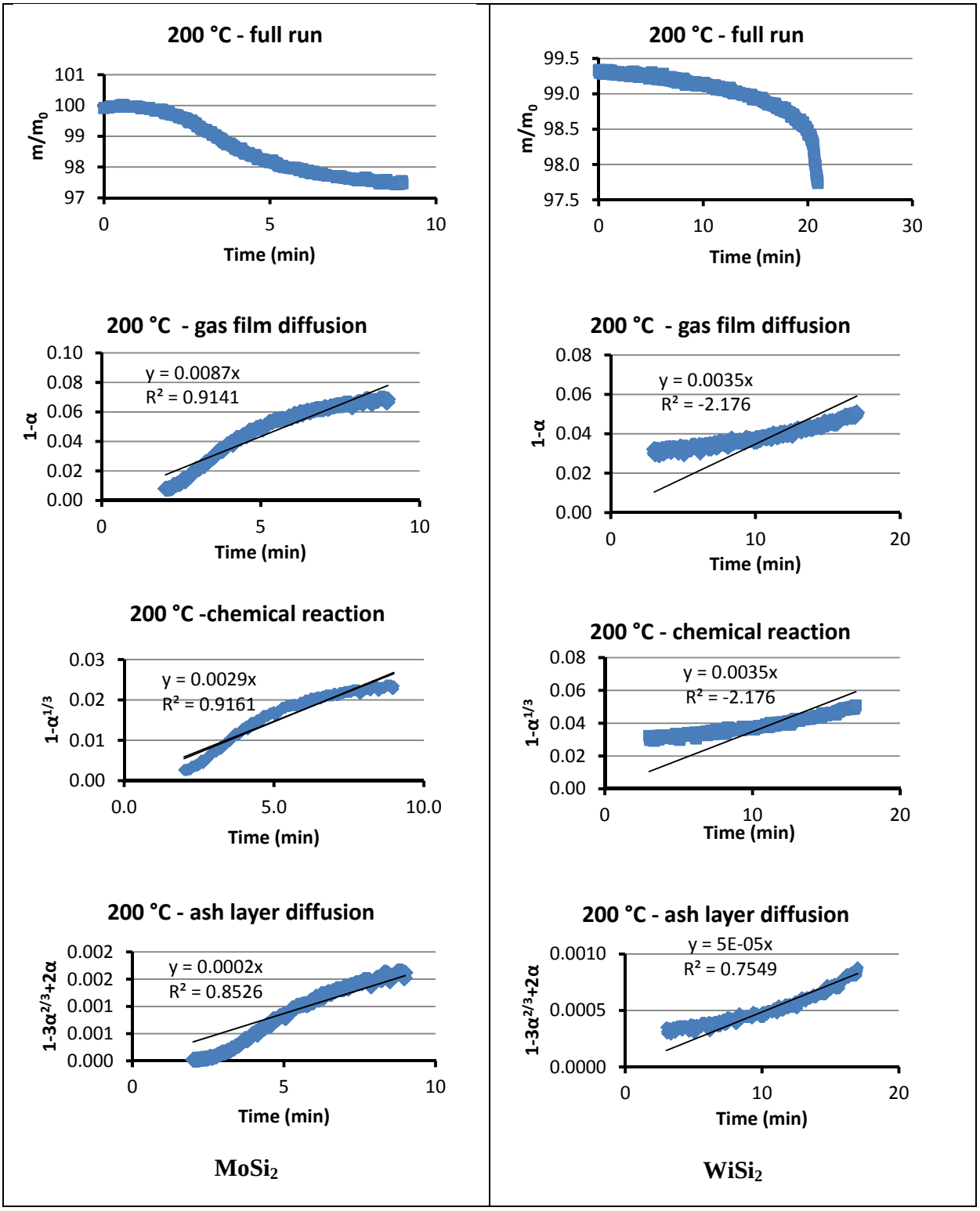

Figure 6.15: Modelled data at 200 °C, for the reactions of HF with $MoSi_2$ and WSi_2

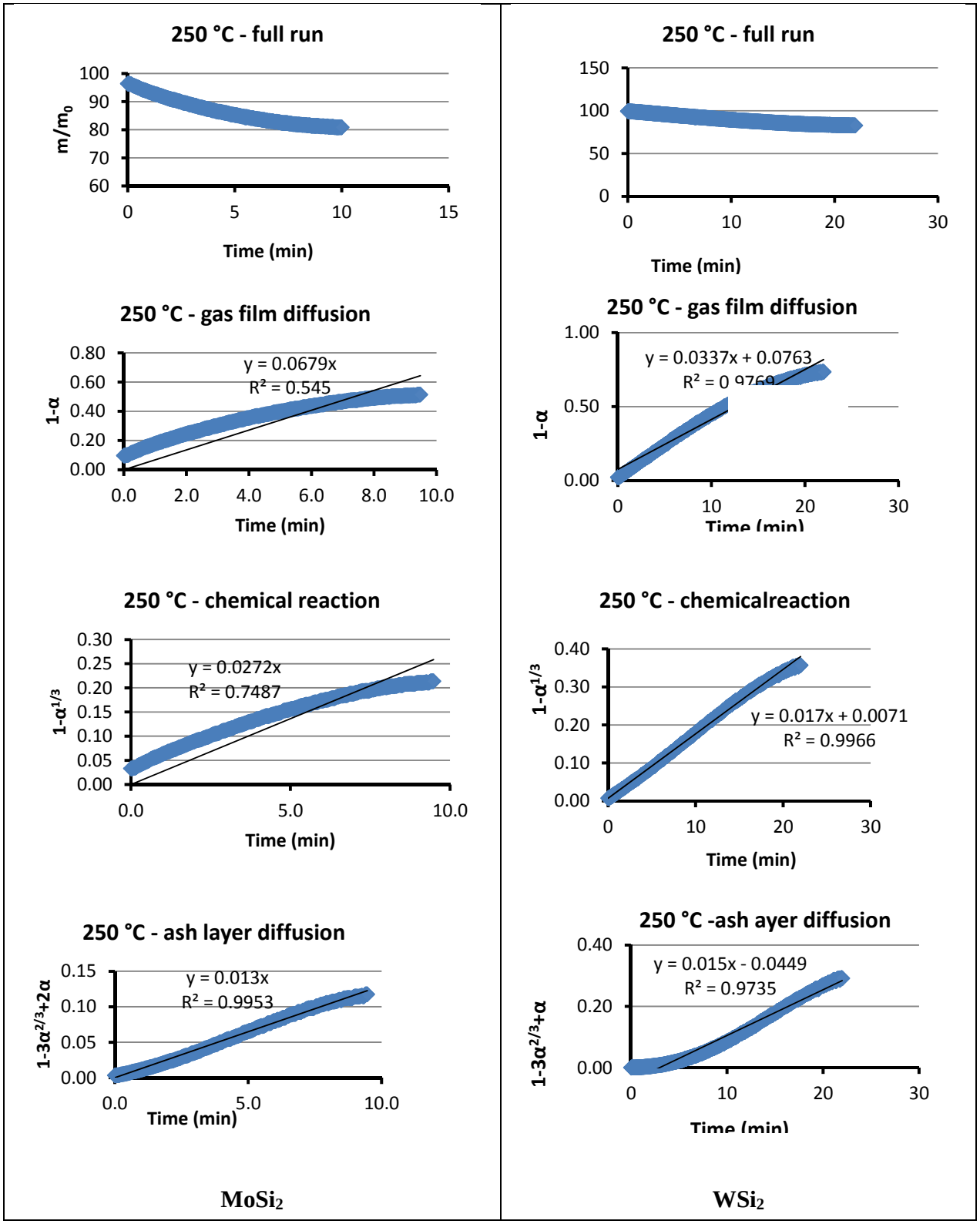

Figure 6.16: Modelled data at 250 °C, for the reactions of HF with $MoSi_2$ and WSi_2

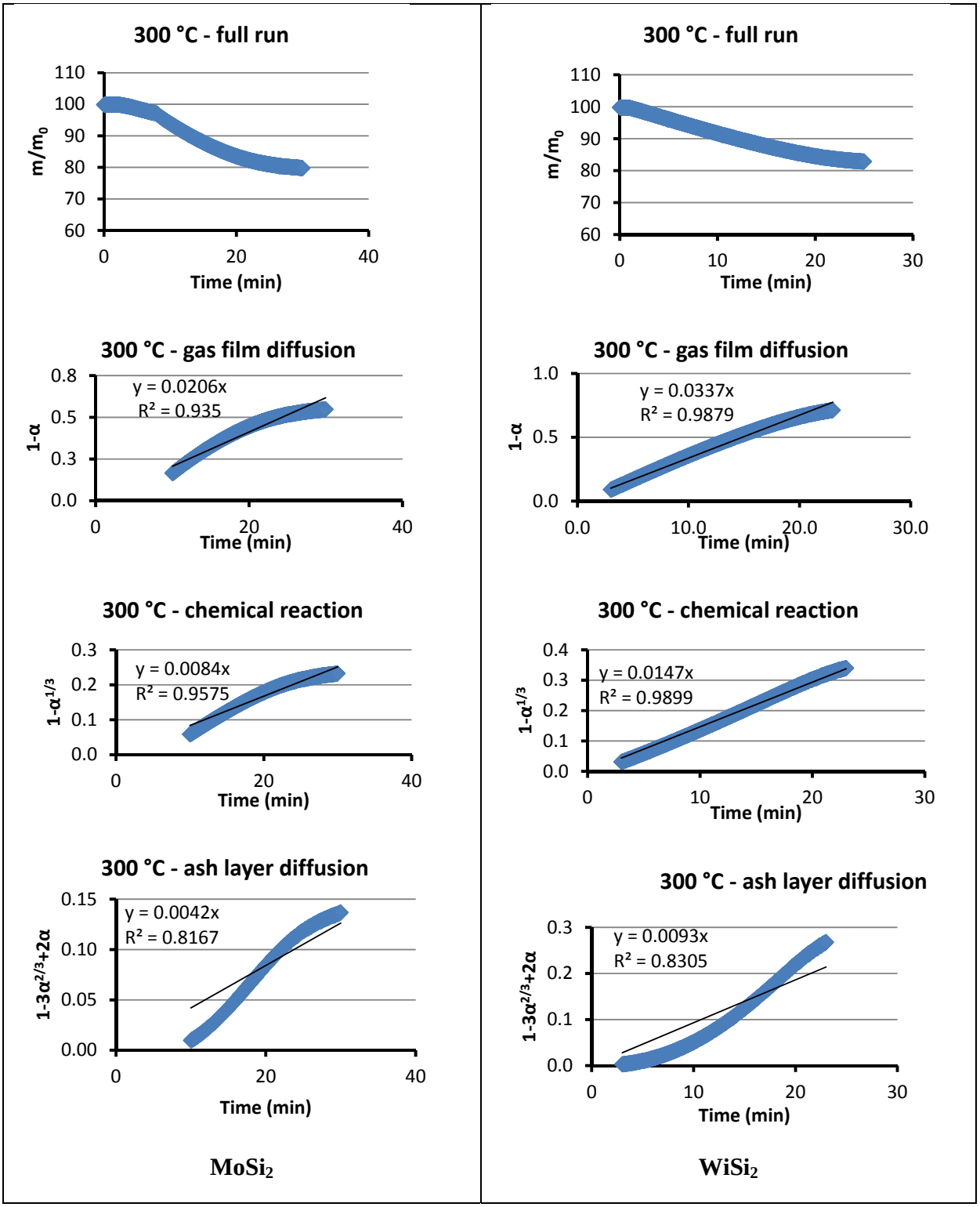

Figure 6.17: Modelled data at 300 °C, for the reactions of HF with $MoSi_2$ and WSi_2.

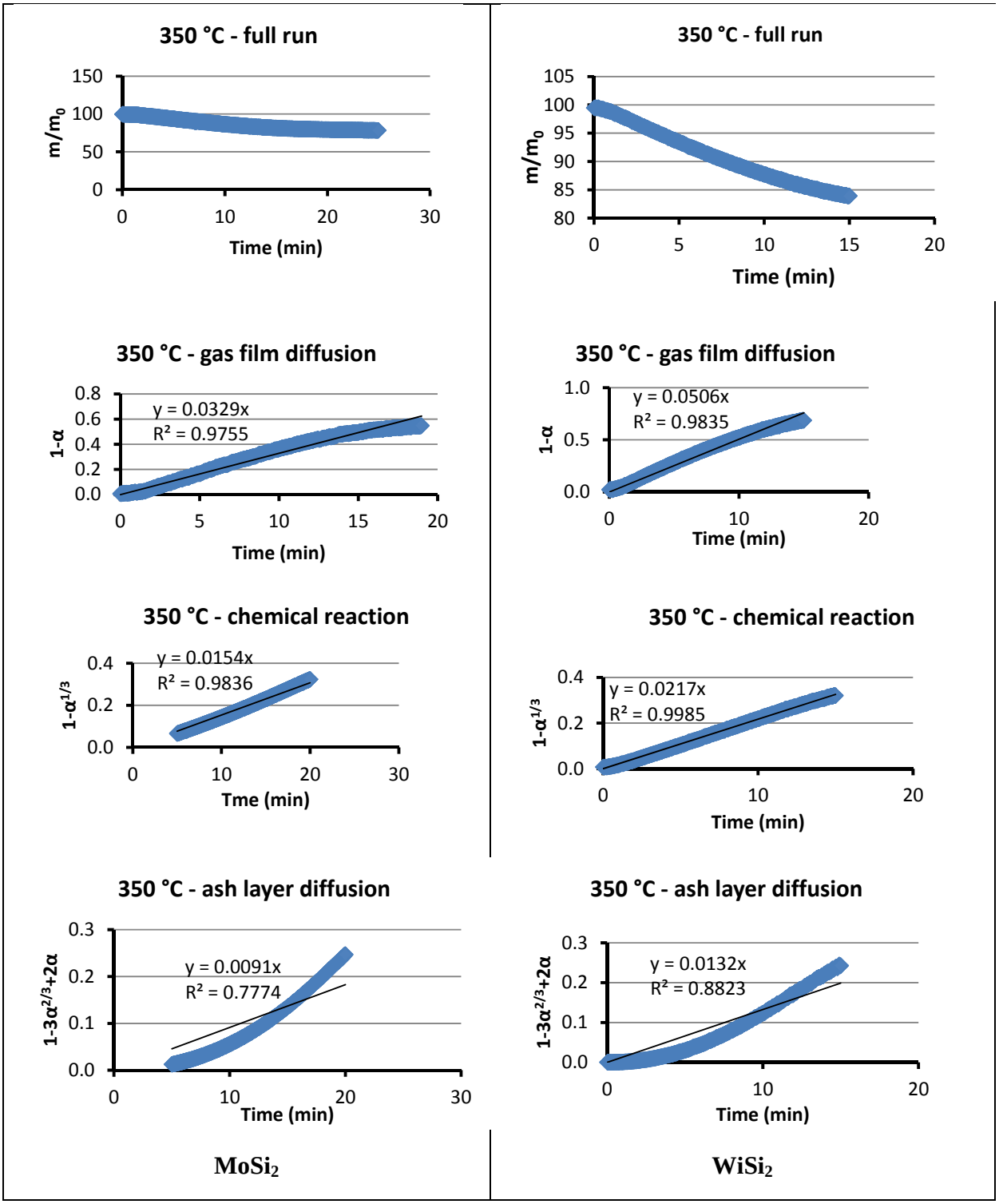

Figure 6.18: Modelled data at 350 °C, for the reactions of HF with $MoSi_2$ and WSi_2.

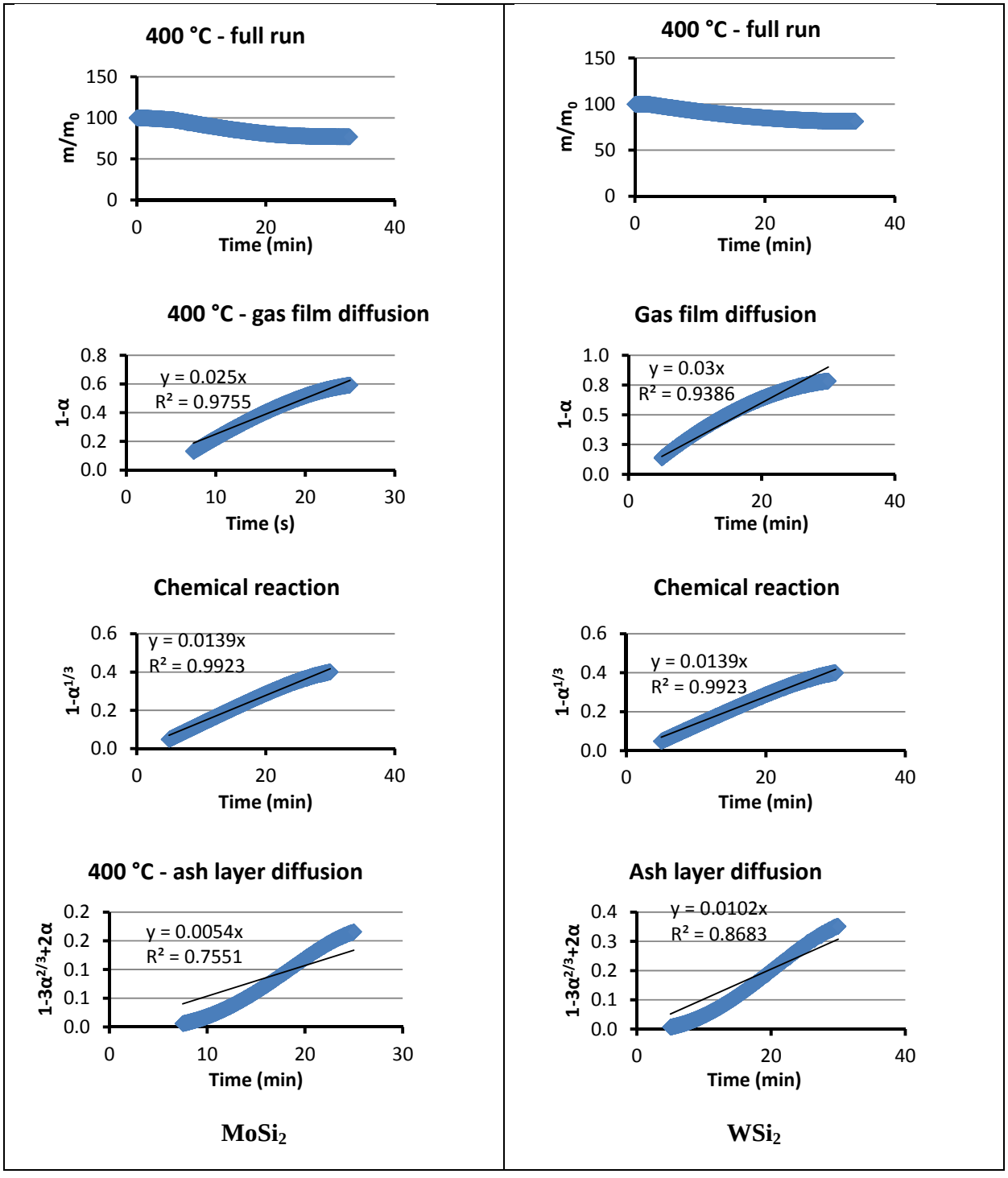

Figure 6.19: Modelled data at 400 °C, for the reactions of HF with $MoSi_2$ and WSi_2.

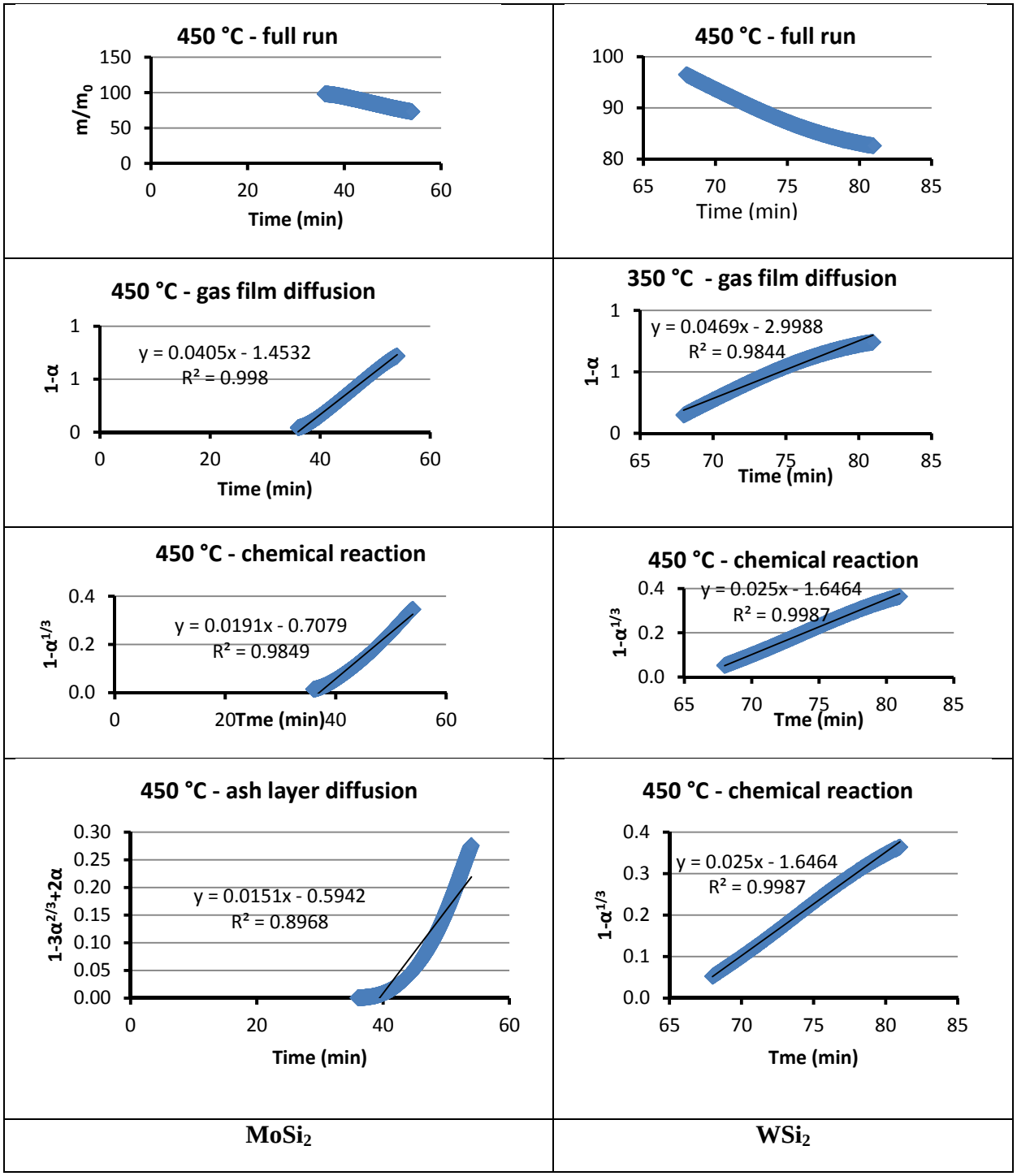

Figure 6.20: Modelled data at 450 °C, for the reactions of HF with $MoSi_2$ and WSi_2.

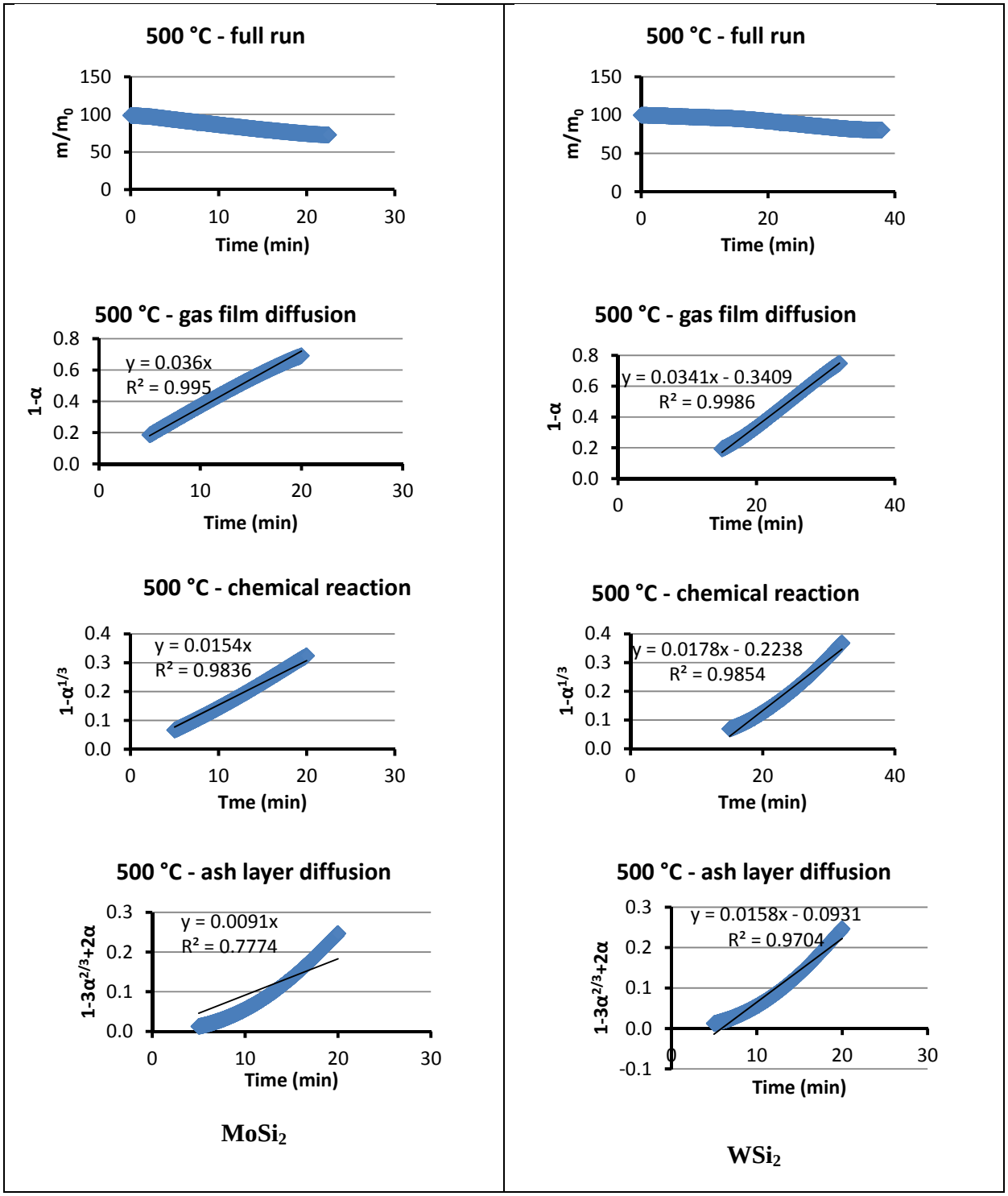

Figure 6.21: Modelled data at 500 °C, for the reactions of HF with $MoSi_2$ and WSi_2.

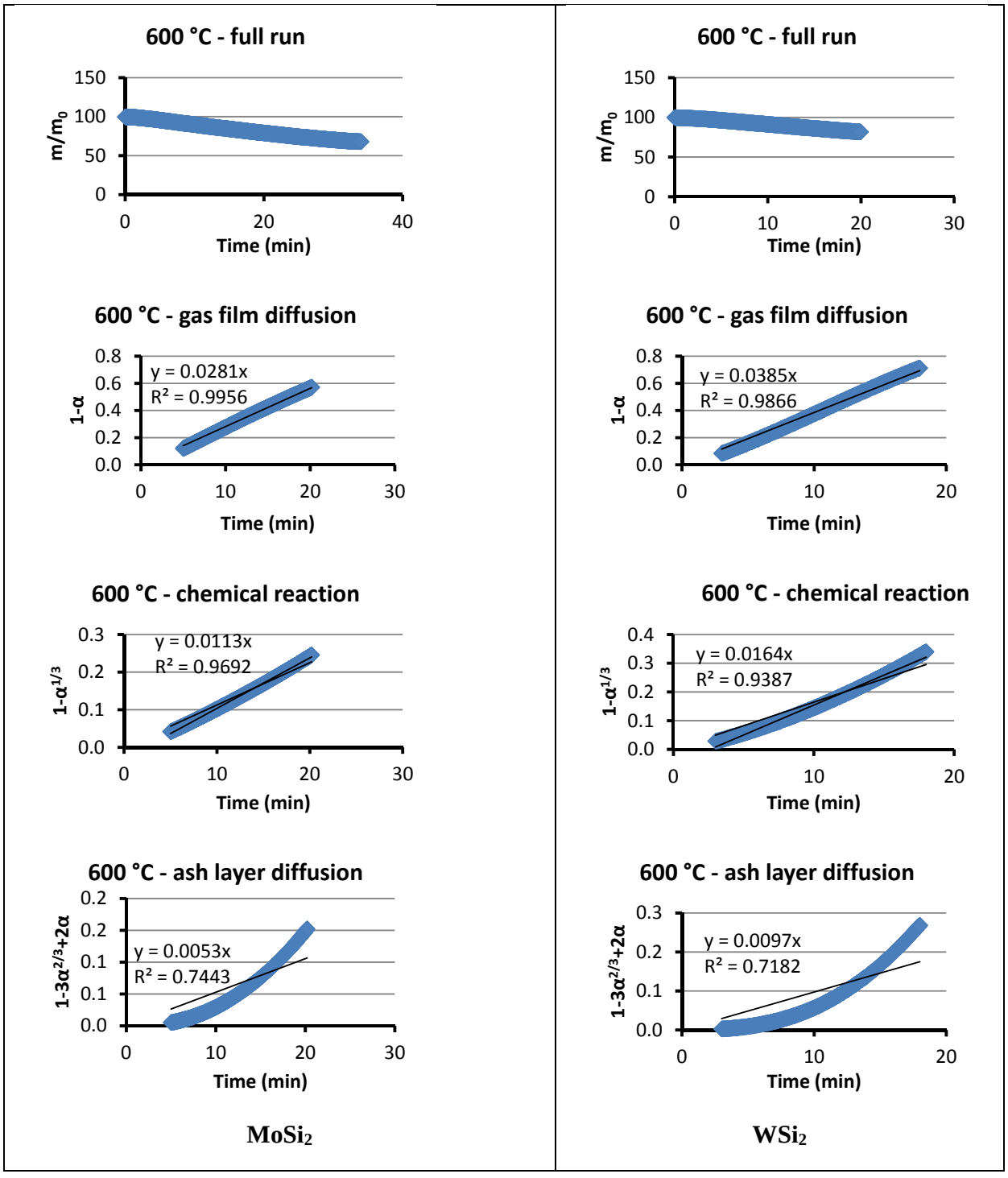

Figure 6.22: Modelled data at 600 °C, for the reactions of HF with $MoSi_2$ and WSi_2.

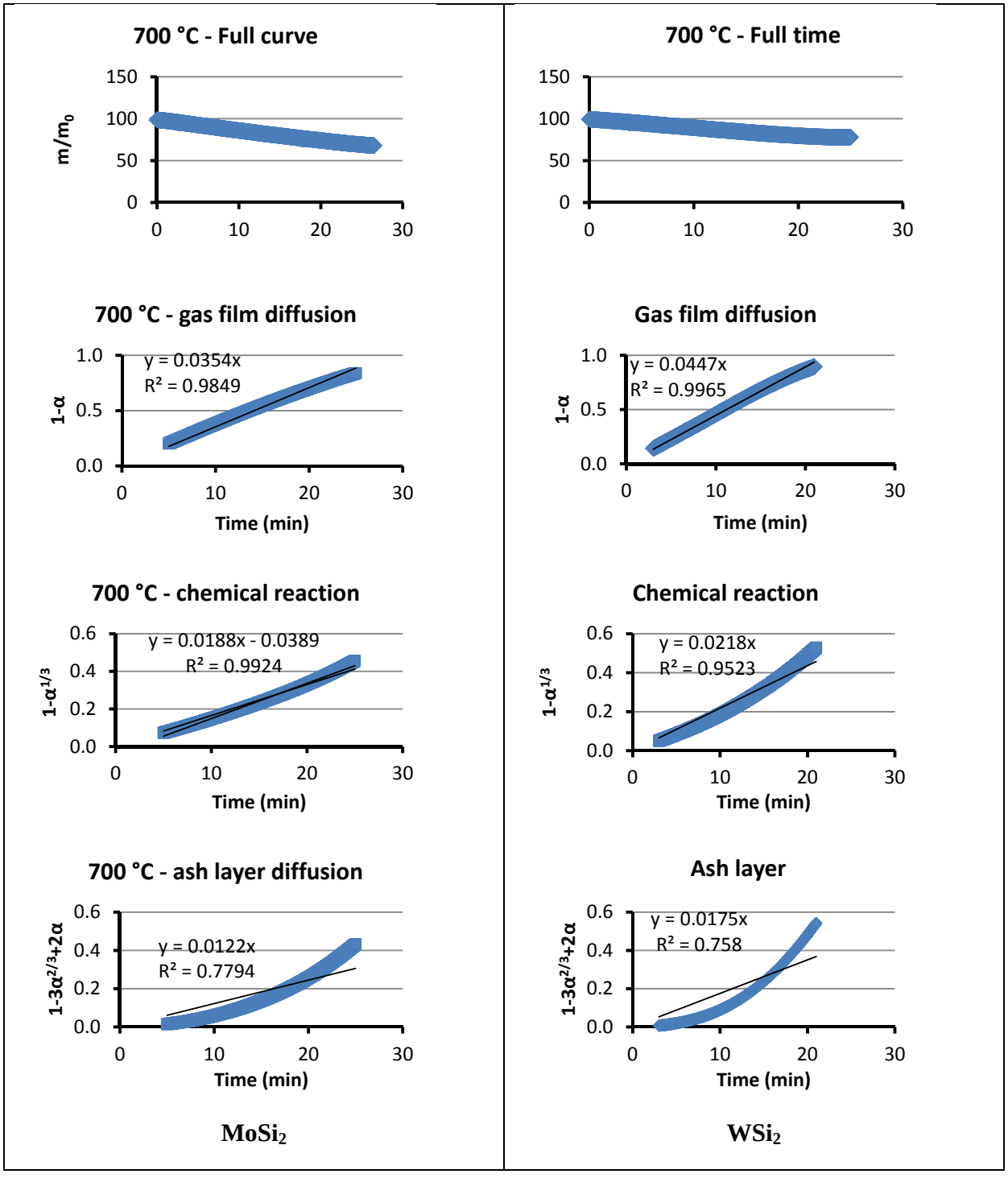

Figure 6.23: Modelled data at 700 °C, for the reactions of HF with $MoSi_2$ and WSi_2.

The kinetic constants and R-squared values for the reactions of WSi_2 and $MoSi_2$ with HF are given in table 6.3 and 6.4 below.

Table 6.3: Kinetic constants and R^2 values at different temperatures for the WSi_2 reactions

	Gas Film diffusion			Ash layer control			Chemical reaction		
T (°C)	τ (s)	k_g (m/s)	R^2	τ (s)	D_e (m^2/s)	R^2	τ (s)	k" (m/s)	R^2
200	-	-	-	-		-	-	-	-
250	1459.9	2.93×10^{-02}	0.9692	5405.4	3.73×10^{-06}	0.8986	3370.8	6.35×10^{-03}	0.9990
300	1780.4	3.07×10^{-02}	0.9879	6451.6	4.66×10^{-06}	0.8305	4081.6	6.70×10^{-03}	0.9899
350	1071.43	4.30×10^{-02}	0.9835	4511.3	4.35×10^{-06}	0.8823	2765.0	8.33×10^{-03}	0.9850
400	2000.0	3.15×10^{-02}	0.9386	5882.4	5.78×10^{-06}	0.8683	4316.5	7.30×10^{-03}	0.9230
450	1279.3	4.00×10^{-02}	0.9844	2469.1	8.47×10^{-06}	0.9842	2400.0	1.07×10^{-02}	0.9987
500	1759.5	4.21×10^{-02}	0.9986	3797.5	1.07×10^{-05}	0.9704	3370.8	1.10×10^{-02}	0.9854
600	1558.4	5.47×10^{-02}	0.9866	6185.6	7.75×10^{-06}	0.7182	3658.5	1.17×10^{-02}	0.9387
700	1342.3	6.97×10^{-02}	0.9650	3428.6	1.51×10^{-05}	0.7580	2752.3	1.70×10^{-02}	0.9523

Table 6.4: Kinetic constants and R^2 values at different temperatures for the $MoSi_2$ reactions

	Gas Film diffusion			Ash layer control			Chemical reaction		
T (°C)	τ (s)	k_g (m/s)	R^2	τ (s)	D_e (m^2/s)	R^2	τ (s)	k" (m/s)	R^2
200	6896.6	7.28×10^{-03}	0.9141	300000.0	9.662×10^{-8}	0.8526	20687.7	1.21×10^{-03}	0.9161
250	1385.7	3.02×10^{-02}	0.9583	4545.5	3.990×10^{-8}	0.9959	3125.0	6.69×10^{-03}	0.9762
300	2912.6	2.26×10^{-02}	0.9350	14285.7	2.881×10^{-6}	0.8167	7142.9	4.61×10^{-03}	0.9575
350	1823.7	3.14×10^{-02}	0.9755	6593.4	4.350×10^{-6}	0.9704	3896.1	7.34×10^{-03}	0.9836
400	2400.0	3.17×10^{-02}	0.9755	11111.1	4.218×10^{-6}	0.7351	5825.2	6.54×10^{-03}	0.9536
450	1481.5	4.22×10^{-02}	0.9980	3973.5	7.381×10^{-06}	0.8958	3141.4	9.94×10^{-03}	0.9849
500	1666.7	5.21×10^{-02}	0.9950	6593.4	8.049×10^{-6}	0.7774	3896.1	1.11×10^{-02}	0.8836
600	2135.2	4.72×10^{-02}	0.9560	11320.8	5.588×10^{-6}	0.7443	5309.7	9.49×10^{-03}	0.9692
700	1694.9	6.58×10^{-02}	0.9849	4918.0	1.415×10^{-5}	0.7794	3636.4	1.53×10^{-02}	0.9759

The dynamic TGA curves as given in figures 6.1 and 6.7 above suggest that in the case of WSi_2 at least two mechanisms dominate the process along the temperature range investigated, while in the case of $MoSi_2$, at least three mechanisms can be detected. Interpretation of the isothermal experimental data is done accordingly.

In line with the dynamic thermograms, poor model fits are obtained at 200 °C. They indicate that the reaction only fully develops somewhat above 200 °C. In the first few hundred degrees above 200 °C, better R^2 values are calculated for chemical reaction control. In the high-temperature region superior fits are obtained for gas-film diffusion control. Isothermal experiments were conducted up to 700 °C. The third mechanism observed dynamically for $MoSi_2$, is evidently above this and was not detected isothermally.

To further decide amongst the three models, Arrhenius plots of the three cases were graphed. An Arrhenius plot is obtained by plotting the logarithms of the left-hand side and right-hand side (i.e. Ink v/s 1/T) of the Arrhenius equation (6.5):

$$k = k_0 e^{\frac{-E_a}{RT}} \tag{6.5}$$

$$Ink = In\,k_0 - \frac{E_a}{RT} \tag{6.6}$$

Here E_a is the activation energy, k_o is the pre-exponential factor, T the temperature and R is the universal gas constant.

Figures 6.24 to 6.29 contain the relevant Arrhenius plots, and the kinetic parameters are tabulated in tables 6.5 and 6.6 below.

For chemical reaction control only data below 400 °C were used. For gas film control, the high temperature data points were used, as shown.

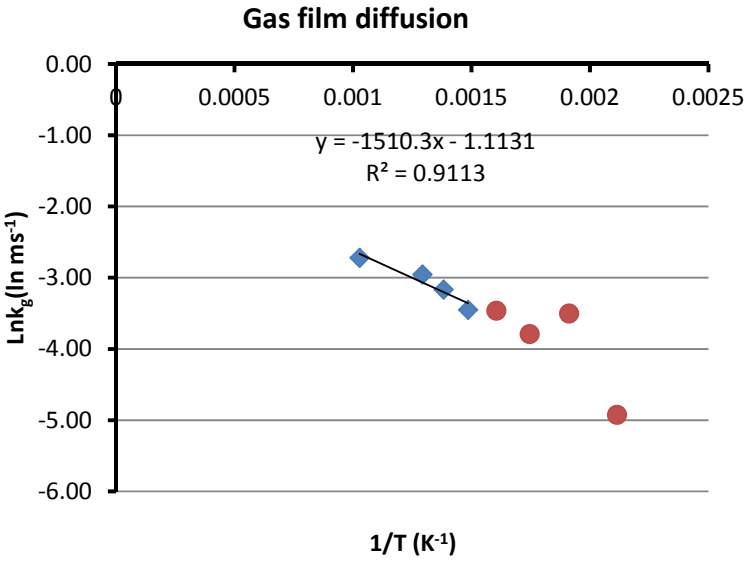

Figure 6.24: Arrhenius plot of the HF mass transfer constant for $MoSi_2$.

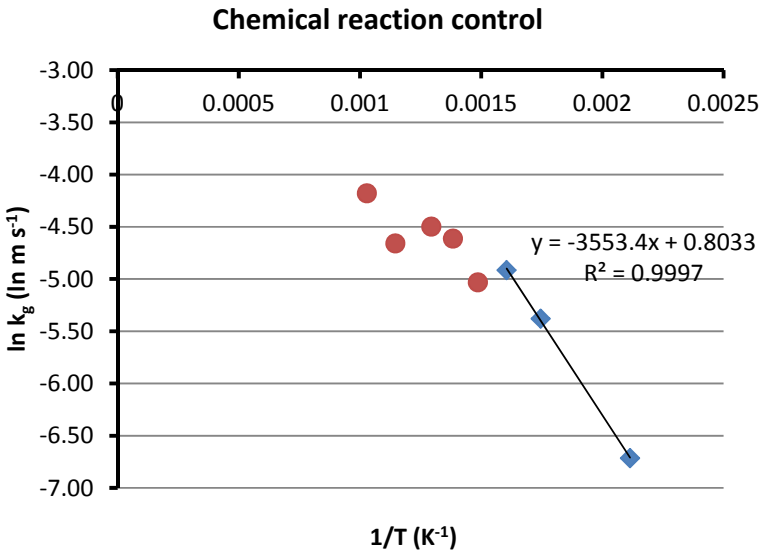

Figure 6.25: Arrhenius plot of the chemical reaction rate constant for $MoSi_2$.

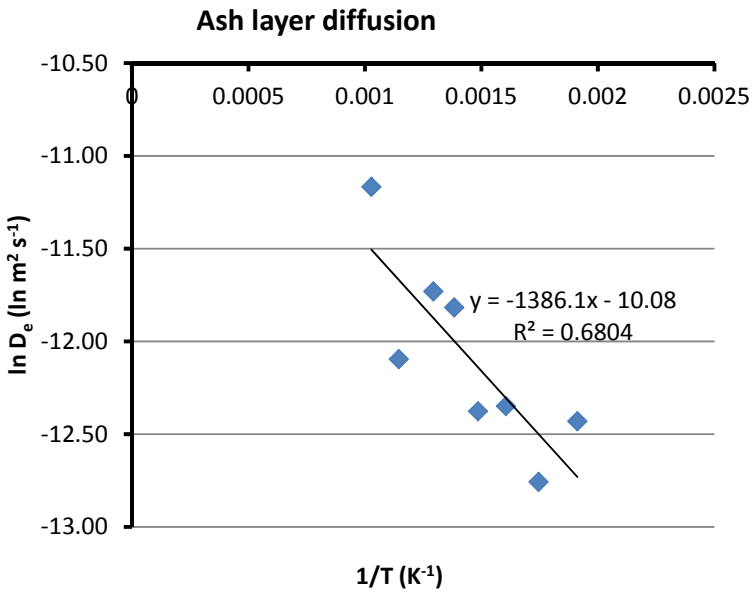

Figure 6.26: Arrhenius plot of the effective diffusion coefficient for $MoSi_2$.

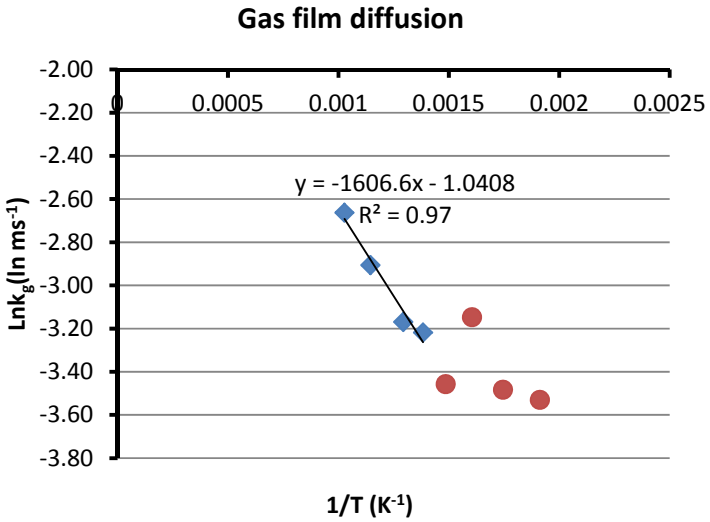

Figure 6.27: Arrhenius plot of the HF mass transfer constant for WSi_2.

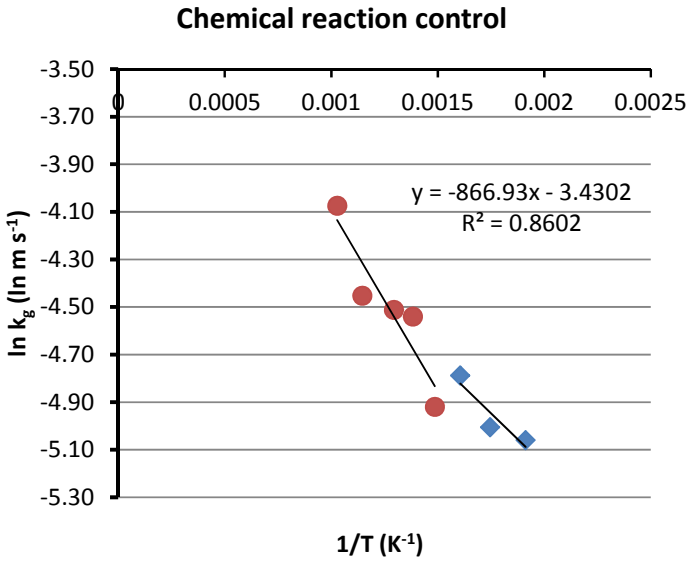

Figure 6.28: Arrhenius plot of the chemical reaction rate constant for WSi_2.

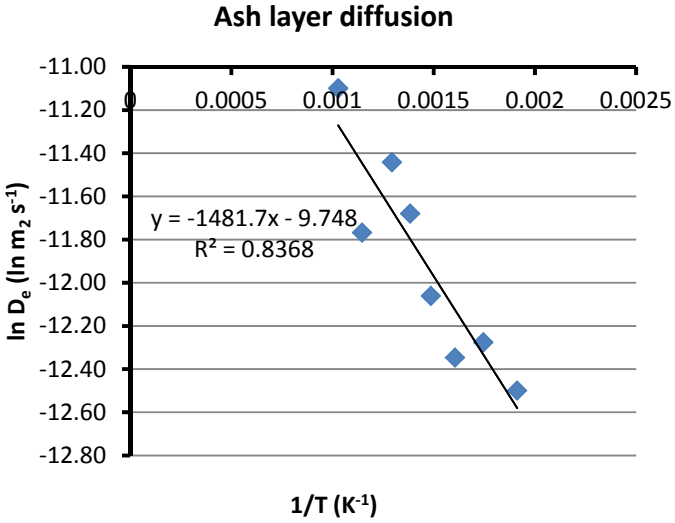

Figure 6.29: Arrhenius plot of the effective diffusion coefficient for WSi_2.

Table 6.5: Activation energy and R-squared values for the $MoSi_2$ reactions

	E_a (kJ/mol)	Pre-exponential factor ($m\ s^{-1}$ or $m^2\ s^{-1}$)	R^2
k_g	12.56	0.329	0.911
D_e	111.52	0.0000419	0.680
k"	29.54	0.032	0.999

Table 6.6: Activation energy and R-squared values for the WSi_2 reactions

	E_a (kJ/mol)	Pre-exponential factor ($m\ s^{-1}$ or $m^2 s^{-1}$)	R^2
k_g	13.4	0.353	0.970
D_e	12.3	0.0000584	0.836
k"	7.2	0.032	0.860

It should be noted that the ash-layer model fitted poorly in all cases. The conclusion is drawn that in the temperature range investigated, and where the reactions proceed relatively easily, two mechanisms are identified as rate controlling – in sequence. Below 400 °C the chemical reaction itself controls the process. Above this up to 700 °C, diffusion through the stagnant gas film surrounding the particles are rate controlling. One could argue that the SiF_4 diffusing away from the surface contributes to this effect.

6.3.2 Chapman-Enskog theory predictions

The Chapman-Enskog theory was used for predicting the gas phase diffusion coefficient values of HF in N_2. These values are compared with the experimental diffusion coefficient values in

order to investigate whether the diffusion of HF(*g*) from the gas stream into the sample holder plays a role in terms of limiting the reactions. The theoretical diffusion coefficient values were calculated using Chapman-Enskog theory, while the experimental values were calculated using Fick's first law, based on the observed flux of HF into the sample vessel and taking part in the reaction.

The Chapman-Enskog theory predicts a gas to gas diffusion coefficient values, while in our case this calculation would be for the diffusion of HF(*g*) through the purge gas (N_2). These values are compared with the typical diffusivity values (Table 6.7) for various compounds (Greankoplis, 1978; Bird et al. 1960).

Table 6.7: Typical diffusivity values for various compounds (Geankoplis, 1978; Bird et al., 960)

System	**T (°C)**	**D ($m^2.s^{-1}$)**
Gas phase		
CO_2 in N_2	25	1.65×10^{-5}
Ar in O_2	20	2.00×10^{-5}
Air in H_2	0	6.11×10^{-5}
Liquid phase		
Ethanol (50 mass %) in water	25	9.00×10^{-10}
Water (50 mass %) in n-butanol	25	2.67×10^{-10}
Acetone in water	25	1.28×10^{-9}
Solid state		
He in Pyrex®	20	4.5×10^{-15}
	500	2.0×10^{-12}
Hg in Pb	20	2.5×10^{-19}

The Chapman-Enskog expression, equation (6.7), and the isothermal reaction between WSi_2 and HF(g) at 500 °C is used as an example:

$$D_{HF} = 0.0018583\left(\frac{1}{M_{HF}} - \frac{1}{M_{N2}}\right)^{1/2} \frac{T^{1/2} f_D}{P\sigma_{HFN2}^2 \Omega_{D.HFN2}} \tag{6.7}$$

Here D_{HF} is the theoretical diffusion coefficient of HF through N_2 in (cm^2/s), M_{HF} and M_{N2} are the molar masses of the two gases, T is the isothermal experimental temperatures in Kelvin, P total pressure in atmosphere, $\Omega_{D,HFN2}$ is the collision integral based on the Lennard-Jones potential, obtained in table 1.6.3 of Christie, 1972, f_D a small second-order correction factor (and normally ignored since it is close to 1.0), and $\sigma_{HF,N2}$ is the collision diameter in Å.

The unknown values in equation (6.7), such as $\sigma_{HF,N2}^2$ and Ω_D, were obtained from the tables published by Geankoplis (1972) and Christie (1972).

The experimental diffusion coefficient values were calculated using equation (6.8). The unknown characters, such as the concentration and the flux, where calculated from the experimental data, while L was a measured value of the nickel TG pan where the reaction occurred.

$$J = -D\frac{\partial c}{\partial x} = \frac{c-0}{L} \tag{6.8}$$

Here J is the flux in $mol.m^{-2}.s^{-1}$, D is the diffusion co-efficient in m^2/s, c is the concentration in mol/m^3 and L is the diffusion length in metres.

The flux was then calculated by considering the stiochiometric reaction between WSi_2 and HF(g) as an example:

$$8HF(g) + WSi_2(s) \rightarrow W + 2SiF_4(g) + 4H_2(g) \quad (6.9)$$

The TG pan has a diameter of 6.55 mm and a height of 1.64 mm, and then the area is given as $4\pi r^2$. By ignoring the induction time and only consider the time for complete conversion of the compounds, the reaction was seen to take about 15 min (900 s). The flux is then given as follows:

$$J = \frac{moles \text{ of HF per reaction time}}{Area}\left(mol.s^{-1}.m^{-2}\right) \quad (6.10)$$

The concentration was calculated using the gas constant equation $PV = nRT$:

$$c = \frac{n}{V} = \frac{P}{RT} \times 10\% \quad (6.14)$$

where the pressure is = 1 bar, T = 773 (K), R is the universal gas constant = 8.314 $\times 10^{-5}$ m^3.bar.K^{-1}.mol^{-1}, and the 10% corrects for the fact that HF(g) was diluted with nitrogen to 10%. D was therefore determined by substituting the values of J, c and L to equation (6.10). Table 6.8 gives the comparison of the calculated experimental and theoretical diffusion coefficients values.

Table 6.8: Comparison of the theoretical and experimental D values

	HF through N_2	WSi_2 + HF(*g*)	$MoSi_2$ + HF(*g*)
Temp (K)	Theoretical D (m^2/s)	Experimental D (m^2/s)	Experimental D (m^2/s)
473	6.29×10^{-03}	3.54×10^{-09}	3.73×10^{-09}
523	6.61×10^{-03}	2.12×10^{-09}	1.76×10^{-09}
573	6.92×10^{-03}	3.68×10^{-09}	5.73×10^{-09}
623	7.22×10^{-03}	1.86×10^{-09}	3.1×10^{-09}
673	7.50×10^{-03}	4.09×10^{-09}	6.42×10^{-09}
723	7.78×10^{-03}	1.90×10^{-09}	3.07×10^{-09}
773	8.04×10^{-03}	5.01×10^{-09}	7.22×10^{-09}
873	8.54×10^{-03}	6.00×10^{-09}	8.84×10^{-09}
973	9.02×10^{-03}	6.69×10^{-09}	9.66×10^{-09}

A conclusion can be made that diffusion from the gas stream to the sample surface is not the rate limiting step, since the values of the theoretical diffusive flux to the sample is some five orders of magnitude higher than the experimentally observed flux. Thus it can be totally eliminated as an option. The theoretical values are two orders of magnitude lower than the gas to gas D values in table 6.7, which is quite comparable.

6.4 Conclusion

The reactions between both disilicides ($MoSi_2$ and WSi_2) with hydrogen fluoride start taking place just above 200 °C. This temperature was higher than the reduction temperatures of the two lower metal fluorides (WF_4 and MoF_3), hence the metals form as pure products.

The diffusion from the gas stream to the sample surface in not the rate limiting step, since the values of the theoretical diffusive flux to the sample is orders of magnitude higher than the experimentally obtained flux.

For both solids (WSi_2 and $MoSi_2$) under an HF(*g*) atmosphere, the behaviour is similar. Below 400 to 500 °C, the chemical reaction itself is rate limiting, while at the higher temperatures gas-film diffusion is rate controlling.

7. THE REACTIONS OF THE METAL DISILICIDES WITH FLUORINE

7.1 Introduction

In this section the reactions of $MoSi_2$ and WSi_2 with diluted gaseous fluorine as a fluorinating agent are described. The experiments were carried out in an open system where the gaseous products were allowed to leave through the gas stream. The thermodynamic calculations showed that fluorine should completely volatilise the disilicides to form $MoF_6(g)$ and $WF_6(g)$ along with $SiF_4(g)$ (Ch.3).

7.2 Thermogravimetric results of the reaction between $MoSi_2$ and F_2

Figure 7.1 shows the thermogravimetric results between the reactions of $MoSi_2$ and dilute fluorine (10% F_2 in N_2). This dynamic experiment was carried out using a thermogravimetric instrument according to the procedure described in Chapter 5. The mass change of $MoSi_2$ as a function of temperature under a fluorine atmosphere was monitored.

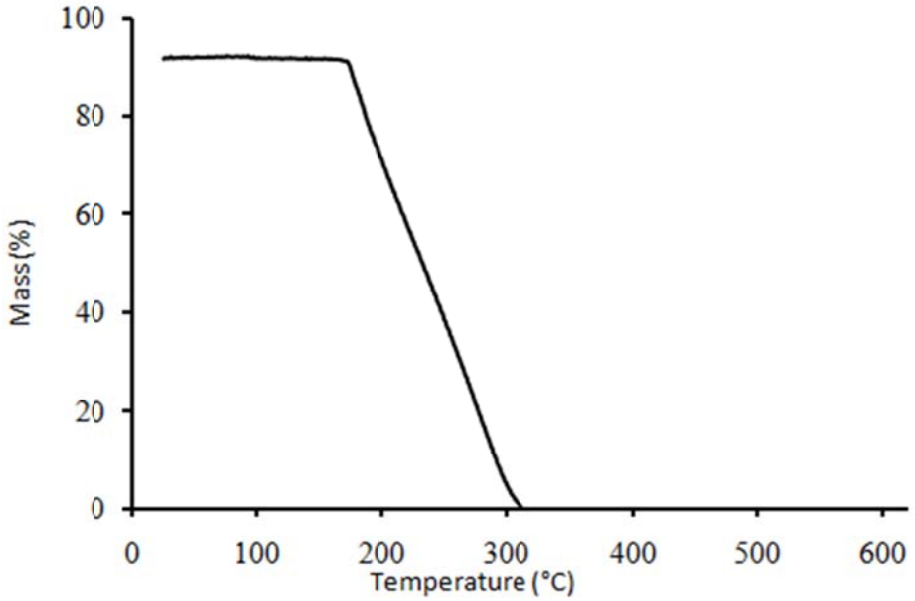

Figure 7.1: Thermogravimetric curve of the dynamic reaction of $MoSi_2$ and F_2

$MoSi_2$ was treated from room temperature up to about 620 °C at a heating rate of 10 °C/min. A total mass loss of 100% was observed, started just above 200 °C.

The results correspond to the theoretical mass loss of the conversion of $MoSi_2$ to MoF_6 and SiF_4 (Chapter 3, Figure 3.2). The results also correspond to the work done by O'Hare (1993), where $MoSi_2$ was completely converted to MoF_6 and SiF_4 with dilute fluorine.

7.3 Thermogravimetric results of the reaction between WSi_2 and F_2

The thermogravimetric results of the reaction between WSi_2 and fluorine are shown in Figure 7.2. The same procedure as described in Section 7.2 was used to treat WSi_2 from room temperature up to 721 °C at a rate of 10 °C/min.

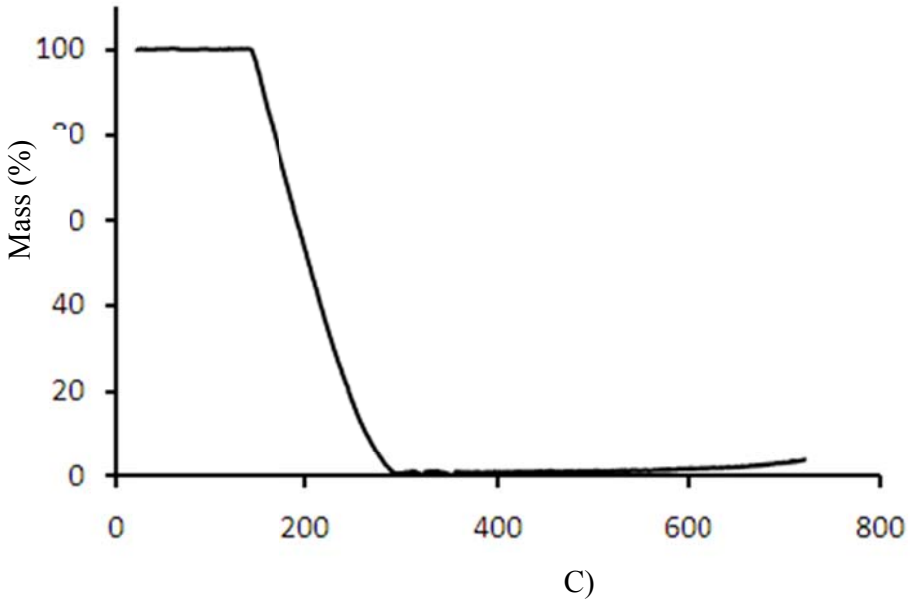

Figure 7.2: Thermogravimetric curve of the dynamic reaction between WSi_2 and F_2

The reaction started below 200 °C, and resulted in a mass loss of 100% at about 300 °C.

Tungsten behaves relatively the same as molybdenum in a fluorine atmosphere. The sharp mass loss starts at approximately the same temperature as the WSi_2 reaction with HF, this is an indication of the simultaneous formation of WF_6 and SiF_4.

The results of WSi_2 with fluorine corresponded to the work done by O'Hare (1992), where WSi_2 was completely converted to volatile products.

The TG results of both $MoSi_2$ and WSi_2 corresponded very well to the theoretical mass loss for the conversion to volatile products, and also agreed very with the predictions done using the HCS program (ch.3).

7.4 Conclusion

The TG results of reactions between the disilicides with fluorine yielded a complete mass loss, which was an indication of the formation of gaseous products. These results corresponded to the thermodynamics and the work done by O'Hare (1992 and 1993), where fluorine was used to fluorinate both compounds in order to obtain the standard molar enthalpy of formation.

8. CONCLUSIONS AND RECOMMENDATIONS

Thermodynamic calculations show that solid $MoSi_2$ and WSi_2 behave similarly under HF and fluorine atmospheres. The reactions of both solids are predicted to yield gaseous products with fluorine and pure metals with HF. Furthermore, the thermodynamics predict different chemical behaviour for the two solids investigated, compared to U_3Si_2. The reaction of U_3Si_2 with HF yields $UF_4(s)$ which is stable up to about 1100 °C before it sublimes.

All the reactions followed the thermodynamically preferred routes. The fluorine reactions resulted in the formation of volatile metal hexafluorides, along with gaseous silicon tetrafluoride. The expected products, solid molybdenum and tungsten metal, where obtained with HF. The solid molybdenum and tungsten metals form through the reduction of the intermediate products (WF_4 and MoF_3) due to the presence of hydrogen.

Diffusion of HF(*g*) from the gas stream to the surface was shown not to be the rate limiting step. The experimental data support two rate limiting steps, *viz*. chemical reaction at lower temperatures, and gas film diffusion at higher temperatures.

The following recommendations for future work can be made:

- Chemical kinetics for the fluorine reactions need to be studied to quantify the reaction rates.
- Implementation of the fluorination study of U_3Si_2 need be started; the results of these alternative materials can be used as guide line in designing the experimental procedure.

9. REFERENCES

Adelhem, M, Bacher, W, Becker FS, Gerster, H, Hohn EG and Jacob, E (1980) "Develpoment of new methods for the reduction of UF6" *J. Fl. Chem.,* 16 (6) 586.

Balluffi, RW, Allen, SM, and Carter, WC (1924) *Kinetics of Materials*, Cambridge, Massachusetts.

Berche, A, Rado C, Rapaud O, Gueneau C and Rogez J (2009) "Thermodynamic study of the U-Si system" *J. Nucl. Materials*, 389 (1), 101 - 107.

Biamino, S, Antonini, A, Pavese, M, Fino, P and Badini, C (2008) "$MoSi_2$ laminate processed by tape casting: Microstructure and mechanical properties' investigation", *J Intermetallics*, 9, 758 - 768.

Bird, RB, and Stewart, WE (1960), *Transport phenomena*, John Wiley and Sons, New York.

Buchholz, BA, and Vandegrift, GF (1995) "Processing of LEU Targets for ^{99}Mo Production - Dissolution of U_3Si_2 targets by Alkaline Hydrogen Peroxide", paper presented at *The international meeting on RERTR,* 18 – 21 September 1995, France.

Brown, ME (1989) *Introduction to Thermal Analysis: Techniques and Applications*, Chapman and Hall, New York.

Chen, L, Dong, D, Buchholz, BA and Vandegrift, GF (1996) "Progress in Alkaline Peroxide Dissolution of Low-Enriched Uranium Metal and Silicide Targets", paper presented at *The*

19th International Meeting on Reduced Enrichment for Research and Test Reactor, Argonne National Laboratory, 7 - 10 October 1996, USA.

Cotton, FA, and Wilkinson, G (1962) *Advanced Inorganic Chemistry*, New York.

Christie, JG, (1972) *Mass Transport Phenomena*, Holt, Reinhart and Winston, New York.

Domagala, RF, Wiencek, TC and Thresh, HR (1983) "U-Si and U-Si-Al dispersion fuel alloy development for the research and test reactor", Technical notes ANL division, 62, USA.

Falconer, WE, Jones, GR, Sunder, WA, Haigh, I and Peacock, RD (1973) "Preparation of lower transition metal fluorides by reduction on a heated filament" *J. Inorg. Nucl. Chem*., 35, 751 - 753.

Gabriac, A, Lamaze, PA, Durand, R and Romano, R (1995) "Process for the recovery and purification of a metal alloy based on highly enriched uranium", *US Patent 5,431,89*1, assigned to Campanie General des Matieres Nucleaires, France.

Gale, GR, Pace, BW, and Evants, RS (date) (2004) "Reclamation and reuse of LEU silicide fuel from manufacturing scrap" Babcock &Wilcox, paper presented at The 7th International topic meeting on the research reactor fuel management,9 – 12 March, 2003, Aix-en Provence, France.

Gates-Anderson, DD, Laue, CA and Fitch, TE (2004) "Dissolution treatment of depleted uranium waste", prepared for the US Department of energy by University of California, Lawrence Livermore National Laboratory, under Contract -7405-Eng-48.

Glemser, O (1986) "Inorganic fluorine chemistry, 1900 - 1945" *J. Fluorine Chem*., 33, 45 - 69.

Gokhale, AB (1990) "Mo-Si phase diagram", http://0-www.asminternational.org.innopac.up.ac.za/AsmEnterprise/APD/ [2010, August 25].

Geankoplis, CJ (1972) *Mass transport phenomena*, The Ohio state University, New York.

Geankoplis, CJ, (1978), *Transport processes and unit operations*, Allyn and Bacon, Inc., Boston.

Gusarov, AV, Perov, VS, Gotkist, IS, Klyuer LI, and Butskii, VD (1974) Doklady Akad. Nauk S.S.S.R, 216.

Greenwood, NN and Earnshaw, A (1984) *Chemistry of the elements*, Elsevier, USA.

Heslop, RB and Robinson, PL (1967) *Inorganic Chemistry*, Elsevier, Amsterdam.

Hutter, JC, Srinivasan, B, Vicek, M and Vandegrift, GF (1994) "Production of Mo-99 Using Low-Enriched Uranium Silicide", paper presented at *The 1994 International Meeting on Reduced Enrichment for Research and Test Reactors, 18 – 23, September, Williamsburg, Virginia, USA.*

Ippei, A and Koji, S (2008) "Reprocessing method by fluoride volatility process using fractional distillation", *US Patent 7,323,153*, assigned to Japan Nuclear Cycle Development Institute (Ibaraki-Ken, JP), US.

Juvenelle, A, Garrido-Berton, Initials, and Tuffery, B, (Date) "RTR fuel processing: Nitric acid dissolution of aluminium alloys", paper presented at *The International Topical Meeting on Research reactor Fuel Management,* 9 – 12 March, 2003, Aix-en-Provence, France.

Jourdan, A and Morel, B (2001) "Recent development in fluorine chemistry for microelectronics applications some examples at comurhex" *J. Fluorine Chemistry*, 107, 255 - 264.

Johnson, RL and Siegel, B (1996) "Tungsten and molybdenum fluorides by metal explosions" *J. Inorg. Nucl. Chem*., 31, 955 – 963.

Kani, Y, Sasahira, A, Hoshino, K and Kawamura, F (2009) "New reprocessing system for spent nuclear reactor fuel using fluoride volatility method" *J. Fluorine Chem.*,130, 74 – 82.

Knacke, O, Laser, M, Merz, E and Riedel, H (1967) "Process for the recovery of uranium from uranium-containing nuclear fuels and the like", *US Patent 3,353,929*, assigned to Kernforschungsanlage, Juelich, US.

Larson, ML (1970) "II. Preparation of some metal halides - anhydrous molybdenum halides and oxide halides - a summary", *Inorganic synthesis*, XII, 165 - 178.

Levenspiel, O (1996) *Chemical Reaction Engineering*, John Wiley, New York.

Lwin, L (2000) "Chemical equilibrium by Gibbs energy minimization on spreadsheets" *Int. J. Engng Edu*., 16 (4), 355 – 339.

LaValle, DE, Steele, RM, Wilkinson, MK and Yaker, Jr HL, (1960) "The preparation and crystal structure of molybdenum (III) fluoride" *J. Am. Chem. Soc*., 82(10), 2433 – 2434.

Muetterties EL, and Castle JE, (1961) "Reactions of hydrogen fluoride with metals and metalloids" *J. Inorg. Nucl. Chem*., (18) 148 - 153.

Mukashev, BN, Tamendarov, MF, Kikkarin, SM and Ustimenko, AB (2002) "Development of a technology of silicon production by recycling phosphorous industry wastes" *Sola energy materials and solar cells*, 72, 605 - 611.

Nagender Naidu, SV, Sriramamurthy, AM and Rama Rao, P (1990) "Si-W phase diagram" http://0-www.asminternational.org.innopac.up.ac.za/AsmEnterprise/APD/ [2010, August 25].

Natesan K, and Deeve SC (2000) "Oxidation behaviour of molybdenum silicide and their composites", *Intermetallics*, (8) 1147 - 1158.

O'Hare, PAG (1992) "Thermodynamic properties of silicides I. Calorimetric measurements of the specific energy of combustion in fluorine of a hyperstiochiometric tungsten disilicide, and the derived standard molar enthalpy of formation $\Delta_f H^0_m$ ($WSi_{2.060}$) at temperature 298.15 K" *J. Chem. Thermodynamics,* 24, 1323 – 1332.

O'Hare, PAG (1993) "Thermodynamic properties of silicides III. Specific energy of combustion in fluorine of a hyperstiochiometric molybdenum disilicide. The standard molar enthalpy of formation $_{\Delta f}^{H0}$ of $MoS_{i2.067}$ ± 0.002 at temperature 298.15 K" *J. Chem. Thermodynamics*, 25, 1333 – 1343.

Okamoto, H (1990) "Si-U phase diagram", http://0-www.asminternational.org.innopac.up.ac.za/AsmEnterprise/APD/ [2010, August 25].

Outotec Research Oy (2007) HSC Chemistry version 6.1, Pori, Finland.

Perry, RH and Green, DW (1997) *Perry's Chemical Engineering Handbook*, McGraw-Hill, New York.

Priest, HF and Schumb, WC (1948) "Tungsten fluorides and related compounds", Contribution from the department of chemistry, Massachusetts institute of technology" *J. Am. Chem. Soc*., 70 (10), 3378 – 3379.

Rampersadh P, (2005) *Removal of hydrogen fluoride from gas streams,* PhD Thesis, University of Witwatersrand, South Africa.

Rodrigues, GC and Gouge Anthony, P (1983) "Reprocessing RERTR silicide fuels", prepared by the US Department of energy, under Contract DE AC09 76SR00001, USA.

Roussel, MR (2004) "Reaction-diffusion equations", University of Lethbridge, Cananda. (study guide)

Settle, JL, Feder, HM and Hubbard, WN (1961) "Fluorine bomb calorimetry. II. The heat of formation of molybdenum hexafluoride" *J. Phys. Chem*., 65(8), 1337-1340.

Tagawa, H and Japan T (1976) "Process for the production of uranium trifluoride", *US Patent 3, 976, 750*, assigned to Japan Atomic Energy Research Institute, Tokyo, Japan.

Touron, E and Cheroux, L (2001) "Silicon behaviour during reprocessing of uranium silicide fuel by purex process", paper presented on *The 5th International Topic Meeting on Research Reactor Fuel Management (RRFM),* 1 – 4 April, 2001, France.

Trusov BG, (2000) “The auxiliary program for service of database on the thermodynamic properties of individual substances”, Bauman Moscow state technical University (study guide).

Yao Z, Stiglich, JJ and Sudarshan, TS “Molybdenum silicide based materials and their properties” *J. Materials Eng. and Performance,* 8 (3), 291 – 304.